REPORT OF INVESTIGATIONS NO. 143

NATURAL STRAIN IN DIAPIRIC AND GLACIAL ROCK SALT, WITH EMPHASIS ON OAKWOOD DOME, EAST TEXAS

M. P. A. JACKSON

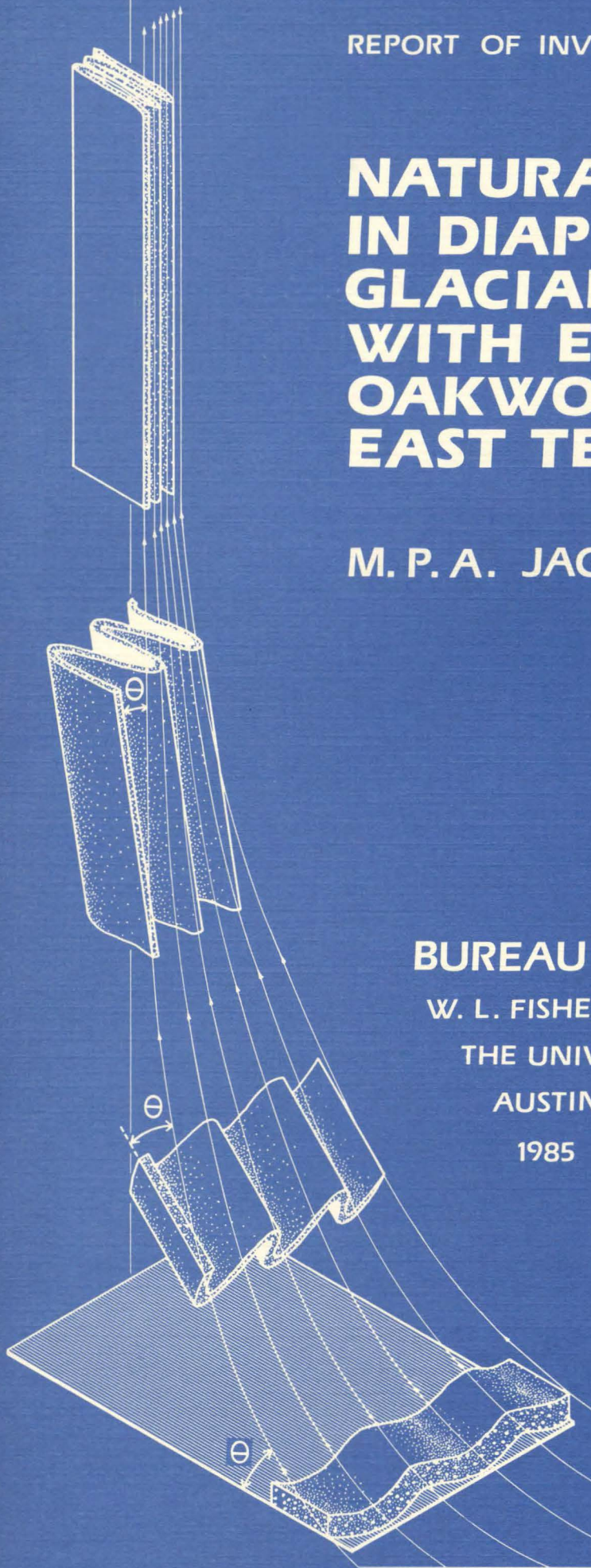

BUREAU OF ECONOMIC GEOLOGY
W. L. FISHER, DIRECTOR
THE UNIVERSITY OF TEXAS AT AUSTIN
AUSTIN, TEXAS 78713
1985

QAe4039

REPORT OF INVESTIGATIONS NO. 143

NATURAL STRAIN IN DIAPIRIC AND GLACIAL ROCK SALT, WITH EMPHASIS ON OAKWOOD DOME, EAST TEXAS

M. P. A. JACKSON

Funded by the U. S. Department of Energy,
National Waste Terminal Storage program,
under Contract No. DE-AC97-80ET46617

BUREAU OF ECONOMIC GEOLOGY
W. L. FISHER, DIRECTOR
THE UNIVERSITY OF TEXAS AT AUSTIN
AUSTIN, TEXAS 78713
1985

CONTENTS

FIGURES

TABLES

ABSTRACT

Structural styles in the gravity-driven, ductile flow processes of glaciers and diapirs are analyzed. When dampened by rainfall, salt glaciers flow rapidly under minute differential stress. Thus, the concentration of water in diapiric rock salt is crucial to predicting creep rates in a repository medium. Natural-strain rates of rock salt range greatly from 10^{-8}/s to 10^{-16}/s; rates of average diapiric uplift are slowest. Contrary to widespread generalization, structural attitudes in dome-salt mines are predominantly moderate to steep (60° to 80°) rather than vertical.

Diapiric folds may be triggered by (1) shear stresses induced by upward flow, (2) shear stresses induced by boundary effects of the salt source layer, and (3) normal stresses induced by convergent flow. Folding in salt stocks follows the similar-fold model, although some folds may have begun as buckles. Closed interference structures are sheath folds formed by intense constriction of originally gentle fold culminations and depressions. Construction of plunge-isogon maps from mapped linear structures allows the flow directions of diapiric salt to be deduced.

Geometric and strain analyses of salt core from Oakwood Dome show that the well bore penetrated the hinge zone and lower limb of an inclined, overturned antiform, which probably represents a salt tongue that has spread outward from the diapir center. Structural evidence indicates truncation of the diapir crest, probably by ground-water dissolution during cap-rock formation. The uppermost 2 m of rock salt recrystallized in the presence of water. Homologous temperatures and present maximum erosion rates suggest that the salt recrystallized at least 3 Ma ago at depths 400 m greater than present.

All the strains recorded in Oakwood halite are of the flattening type. The ratio of flattening to constriction increases upward, whereas strain intensity decreases upward. This strain pattern may represent a transition to an originally "neutral" zone in the diapir, since removed by dissolution. Orientations of maximum-extension axes in rock salt vary widely.

Keywords: diapirs, East Texas, fabric, finite-strain analysis, flow structures, folds, glaciers, salt domes, salt tectonics, shear zones, structural geology

INTRODUCTION

Oakwood Dome is one of 15 shallow salt domes in the East Texas Basin (fig. 1) studied since 1977 by Bureau of Economic Geology researchers to evaluate the suitability of using these and other domes for storing high-level nuclear wastes (for example, Kreitler and others, 1981; Jackson and Seni, 1984a,b). As part of the East Texas Waste Isolation Feasibility (ETWIF) project, a 10-cm-wide continuous core was extracted from a vertical borehole (LETCO TOG-1) near the axis of the salt stock. Cap rock was intersected at a depth of 217.3 m and rock salt at 354.5 m; the hole ended at a depth of 411.8 m. The lithology, microstructures, fluid inclusions, and geochemistry of the rock salt and cap rock have been documented by Dix and Jackson (1982) and Kreitler and Dutton (1983).

The present companion study describes and analyzes the structural geology of the salt core. Through geometric and strain analyses, the structure is examined on all scales from 10^{-3} to 10^{1} m. For scales less than 10^{-3} m, the reader is referred to the paper by Dix and Jackson (1982), which also presents the geologic setting of Oakwood Dome.

Chief practical goals of this study were to assess the structural stability of Oakwood salt stock and to evaluate its fabric to assist mining engineers who might one day excavate storage caverns within the stock. Some important hydrologic aspects, such as evidence of truncation by subsurface dissolution, also derive from these structural studies. To the writer's knowledge, this is the first geometric analysis in cross section and the first strain analysis of a Gulf Coast salt stock.

To evaluate the results of these analyses from just a single core, old data from other salt domes were reinterpreted using current structural concepts and techniques and compared with data on gravity structures of ice and salt exposed at the Earth's surface. This general survey of other salt domes and glaciers received major impetus when Oakwood Dome was given lowest priority, after Richton, Vacherie, and Cypress Creek Domes in Mississippi and Louisiana, as a candidate for storing high-level nuclear wastes (Office of Nuclear Waste Isolation, 1982). In terms of Nuclear Regulatory Commission licensing criteria, the presence of many boreholes in the Oakwood salt stock was considered "adverse" and the proximity of potential Quaternary faulting, possible evidence of dissolution, and aspects of the surface hydrology were termed "less favorable" (Office of Nuclear Waste Isolation, 1982). In their summary of all results from the ETWIF project, Jackson and Seni (1984b) concluded that in terms of guidelines of the U.S. Department of Energy (1983), Oakwood Dome was disqualified as a candidate dome because 62 exploration and production boreholes are drilled through the overhang, 3 of which have not been located, and because petroleum reserves lie below the overhang and 4 km to the southeast. These adverse evaluations mean that structural data, techniques, and models should not be confined to Oakwood Dome but should be sufficiently broad in scope to be applied to understanding other domes. Thus, part I of this report is a generic account of the internal structure of salt domes and related structures for application to any salt dome; it also provides background concepts and data for assessing part II, which is specific to Oakwood Dome.

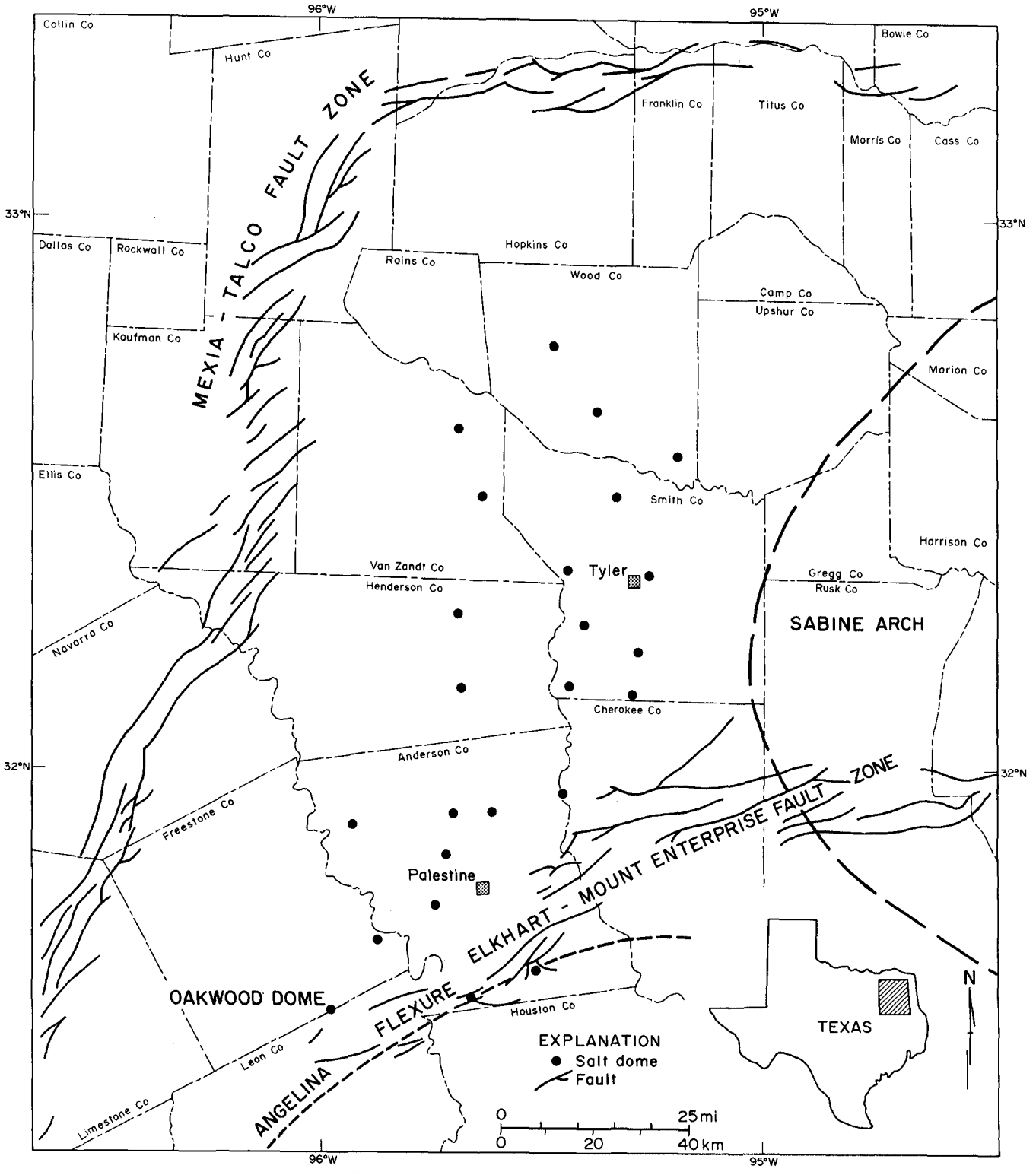

FIGURE 1. Map showing the East Texas Basin and location of Oakwood Dome. (From Dix and Jackson, 1982.)

PART I: GRAVITY-DRIVEN DEFORMATION: COMPARISON BETWEEN GLACIERS, NAMAKIERS, AND SALT DIAPIRS

RELEVANCE OF GLACIERS AND NAMAKIERS TO SALT-DIAPIR STUDIES

Glaciers and diapirs have several features in common. Both represent gravity-driven movement of large masses of fairly pure metamorphic rock. Likewise, both contain a complex array of superposed fabrics, recrystallization zones, and zones of inhomogeneous shear. However, certain major differences separate glaciers from diapirs. Glaciers move down and diapirs move up, and their boundary conditions are quite different. Despite these dissimilarities, it is surprising that geologists studying the internal structure of salt diapirs have made so little use of the enormous amount of data on and models of the gravity flow of glaciers. One purpose of this paper is to compare the fabrics and flow mechanisms in ice glaciers, salt glaciers, and salt diapirs so that glacial analogs can be used in interpreting the internal structure of salt diapirs. Only those aspects of glacial flow relevant to diapiric flow will be described.

Glaciologists have intensively studied ice glaciers on all scales. Ice glaciers and sheets are abundant, covering 10 percent of the Earth's land surface. Their complete sequence of deformation can be studied in marginal cliffs, crevasses, and drill cores.

Salt glaciers, described as "one of the geological wonders of the world" (Kent, 1979), are comparatively rare. They are best developed in southern Iran. A full sequence of glacial deformation is exposed, but unlike ice, the salt has already been deformed many times before it begins glacial flow. Because the origin of salt glaciers is fundamentally different from that of ice glaciers, Talbot and Jarvis (1984) have proposed that salt glaciers be renamed "namakiers," a combination of "*namak*" (Farsi word for salt) and "glacier." This usage is followed here, and ice glaciers are hereafter referred to simply as glaciers.

Namakiers are fed by exposed diapirs. The Hormuz Salt, part of a late Proterozoic evaporite sequence, has risen diapirically from depths of 5 to 10 km through a virtually continuous carbonate overburden to breach the surface in the form of more than 200 salt diapirs (Ala, 1974; Kent, 1979). Diapirism and salt intrusion began in the Jurassic and Early Cretaceous and were followed by salt extrusion by Early to Late Cretaceous time (Kent, 1979). The bedded Hormuz Salt provided a décollement zone for Zagros folding, which began after salt extrusion in the middle Miocene and peaked in the Pliocene-Pleistocene. Folds propagated serially toward the southwest and were partly controlled by weak points represented by preexisting salt diapirs (Kent, 1979). Folding continues today along the Persian Gulf coast of Iran; shortening rates have been estimated at 14 to 18 mm/a (1 a = 1 year, 1 Ma = 10^6 years), and anticlinal rising rates at an average of 1.4 to 1.9 mm/a (Vita-Finzi, 1979). The bellows action of Zagros folding is pumping salt out from exposed orifices at geologically rapid rates (discussed on p. 11). One of the largest namakiers flows northeast from the summit of Kuh-e-Namak (Mountain of Salt) in Dashti Province, southwest Iran. Because it is the only one whose detailed internal structure, flow dynamics, and salt budget have been studied (Talbot, 1979, 1981; Talbot and Rogers, 1980; Talbot and Jarvis, 1984), this namakier is regarded here as the type namakier.

Salt diapirs are common in many basins containing buried evaporites. Almost all information on the internal structure of salt diapirs is based on excavation of caverns and drilling in salt mines of Texas, Louisiana, and Germany. The floors and ceilings of large caverns provide horizontal cross sections allowing meticulous structural mapping (for example, Balk, 1949, 1953; Muehlberger, 1959; Hoy and others, 1962; Kupfer, 1962). Because almost all structures in the trunk of salt diapirs dip or plunge steeply, these mine levels provide structural profiles; walls and pillars in plan section correspond to areas of no outcrop. Because of the paucity of stratigraphic markers in the rock salt, the Gulf Coast domes have not yielded the information needed to interpret their fold patterns. In German salt diapirs, the stratigraphy, defined by complete sequences of evaporite minerals, enables the three-dimensional shape of extremely complex major folds to be elucidated (Richter-Bernburg, 1980). In the Great Kavir in north-central Iran, the Semnam salt diapirs breached by erosion display superb

exposures of major folds within them (Stöcklin, 1968) and represent a major frontier for the study of the interiors of salt domes.

The following sections compare properties related to the flow of glaciers, namakiers, and salt diapirs. Properties of glaciers and salt diapirs are generalized because of the large number of examples studied; namakier description is based on Kuh-e-Namak.

LITHOLOGY

All three types of gravity-driven structures–glaciers, namakiers, and salt diapirs—consist of largely monomineralic crystalline rock:

Glaciers consist of ice and entrained air bubbles, dirt, rock fragments, and atmospheric fallout; they are mantled by firn, snow, and residual foreign matter. Foreign fragments are locally derived from the glacier sole, valley walls, and cirques. Foreign materials are concentrated because their melting points are higher than that of ice.

Namakiers consist of halite (as coarsely crystalline aggregates, porphyroclasts, and fine-grained groundmass) and disseminated anhydrite, magnetite, hematite, sulfur, and foreign rock fragments. These impurities, which are derived from the salt diapir feeding the namakier, are concentrated because their solubilities are lower than that of halite (Harrison, 1930).

Salt diapirs also consist of halite (as coarsely crystalline aggregates or megacrysts) enclosing or interlayered with other evaporite minerals like anhydrite, carnallite, and sylvite. In the Gulf Coast and German domes, foreign (nonevaporitic) inclusions are rare; however, Iranian diapirs, generally 5 to 10 km across, contain entrained debris that ranges in size from sand grade to enormous rafts of Cambrian sediments up to 7 km^2 in exposed area (Chah Benu diapir). These large rafts are undeformed apart from gentle curvature and rock salt is horizontally stratified in some diapirs (for example, Jehani), suggesting emplacement in a pistonlike manner with little internal deformation (Ala, 1974; Kent, 1979). This hypothesis cannot explain the highly deformed interiors of diapirs elsewhere in Iran (Stöcklin, 1968, his pl. 3; Richter-Bernburg, 1980, his figs. 21 and 22) and in Germany and the Gulf Coast (described on p. 20). The apparent horizontal stratification in diapirs like Jehani may be a response to the boundary effects imposed by the upper free surface (compare Talbot, 1981) rather than a result of pistonlike flow; flow banding in salt becomes parallel to its boundaries. Furthermore, some of the large rafts of country rock conceivably represent downfaulted roof rocks separated by dikes of salt (C. J. Talbot, personal communication, 1983). Where many cubic kilometers of country rock displaced from the diapir neck are missing, salt must have originally extruded at much higher stratigraphic levels before being deeply eroded (Kent, 1979).

MASS BALANCE

Glaciers and namakiers advance, recede, and even disappear according to the balance between the rate at which they are supplied at their heads with new ice or salt and the rate at which these rocks are lost flowing toward their snouts. The gain and loss of salt to and from diapirs is more speculative, but evidence from hydrological studies, cap-rock studies, and basinwide mass-balance studies (summarized in, for example, Jackson and Seni, 1984b) suggests that at least some salt diapirs are not fossil structures but have lost (and presumably gained) considerable volumes of salt during their long evolution.

Glacial ice accumulates by transformation of snow replenished by snowfall, avalanches, and freezing rain. Ice is lost by ablation: meltwater runoff, evaporation, wind erosion, and iceberg calving.

Namakiers are fed by gravity spreading of extrusive topographic domes of salt representing the crests of erosionally breached diapirs. Salt is removed by dissolution and minor mass wasting. Kent (1966, 1970) emphasized that active flow is needed to maintain the elevated topography of namakiers against continuous climatic attrition.

Diapiric salt is fed by gravity-induced rise of a buried salt source layer. Diapirism is propelled by buoyancy, differential loading, thermal convection, or tangential extension or contraction of the crust. Salt is lost by dissolution, erosion, or extrusion.

MORPHOLOGY

Valley glaciers are long, narrow, thick sheets. Their upper surfaces are all depressed below the surrounding landforms. The glaciologists' parameter W (half-width divided by thickness) ranges from 2 to 4 (Paterson, 1981). Piedmont glaciers are much thinner and broader. They commonly form on the plains fronting the mountainous terrain containing valley glaciers.

Namakiers are broad, thin sheets connected to extrusive topographic domes of salt. Kuh-e-Namak is estimated to have a W ratio of 10 to 20 (Talbot and Jarvis, 1984). The topographic expression depends on the relative rates of extrusion and rain-induced solution. Where solution predominates, the diapir is depressed in a crater. Where extrusion predominates, both the salt plug and the namakier are raised above their immediate surroundings, and the plug typically has concentric crestal ridges. Exceptionally active extrusion is required for salt in a plug to overflow its confining scarps and descend as one or more namakiers. Kuh-e-Namak rises more than 1,500 m above the surrounding plains.

Salt diapirs range from squat to spinelike. In vertical cross section, they can be conical, barrel shaped, or mushroom shaped. They need not be exposed to influence the topography, but, like namakiers, their topographical expression depends on the balance between supply and attrition. The surface expression of shallowly buried diapirs in the East Texas Basin is subdued or nonexistent because the rates of diapir rise are too low to offset the effects of erosion (Seni and Jackson, 1983b, 1984; Jackson and Seni, 1984b). Diapirs buried in the Gulf Coast, onshore and offshore, tend to have a more marked relief than do those in East Texas because the Gulf Coast domes are younger and more active (Seni and Jackson, 1983a).

BOUNDARY CONDITIONS

Glaciers and namakiers have similar boundary conditions. Rigid country rocks underlie and flank both types of structures. Incohesive residual debris (till) is common near their snouts, and the upper surface is a free-air boundary. On the basis of observations at Kuh-e-Namak, Talbot (1979, 1981) concluded that namakiers do not erode their bedrocks to the same degree as do glaciers.

Salt-diapir boundaries are much more confining because diapirs are intrusive. They are laterally confined by country rocks of various rigidities and are vertically constrained to different degrees by cover sediments, water, or air.

BULK-STRAIN PATTERN

The overall strain pattern in glaciers, namakiers, and diapirs provides a framework within which to examine the detailed structure of these bodies. The bulk strain of glaciers is calculated from direct measurements of the flow velocity in different parts of the glaciers (Milnes and Hambrey, 1976; Hudleston and Hooke, 1980). The strain state of glaciers can be broadly summarized as pure shear (coaxial strain) in the center and simple shear (noncoaxial strain) along the margins (Hambrey, 1979). The Barnes Ice Cap on Baffin Island, Canada, undergoes simple shear (Hudleston and Hooke, 1980). Near the margins, simple shear is restricted to the basal ice; above the base, the ice shortens tangentially and extends vertically, increasingly modifying the shear component toward the surface. Mathematical modeling by Hudleston and Hooke (1980) indicates that flow surfaces (surfaces containing flow lines along which ice particles move during glacial flow) are listric (spoon shaped and concave upward). On the top of the ice, the trace of each listric flow surface is arcuate; along the center line, ice is being compressed in the direction of flow; along the margins, ice is being sheared into parallelism with the confining valley sides.

The morphology of the layering in namakiers suggests that their bulk-strain patterns are similar to those of valley glaciers, although no quantitative studies are available to check this. Field observations indicate that simple shear dominates (1) in a vertical plane above bedrock obstructions and at the junction of dome and namakier and (2) in a horizontal plane between mainstream salt and salt dammed by obstructions projecting laterally into the namakier (Talbot, 1979, 1981).

The difficulties of understanding or generalizing the bulk strains within salt diapirs are exemplified by Richter-Bernburg's (1980) conclusion that within a diapir, folds of all imaginable, or even unimaginable, geometries are possible. Nevertheless, we can describe, on the basis of intuitive reasoning, the general nature of these large-scale strains at different levels of a diapir. The flow circulation in a diapir has the form of a toroid: The diapir either occupies the "hole in the doughnut" (Carey, 1962) or includes the doughnut itself. Thus, flow is initially centripetal in the source layer, upward in the diapir trunk, and centrifugal in the overhang region of the diapir cap. A later section of this report (p. 26) examines the implications of this simplified flow pattern for the formation of folds in diapirs.

Experimental modeling by Talbot (1974, 1977) has shown that diapirs tend to grow asymmetrically and to overhang preferentially a quadrant with a

source layer or overburden that has nonuniform thickness, density, dip, or strain rate. Thus, if the source layer is inclined or wedge shaped, model diapirs preferentially overhang the downdip or thinner side.

FABRICS

As with many deformed crystalline rocks, two main structural elements in glaciers, namakiers, and diapirs can be distinguished: layering and mineral fabric. Layering is defined by differences in mineral composition, color, or grain size; most layering represents the deformed remains of primary structures. Mineral fabric is defined by crystallographic or morphologic preferred orientation of mineral grains. Fabrics of most rocks deformed by penetrative strain contain a planar preferred orientation (schistosity), a linear preferred orientation (lineation), or both. In the L-S system of Flinn (1965), rocks containing no linear preferred orientation within the schistosity plane are termed S tectonites, whereas those containing a lineation but no planar preferred orientation are termed L tectonites. Intermediate categories also exist, so that there are five basic categories, the middle one having lineation and schistosity of equal strengths: L, L > S, L = S, S > L, and S. The equivalent strain ellipsoids are prolate (cigar shaped and forming by constriction) and oblate (pancake shaped and forming by flattening) spheroids for L and S fabrics, respectively, and orthorhombic triaxial ellipsoids for the composite L-S fabrics. Shape fabrics are defined by the preferred orientation of elongated aggregates of minerals rather than by individual mineral grains that define mineral fabrics.

Individual layers in glaciers are commonly 1 to 10 cm thick and are rarely continuous for more than a few meters (Paterson, 1981). Stratification is primary sedimentary layering in the form of dirt layers concentrated by summer melting or alternating thick layers of coarse, bubbly ice formed from winter snow and thin layers of coarse, clear "blue" ice formed from refrozen meltwater. Foliation is a secondary layering formed during glacial flow. It has been convincingly argued with the aid of numerical modeling that layering forms by strain modification of primary glacial features (Hooke and Hudleston, 1978; Hudleston and Hooke, 1980). For instance, irregularities such as ice glands (refrozen vertical pipes of meltwater) and ice lenses (refrozen horizontal lenses of meltwater) and crevasse fillings that were initially normal to sedimentary stratification rotate toward the plane of maximum flattening to within 1° of parallelism to the stratification in distal parts of the glacier.

Layering in namakiers is defined by differences in the shape and size of grains and in the type and concentration of entrained impurities in the rock salt. Layering probably represents highly deformed bedding (Talbot, 1979, 1981). Color intensity of the layering increases down the length of the glacier, apparently because entrained insoluble minerals are comminuted and dispersed and transparent coarse-grained halite is converted to translucent fine-grained halite (Talbot and Jarvis, 1984). Progressive solution of halite is considered to be merely superficial. Layering in salt diapirs is generally defined by different proportions of disseminated anhydrite and probably also represents deformed bedding in the original evaporite sequence.

Ice in glaciers and halite in salt structures show evidence of frequent recrystallization in which new, unstrained grains replace older, strained grains or subgrains. This is especially true of glacial ice, which deforms at temperatures close to its melting point. In this respect, both ice and halite have short strain memories; only the last few increments of strain are recorded before the rock recrystallizes either statically between strain increments or dynamically during strain. Because their strain memories are short, ice and halite can be repeatedly deformed (as evidenced by the distortion or rotation of primary structures like layering or fissures) and yet be composed of strain-free grains.

In the Barnes Ice Cap on Baffin Island, Canada, the ice initially consists of equant polygonal grains having either no preferred orientation or a weak vertical concentration of *c* axes (Hudleston, 1980). Down the length of the glacier, this almost isotropic fabric becomes progressively deformed near the glacial margins. The first sign of strain is the formation of shear zones having an aspect ratio of 20:1 parallel to bedrock. Each ductile shear zone is outlined by sigmoidal patterns of elongated air bubbles and is differentiated by (1) decrease in plunge of elongated air bubbles, (2) increase in degree of *c*-axis preferred orientation, (3) formation of weakly sutured grain boundaries, and (4) increase in grain size (Hudleston, 1980). Despite the high shear strains shown by bubble inclination and elongation, the ice grains are equant, indicating recrystallization and grain growth during or after

shearing. Growth and coalescence of shear zones further deform the glacier. Eventually the glacier margin represents a single, large, highly strained shear zone, and only scattered pods of weakly deformed ice remain.

As with glaciers, deformation increases down the length of namakiers (Talbot, 1979, 1981). Grain size progressively decreases and the proportion of insoluble residue increases distally. The exposed diapir of Kuh-e-Namak consists of coarse, clear crystals of halite. Salt at the namakier snout contains only about 0.1 percent of these crystals in the form of porphyroclasts set in a fine-grained, cloudy matrix of halite and entrained insoluble minerals.

Linear (L > S) fabrics appear to dominate in salt stocks. In Grand Saline Dome, Balk (1949) observed so many true lineations (as opposed to apparent lineations representing the trace of planar structures on mine walls) that he concluded that the entire stock was lineated. The longest axes of halite crystals plunge steeply to vertically. Most axial ratios of vertical elliptical sections through these crystals were close to 1.5. Balk's "pencil anhydrite," in cigar-shaped aggregates 5 to 8 cm long having elliptical cross sections, indicates an L > S fabric as well. Linear fabric in Winnfield Dome takes the form of cigar-shaped aggregates of anhydrite and crenulation lineation (Hoy and others, 1962). In Jefferson Island Dome, halite defines an L fabric having mean axial ratios of 1.6 and mean horizontal axial ratios of 1.0. This lineation is axial to subvertically plunging folds (Balk, 1953). Linear fabrics were also reported from parts of Avery Island Dome and Weeks Island Dome (Rogers, 1918; Balk, 1953). In addition, steeply oriented and elongated halite having elliptical cross sections define L > S fabrics throughout 767 m of vertical salt core from Vacherie Dome (Nance and others, 1979) and 762 m of vertical salt core from Rayburn's Dome (Nance and Wilcox, 1979); axial ratios in the vertical plane average 3 and 2, respectively. In both Vacherie and Rayburn's Domes, these linear fabrics alternate with isotropic fabrics composed of equant halite crystals.

Geologists tend to overestimate the strength of lineations when making qualitative judgments of rock fabrics (Schwerdtner and others, 1977). Nevertheless, L > S fabrics appear to genuinely dominate in regions where salt stocks have been sampled.

Petrofabric analysis of halite in Winnfield, Grand Saline, and Avery Island Domes has yielded information on fabric orientation (Clabaugh, 1962a, b; Schwerdtner, 1966; Muehlberger and Clabaugh, 1968; Carter and Hansen, 1980). Because halite is isotropic, poles of all three of its crystallographic planes parallel to cubic cleavage must be plotted on the same stereogram. The resulting confused appearance of multiple maxima, submaxima, and girdles provides fertile ground for subjective interpretation. Matching these fabrics with larger structures like folds is difficult. Comparing the fabric patterns with those derived by mathematical models elucidates the mechanism of deformation: Translation gliding appears to dominate (Schwerdtner, 1967). Because isometric minerals like halite do not have unique crystallographic axes, all mineral fabrics and preferred orientations in salt described in this paper are based on grain shape.

FLOW MECHANISMS

Slow, solid-state flow of ice and salt is made possible by continual readjustments between and within the grains of the rocks. Several mechanisms have been proposed for the creep of glaciers, namakiers, and salt diapirs; some of these mechanisms have been proposed for all three types of gravity-driven structures and are common to many other metamorphic rocks.

Ice flows principally by dislocation slip, dominated by basal glide, within individual crystals (Paterson, 1981). During flow, ice recrystallizes dynamically and crystals enlarge by annealing between episodes of flow; this removes the strain and allows further deformation during the next strain increment. Some grain-boundary sliding and grain cataclasis have also been inferred (Hudleston, 1980); voids would open without these adjustments because ice deformation is predominantly on only one slip system.

Several deformation mechanisms were inferred to operate in the namakier studied by Talbot (1981). Down the length of the namakier, dynamic recrystallization of halite allows high strains to build up in the rock as a whole, whereas individual crystals are only moderately strained. Annealing recrystallization takes place in zones of stress drop, such as in layers being passively carried. In high-strain zones along the base of the structure or in slides, intracrystalline deformation takes place in two ways: slip parallel to cleavage and dilation of microfractures parallel to cleavage. Down the length of the

namakier, cataclastic milling of impurities increases to the snout, where the salt deforms so easily that it seems to have reached a state of superplasticity similar to that recorded in fine-grained, highly deformed metals; under such conditions, grain-boundary sliding may take place. The presence of veins of reprecipitated halite in salt near zones where slides form suggests that halite is removed in solution from high-stress zones by pressure solution and accumulates in dilation zones; diffusion of halite also facilitates flow.

Diapiric salt almost certainly undergoes some form of recrystallization, so that strains are continually neutralized. Contortions of the layering indicate that the rock mass has been extremely distorted, yet grain size has remained coarse. Despite their elongated shapes and preferred orientation, the halite crystals generally show little sign of internal strain. How the rock recrystallizes is unclear. As in the case of namakiers, diapiric flow may occur by means of pressure solution and diffusional mass transfer of the halite.

DEFORMATION TEMPERATURES

The homologous temperature (T_h) is useful for comparing the temperatures of deformation of different minerals. Homologous temperature is the ratio of a mineral temperature to the melting temperature of the mineral in Kelvins.

For glacial ice, deformation temperatures of -30°C to 0°C correspond to T_h = 0.89 to 1.00. Such high homologous temperatures are comparable to those of migmatites 20 km deep in the crust, which are partially melting at amphibolite-facies temperatures of more than 700°C. This abundance of heat (relative to melting point) in glacial ice may allow coarse textures to be built up by recrystallization.

Rock salt in namakiers and diapirs deforms at much lower homologous temperatures than does ice. The temperature range of 0°C to 40°C in namakiers corresponds to T_h = 0.25 to 0.29. The temperature range of 0°C to 550°C in salt diapirs corresponds to T_h = 0.25 to 0.77. The high end of this range is estimated for the base of the Louann Salt, more than 10 km below the continental slope of the northern Gulf of Mexico.

STRAIN RATES AND STRESSES IN HALOKINESIS AND THEIR RELATION TO EXPERIMENTAL DEFORMATION OF ROCK SALT

All gravity-driven structures deform against the resistance of internal or surface stresses induced by their viscosity or frictional sliding (where sliding occurs). They are also subject to external forces. During their flow, both glaciers and namakiers are under low confining pressures; their upper surfaces are free and their lower and lateral surfaces are pressured only by the weight of ice or salt. Glaciers deform by gravity spreading and gravity gliding of the plastic ice. Namakiers apparently deform only by gravity spreading, the basal layers of salt being essentially inert, or "dead." In contrast, diapirs are under moderate to high confining pressures, and the stresses that cause them to rise are set up by buoyancy, differential loading, thermal convection, or regional tangential stresses. The shear stresses that drive namakiers (and glaciers) can be calculated from their thickness, density, and surface gradients; these stresses are low (table 1, notes b and d). Differential stresses that drive diapirs or bedded salt have been estimated from experimental data on the rheology of rock salt (table 1, note e). This stress is high, as might be expected surrounding newly formed underground openings.

Strain rates estimated for natural deformation of rock salt vary over eight orders of magnitude, from 10^{-8}/s to 10^{-16}/s (table 1; strain rate defined in note a). By comparison, the estimated rate of flow in the asthenosphere—a standard datum for steady-state geologic strain—is about 10^{-14}/s (Carter, 1976). Average strain rates for orogeny have also been calculated as 10^{-14}/s (Pfiffner and Ramsay, 1982). The wide range in halite strain rates reflects the diverse conditions of observed flow. The most rapid rates are those of borehole closure, where rock salt under high lithostatic pressure expands by primary creep toward a free surface to fill a borehole. After a few weeks of accelerating flow, the rate of flow declines roughly exponentially. The measured rate of closure in mined cavities is probably slower because the observation period for cavity closure was 40 to 120 times longer than that for the borehole and included a lengthy period of decelerating flow

Table 1. Natural-strain rates in the deformation of rock salt.

Environment		Strain rate[a]
		per second
Glacial salt		
Direct measurement of flow[b]		1.1×10^{-11} to 1.9×10^{-9}
Comparison of theoretical profile with actual profile[c]		6.7×10^{-13} to 9.0×10^{-13}
Estimate from namakier morphology[d]		2×10^{-13} to 2×10^{-8}
Diapiric salt		
Direct measurement of closure of mined cavity[e]		1×10^{-9} to 9×10^{-12}
Direct measurement of peak borehole closure[f]		3×10^{-8}
Direct measurement of long-term borehole closure[g]		7.4×10^{-11} to 3.5×10^{-9}
Measurement of topographic mound[h]		2×10^{-14}
Comparison of theoretical profile with actual profile[c]		8.4×10^{-13}
Estimates from stratigraphic thickness changes around diapirs		
Overall rates:	range[i]	1.1×10^{-15} to 1.1×10^{-16}
	mean[i]	6.7×10^{-16}
Fastest rates:	range[i]	3.7×10^{-15} to 6.2×10^{-16}
	mean[i]	2.3×10^{-15}
Average growth for Zechstein domes[j]		2×10^{-15}

[a]Conventional strain rate, $\dot{e} = e/t$, where elongation e = change in length/original length and t = duration of strain in seconds.

[b]Talbot and Rogers (1980). Survey of markers distorted by glacial flow of Hormuz Salt, Kuh-e-Namak namakier, Dashti Province, Iran. Duration of strains = 292 days (2.5×10^7 s). Maximum flow after 5 mm rainfall. Calculated shear stress = $\tau \leqslant 0.25$ MPa.

[c]Talbot and Jarvis (1984). Observed longitudinal profile of Kuh-e-Namak exposed stock and namakier fitted to profile of numerical model of viscous fluid extruding from a narrow orifice. Stock height = 6.4 km, namakier length = 6 to 8 km.

[d]Wenkert (1979). Average shear-strain rates for five Iranian glaciers of Hormuz Salt, assuming steady-state equilibrium between extrusion and wasting, and based on erosion rates of 0.08 to 0.25 cm/a. Calculated shear stress = $\tau \approx 0.03$ MPa.

[e]Serata and Gloyna (1959), Reynolds and Gloyna (1960), and Bradshaw and McClain (1971). Peak rates in Grand Saline Dome (East Texas Basin) and bedded rock salt (Hutchinson and Carey Mines, Kansas). Upper limit corresponds to wall temperatures of ~ 100° C. Estimated stress difference = $\Delta\sigma \approx$ 10 MPa. Duration of strains = 10 to 30 a (3.2×10^8 s to 9.5×10^8 s).

[f]Martinez and others (1978). Vacherie Dome (Louisiana interior basin). Duration of strain = 3 mo (7.8×10^6 s).

[g]Thoms and others (1982). Vacherie Dome (Louisiana interior basin). Slowest at 100° C 351 m deep under $\Delta\sigma = 4.2$ MPa; fastest at 160° C 1,509 m deep under $\Delta\sigma = 18.1$ MPa. Duration of strain = 890 days (7.7×10^7 s).

[h]Ewing and Ewing (1962). Sigsbee Knolls (Gulf of Mexico abyssal plain). Calculation based on salt-stock height of 1,300 m (seismic section in Martin, 1980). Duration of strain = 11,000 a (3.5×10^{11} s).

[i]Seni and Jackson (1983b, 1984). Based on salt diapirs in the East Texas Basin. Overall rates are those during entire known diapiric history of 16 diapirs; duration = 30 to 56 Ma (9.5×10^{14} s to 1.8×10^{15} s). Net rates calculated by maximum rate of deposition in salt-withdrawal basins. Fastest rates are those of five diapirs during stratigraphic intervals characterized by the most rapid diapirism; duration = 1 to 13 Ma (3.2×10^{13} s to 4.1×10^{14} s). Gross rates calculated by dividing the volume of sediments in a salt-withdrawal basin by the product of the maximum cross-sectional area of the diapir and the duration of the stratigraphic interval whose sediments constitute the salt-withdrawal basin.

[j]Sannemann (in Trusheim, 1960). Based on stratigraphic-thickness data and salt-stock height of 4 km. Duration of strain = 35 to 130 Ma (1.1×10^{15} s to 4.1×10^{15} s).

(table 1, note e). Salt glaciers are driven downhill by geologically minute shear stresses resulting from gravity (table 1, notes b to d). The glacial salt overcomes internal friction and bedrock drag and undergoes geologically rapid seasonal flow. Although Wenkert's (1979) estimates of flow rates are similar to the direct measurements by Talbot and Rogers (1980), they may be slightly too high because Wenkert assumed a steady-state equilibrium between extrusion and wasting (by solution); most salt glaciers are actually in overall retreat despite seasonal advances after rainfall (Kent, 1979).

The rate of salt uplift during diapirism cannot be estimated with the precision of the direct measurements referred to on p. 9. All methods for studying diapirs entail certain assumptions (Seni and Jackson, 1983b, 1984) and rely on paleontologic-radiometric dating of variable accuracy. Ewing and Ewing (1962) directly measured the thickness of sedimentary strata draped

over an abyssal salt diapir at the Sigsbee Knolls. They assumed that the strata had been folded after deposition. However, because the strata are composed almost entirely of pelagic ooze, they could have draped over the seafloor mound without giving evidence of angular unconformity on seismic reflection profiles. The calculated strain rate for the Sigsbee Knolls may thus be too high because the draped strata may be younger than the rise of the mound.

Different methods must be applied to older salt diapirs in the interior salt basins such as the East Texas Basin. Estimates based on the upward flexure of overburden are likely to be too low because they ignore the effects of dissolution or extrusion of salt and record only the late, declining phase of growth. Carter and Heard (1970) crudely estimated a strain rate at 10^{-15}/s by calculating areal strain from the difference in plan-view area between the peripheral sink and the salt stock. These authors assumed a conservatively long period of diapiric growth (120 Ma); stratigraphic thickness measurements of East Texas domes, however, suggest that more than 90 percent of the growth of each diapir took place over only 30 Ma (Seni and Jackson, 1983b, 1984).

The distinction between rates of gross and net growth is important. Gross rates are a function of the volume of salt evacuated from a withdrawal basin and moved up the diapir. Net rates are a function not only of this process but of all other processes that affect diapir height, such as salt dissolution, extrusion, and lateral intrusion. Strain rates calculated for the diapirs of East Texas are shown in table 1, note i (from Seni and Jackson, 1983b, 1984). These calculations are based on borehole information, which is commonly lacking for the deeper intervals that record early stages of diapir growth. Hainesville Dome is an exception. Because diapirism started anomalously late, subsurface data reflect almost all the growth history of Hainesville Dome. Its peak growth rate is about seven times that of its average rate. For the Zechstein salt basin in northern Germany, Sannemann (1968) (and in Trusheim, 1960) estimated average flow rates of 0.3 mm/a in both horizontal and vertical directions by measuring stratigraphic thickness. The strain rate of 10^{-15}/s calculated by Sannemann was based on an average for all diapirs.

In summary, we can be reasonably confident that under natural geologic conditions, rock salt flows at strain rates as rapid as 10^{-11}/s to 10^{-9}/s in namakiers, about 10^{-13}/s in diapirs in active fold-and-thrust belts, and 10^{-14}/s to 10^{-15}/s in diapirs deforming only in the field of gravity.

How do these estimates of strain rate for the different manifestations of salt flow relate to experimentally determined flow properties of rock salt? Using the inverse relation between the spacing of subgrain boundaries in halite and the differential stress that caused them, Carter and Hansen (1983) inferred that steady-state differential stresses were between 0.5 and 1.5 MPa (1 MPa = 10 bars) in a wide variety of bedded and dome rock-salt data. The following flow law for steady-state deformation of rock salt in the temperature range of 100°C to 200°C was derived by Hansen and Carter (1982) (modified according to Hansen, personal communication, 1983):

$$\dot{\varepsilon}_{ss} = 7.6(10^{-4}) \pm 6.9(10^{-4}) \exp\left[\frac{-15.9 \pm 1.0}{RT(10^{-3})}\right] \sigma^{4.5 \pm 0.3}$$

where $\dot{\varepsilon}_{ss}$ = steady-state creep rate (/s)
R = universal gas constant
$= 1.987 \times 10^{-3}$ (kcal/mol·K)
T = absolute temperature (K)
σ = differential axial stress (MPa)

Carter and Hansen (1983) regarded this equation as the best representation of steady-state creep for natural rock salt. The relation between this flow law and the inferred limits of differential stress of 0.5 to 1.5 MPa is shown in figure 2, which was the basis for comparison with estimates of natural-strain rate in table 1. The flow law accords well with the slower rates of halokinesis characteristic of diapirism in the absence of crustal shortening. At the lower limit of stress (0.5 MPa), the mean overall rate and fastest rate of diapiric growth (table 1, note i) would require temperatures of 45°C and 75°C, respectively. In a geothermal gradient of 30°C/km, these temperatures would exist under burial of 600 and 1,620 m, respectively. The first stage of salt flow (gradually accelerating growth of pillows) began in the East Texas Basin beneath an overburden of about 500 m (Jackson and Seni, 1983). At the mean stress levels inferred from subgrain studies (1.0 MPa), flow could occur at ambient temperatures characteristic of zero burial. These experimental data on the deformation of dry rock salt therefore indicate that steady-state flow can begin to accelerate below an overburden as thin as 600 m or even 0 m, depending on the differential stresses present. This accords with the seismic evidence for

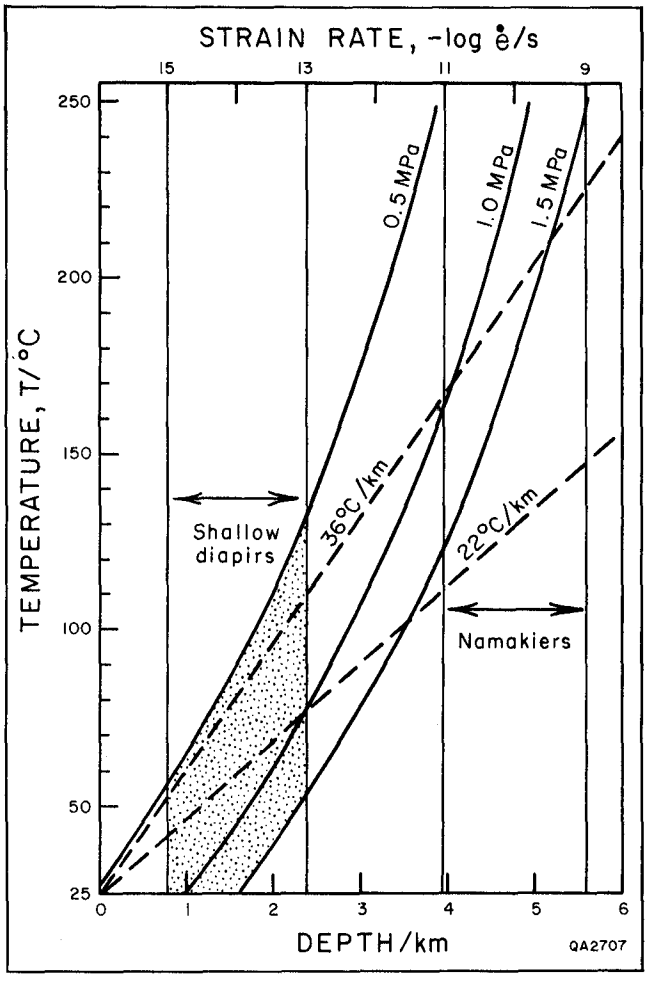

FIGURE 2. Experimentally deduced flow properties of dry rock salt (solid lines) under varying conditions of temperature, strain rate, and differential stress. Dashed lines show present-day extremes of geothermal gradient in the Gulf of Mexico. (Adapted from Carter and Hansen, 1983.)

overburden thickness at the onset of salt flow in the East Texas Basin.

In contrast, the experimental data are difficult to match with the measured or calculated rates of rapid flow associated with an exposed diapir and namakiers in Iran (table 1, notes b, c, d). Three rates have been derived by Talbot and coworkers at Kuh-e-Namak: rate of diapiric rise (numerically modeled), steady-state rate of namakier flow (numerically modeled), and short-term namakier flow after rain (measured directly). These rates are more than 10^3, 10^4, and 10^6 times faster, respectively, than the flow law "allows," even if the estimated shear stress driving the namakier is doubled. Periods of accelerated flow of the Kuh-e-Namak namakier have been found to correspond to periods when the salt had been dampened by rainfall (Talbot and Rogers, 1980), and both Talbot (1979, 1981) and Wenkert (1979) have emphasized the importance of small amounts of interstitial water in promoting namakier flow. However, experimental deformation has concentrated on dry rock salt containing little water (0.001 to 0.1 percent). So although this flow law appears applicable to dry salt, it is inadequate to explain the greatly accelerated rates possible in slightly damp salt, in which other deformation mechanisms, such as pressure solution and diffusion mass transfer, may operate. At present, neither the mechanism of rapid strain in damp rock salt nor the minimum water content required is known. Nevertheless, experimental deformation of another evaporitic chloride, bischofite ($MgCl_2 \cdot 6H_2O$), by Urai (1983) has shown that addition of about 0.1 weight-percent water to dry, artificially prepared specimens decreases the flow stress by a factor of 5. A thin fluid film on bischofite grain boundaries enhances dynamic recrystallization by movement of high-angle grain boundaries and possibly by increasing intracrystalline plasticity.

DUCTILE SHEAR ZONES

Having surveyed the large-scale and small-scale structures within glaciers, namakiers, and diapirs and the timespan over which they formed, let us examine the intermediate-scale structures. Ductile shear zones are present in all three types of gravity-driven structures. These are high-strain zones having large length-to-width ratios. They mark zones of differential movement between sheets or tongues of ice or salt moving at different rates.

High simple-shear strains in ductile shear zones generate schistosity parallel to the XY principal plane of maximum flattening and rotate older structures such as layering toward this plane (Ramsay and Graham, 1970; Ramsay, 1980). The ductile shear zones are therefore recognized as roughly vertical tabular zones of highly drawn out subparallel structures that pass outward into progressively less rotated structures on the edges of the shear zone. Layers trending obliquely across the shear zone may be thickened or thinned, depending on their relation to the shear directions (fig. 3). Displacement between salt lobes can potentially be quantified (Ramsay and Graham, 1970; Coward,

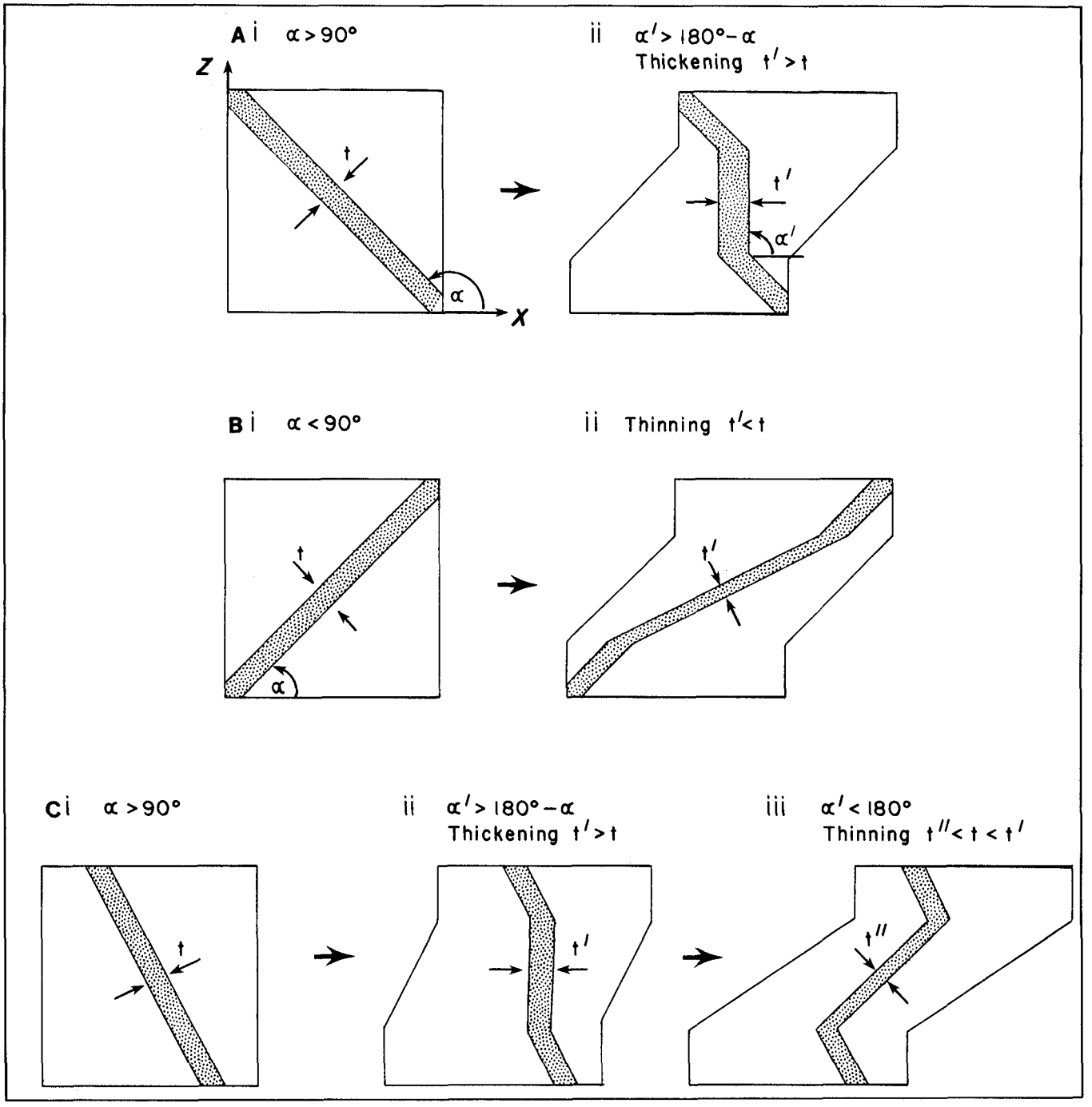

FIGURE 3. Homogeneous change in thickness from t to t′ of a stippled layer in a matrix of similar viscosity by uniform simple shear parallel to x. (A) Thickening. (B) Thinning. (C) Thickening followed by thinning. (Adapted from Ramsay, 1980.)

1976; Cobbold, 1977; Ramsay and Allison, 1979; Ramsay, 1980).

Shear zones in glaciers have already been discussed in connection with fabrics (p. 6). Glacial shear zones mark the first stages of ice deformation before they amalgamate into a zone of continuous shear, where the bulk of the glacier margin becomes a single large shear zone (Hudleston, 1977, 1980).

Shear zones in a namakier were described by Talbot (1981). These shear zones are slides: ductile faults formed by extreme attenuation of fold limbs during folding and having normal or reverse senses of displacement. The slides form as ramps within the namakier, where salt slows and thickens to surmount the bedrock obstructions to its general downslope flow (fig. 4). These slide-propagation

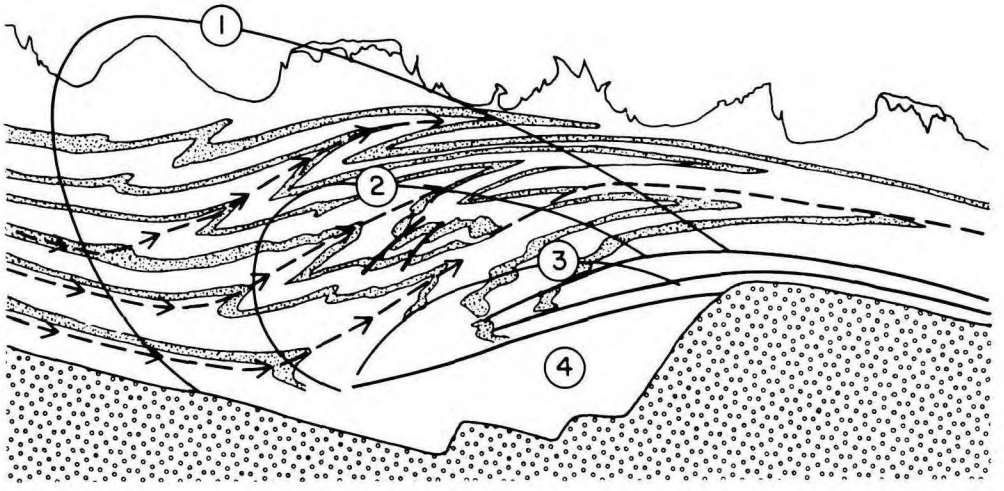

A

EXPLANATION

	Layering	1	Flow-fold boundary
	Lag	2	Crenulation boundary
	Thrust	3	Salt-vein boundary
	Flow line	4	Static salt

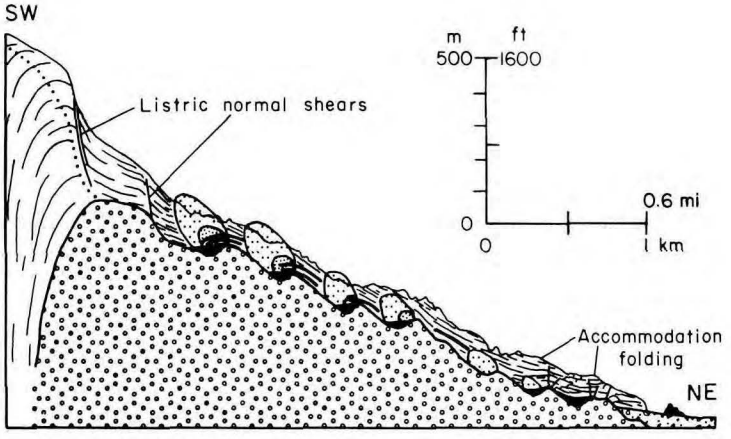

B

EXPLANATION

	Country rock		Color banding
	Static salt		Slides
	Flow folding	.....	Upstream boundary of granulation
	Crenulation		

QA2424

FIGURE 4. Schematic longitudinal profiles of flow folds in the northern namakier of Kuh-e-Namak, Dashti Province, southern Iran. (A) Idealized reconstruction of a deformation zone based on partial exposures of several such zones. Flow is left to right over a scarp slope in bedrock. (B) The entire namakier showing several deformation zones and the change in their geometry as salt becomes increasingly mylonitized toward the terminus. (Adapted from Talbot, 1979, 1981.)

zones are stationary, and the salt folds and tears as it flows through and beyond them. The upstream part of these thickened zones contains large folds and small crenulations. Slide ramps form closer to the obstruction and assist the salt in surmounting it. Downstream, over the obstruction, the slide ramps curve into flat zones parallel to the upper and lower surfaces of the namakier (fig. 4). In the shear zones, halite deforms principally by segmenting along cleavage planes, forming several small, new, equant grains from one large, elliptical grain having an axial ratio of 3 or 4 to 1; cleavage slip, a type of low-temperature crystal plasticity, also occurs in the slide zones. Downstream of the obstruction, where the stress presumably drops, some slides heal by annealing of their fabrics.

Shear zones in salt diapirs probably mark zones of differential movement between adjacent spines or tongues of rock salt (Muehlberger, 1959; Kupfer, 1974, 1976). Vertical lobes of differential movement have also been documented in the Five Island domes of coastal Louisiana (Atwater and Forman, 1959; Kupfer, 1968, 1974). Balk (1949) and Muehlberger (1959) suggested that displacements on regional faults triggered a local flow of salt, so that Grand Saline diapir rose by successive differential intrusions of spines and lobes, as has been proposed for granite diapirism (Cloos, 1936; Balk, 1937). Alternatively, the growth of lobes may be an inherent part of the intrusion mechanism (Howard, 1971) rather than fault controlled.

Kupfer (1968) equated planar zones of halite megacrysts with former fractures or faults closed by salt recrystallization. This conclusion is supported by the presence of coarse-grained ice in the cores of partly annealed shear zones along the margins of the Barnes Ice Cap, Baffin Island, Canada (Hudleston, 1980). Because its homologous temperature of deformation is high, this type of recrystallization is probably much more common in ice than in salt.

Septa of cataclastically deformed country rock trapped between rising lobes also delineate the shear zones (Kupfer, 1976). The large differences in effective viscosity between sandstone in these septa and the enclosing matrix of highly ductile rock salt provide rheologic contrasts equivalent to those at much higher temperatures than are found in salt diapirs. Under high temperatures, quartz is extremely ductile and feldspar only moderately ductile, thus forming mylonite under high strain. Large extension of sandstone layers therefore forms low-temperature mylonite in which sandstone is preserved as porphyroclasts in a recrystallized rock-salt matrix (fig. 5).

FOLDED GLACIAL MORAINES

Folds in glaciers, namakiers, and salt diapirs all result from gravity-induced ductile flow of the rock masses in which they are found. Thus, it is not surprising that the folds in each type of moving mass look similar over a wide range of scales. Valley and piedmont glaciers represent unusually large and accessible working models of rock folding by flow, so it is appropriate to examine them before the salt structures.

This section describes the geometry, origin, and significance of folds defined by lateral and medial moraines in valley and piedmont glaciers. Ogives are arcuate bands or undulations on the surface of a glacier, convex downstream and usually recurring in a periodic pattern speculated to be annual (Post and LaChapelle, 1971). Another type of fold is represented by the recumbent flow folds in the Barnes Ice Cap of Baffin Island, Canada, described and numerically modeled by Hudleston (1976, 1977). This type of folding is examined in the section that follows on geometrically similar folds in namakiers (p. 18).

Glacial surges, popularly known as galloping glaciers, represent periodic, rapid flow of ice in a glacier. Surges alternate with much longer periods of slower flow or stagnation (Meier and Post, 1969; Post and LaChapelle, 1971). Contorted medial and lateral moraines record glacial surges. The stagnant tributaries of a valley glacier are sealed at their mouths by lateral moraines lining the main trunk glacier (fig. 6A). Renewed flow of a sealed tributary pushes out the main lateral moraine into a loop (fig. 6B). If this is a surge flow, the loop may project far into the main stream of ice. When the main glacier again dominates, either through decline of the tributary flow or by a surge in the main trunk, the original surge loop can be contorted by refolding (fig. 6C) or can be flattened isoclinally. Each surge of a branch of a compound valley glacier relative to a conjoining ice stream is marked by the formation of a surge loop; the source of each loop can be traced upstream to its root in a tributary (fig. 7).

Geometrically similar fold loops may also form in the stems of diapirs receiving salt from different stratigraphic levels, such as the Semnam diapirs in the Great Kavir of central Iran (Stöcklin, 1968). Younger salt being drawn in could push aside loops in the curtain folds of older salt from a lower level. Formation of loops would require either a

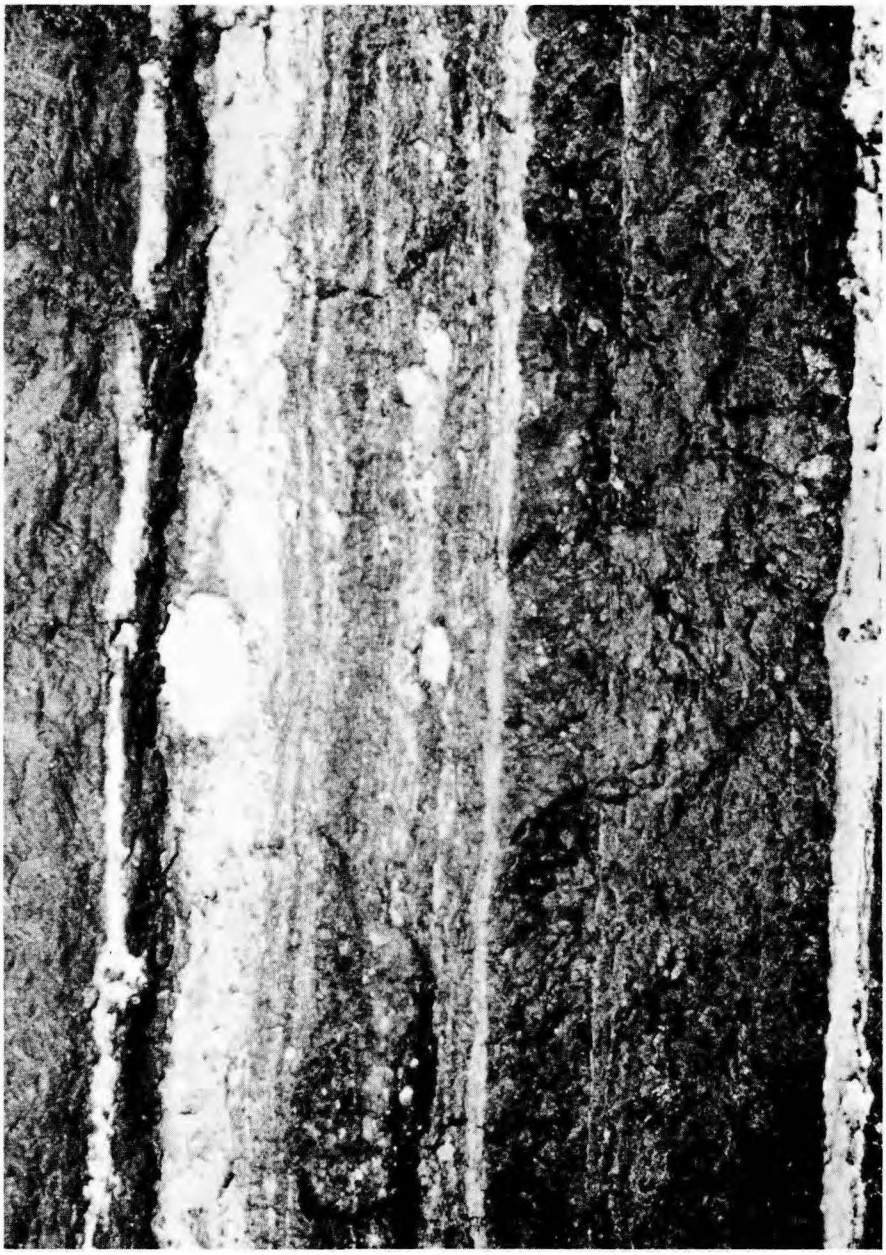

FIGURE 5. Low-temperature mylonite comprising porphyroclasts and highly strained streaks of competent, pale sandstone in an incompetent matrix of dark rock salt. Vertical rock face in underground mine, Avery Island Dome, Louisiana. Width of view is 0.5 m.

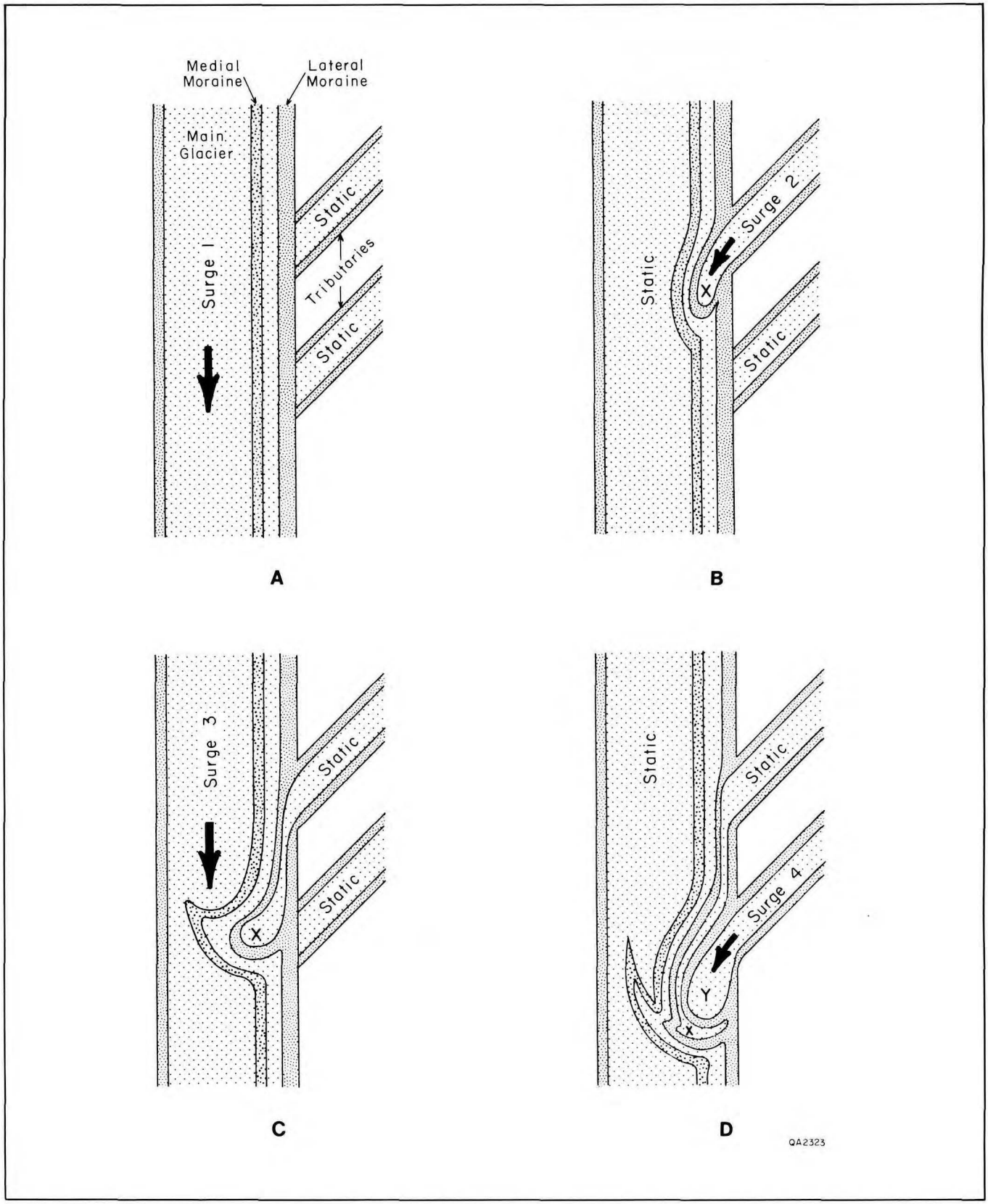

FIGURE 6. Schematic evolution (A through D) of loops in glacial medial moraines caused by differential ice flow in main trunk and two tributary ice streams. For simplicity, this diagram assumes that periods of surge alternate with periods of stagnation in all three ice streams, but the same pattern of surge loops can form where some streams surge and others flow steadily. X and Y are reference points within the two surge loops.

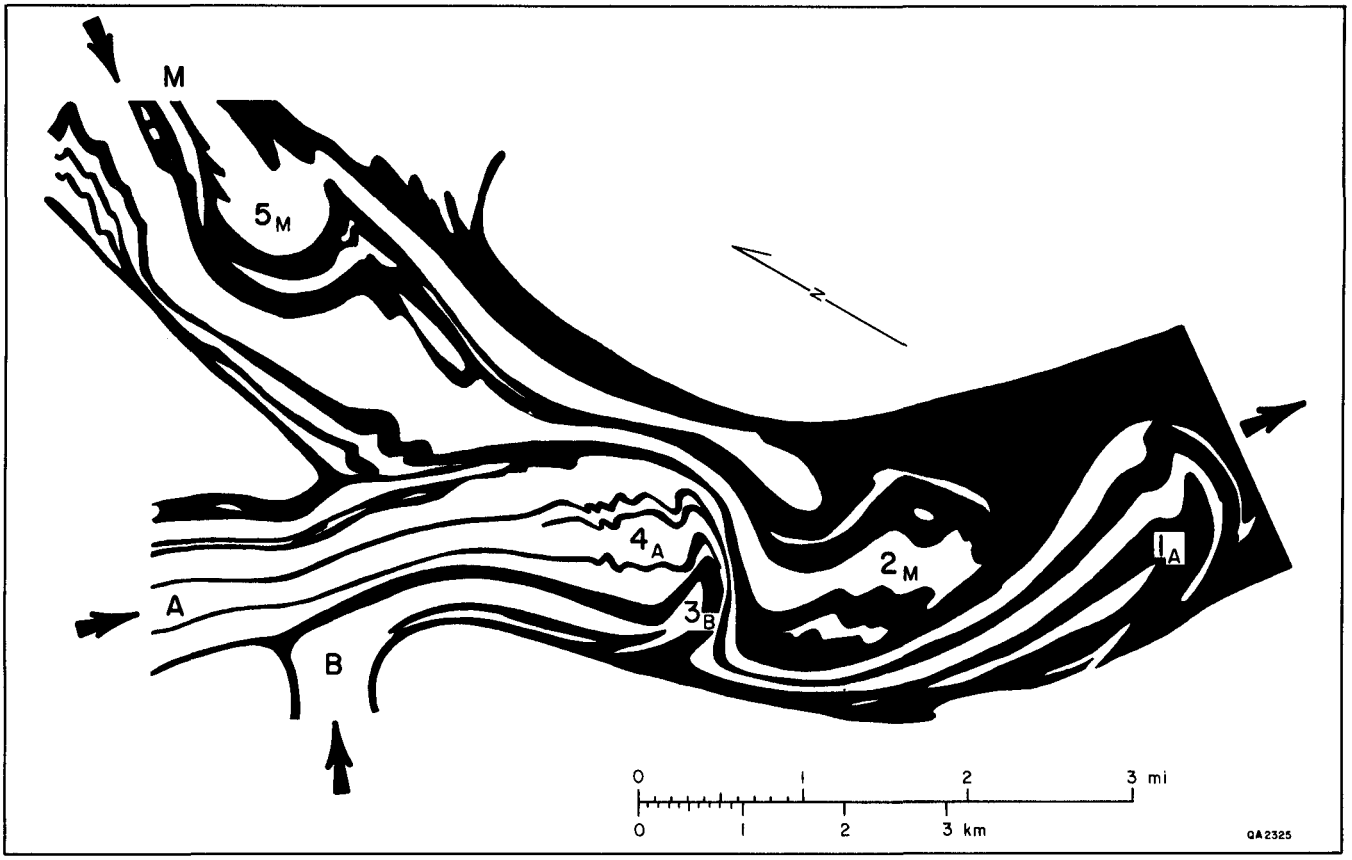

FIGURE 7. Fold patterns in medial moraines of the lower Susitna valley glacier, central Alaska (adapted from Meier and Post, 1969; Post and La Chapelle, 1971). Numbers refer to sequence of surges, and letters refer to source of surge, which is indicated by the root of each surge loop. Loop 4_A surged before 1941, whereas loop 5_M surged down to the present position of loop 2_M in 1952 just after the aerial photographs on which this map is based were taken.

temporary decrease in flow of older salt or a temporary increase in flow of younger salt; either change would trigger the formation of a loop.

Where a valley glacier debouches from mountains not in tidewater but on a coastal plain, as in the northern Gulf of Alaska, a fan-shaped piedmont glacier forms. The type example is the Malaspina Glacier, the medial moraines of which define spectacular folds (fig. 8). These arcuate, subsimilar, mostly isoclinal folds were originally mapped by Sharp (1958) and are now known in much more detail. By inverting the map and distorting it by shortening its north-south axis, Carey (1962) proposed analogy with a rooted, basement-cored nappe in cross section. But the cap of a spreading diapir in cross section is an even more irresistible analogy. If the piedmont folds are flow folds, the lines of flow are parallel to their axial traces. This flow pattern implies a southward-flowing central stream of ice from which side streams branch off at right angles and curve back northward because they encounter barriers of static ice, bedrock ridges, or terminal or lateral moraines. An alternative model, proposed by Sharp (1958), is that the moraines buckle when compressed parallel to their length. Compression and flattening of the buckles are induced by the radial flow of ice against barriers at the edge of the piedmont apron.

Neither of these models has been tested against observed movements of the Malaspina Glacier. But the Bering Glacier, a slightly smaller but geometrically similar piedmont glacier, fortuitously surged in 1957–60 and 1965–66, and its flow pattern was documented by aerial photographs (Post, 1972). The flow pattern is unequivocally radial, confirming Sharp's (1958) hypothesis (fig. 9). Two structural domains are recognized. Over most of the piedmont glacier (fig. 9, domain I), flow is across the axial traces of the arcuate folds. Gentle folds are present in medial moraines at the apex of the fan. These

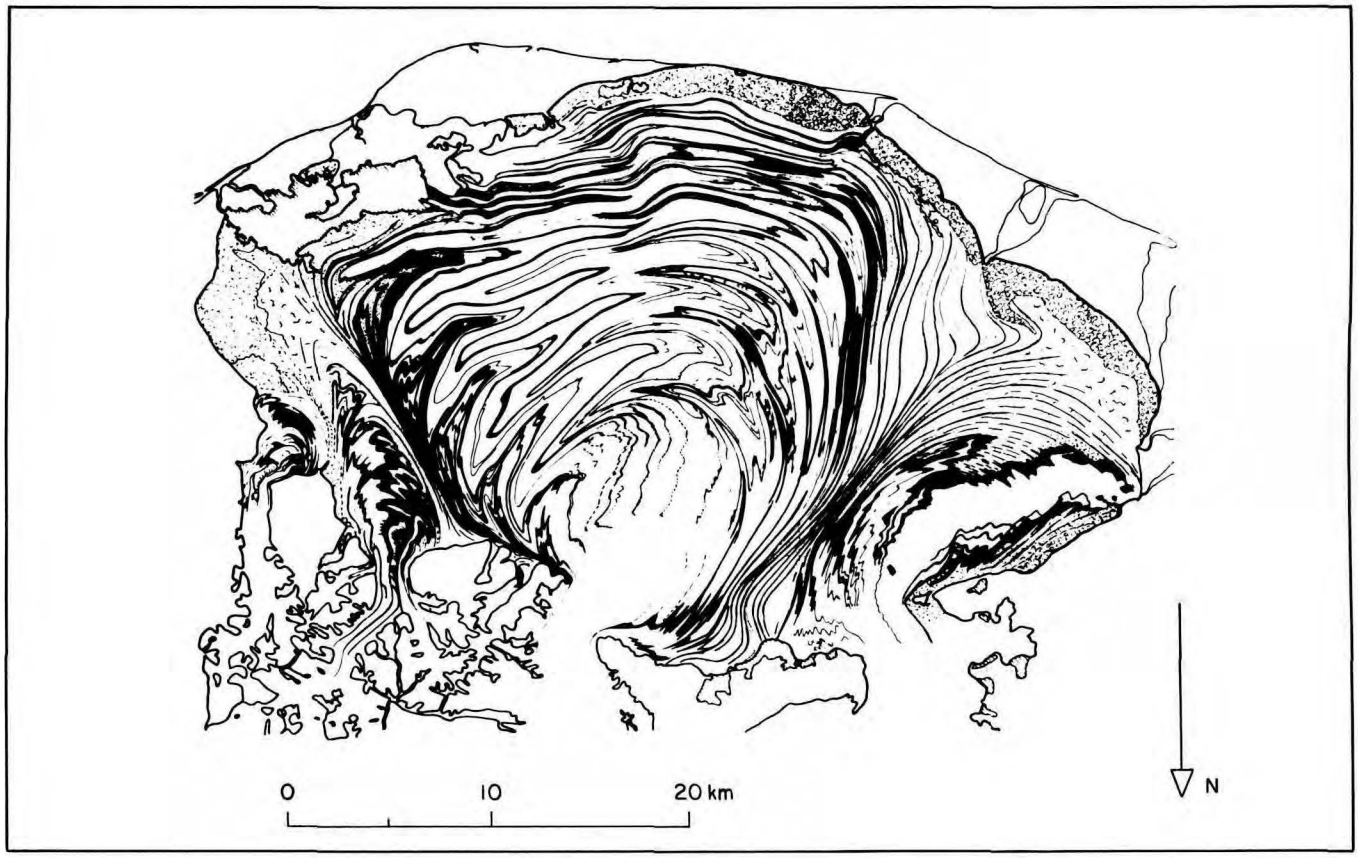

FIGURE 8. Folds defined by medial moraines in the Malaspina piedmont glacier, southeast Alaska. Terminal moraine near the coastline is forested. (From Post and LaChapelle, 1971.)

folds may be produced by tributary ice streams deflecting the main trunk, or they may represent the onset of buckling as the ice begins to encounter resistance. The folds are magnified and tightened by intense radial flattening and tangential stretching.

Along the sides of the ice apron (fig. 9, domain II), flow is predominantly subparallel to the fold axial traces. In plan view, these are zones of strong simple shear as opposed to the pure shear in domain I. Frictional drag progressively slows the ice toward the sides of the apron, shearing the ice and enclosed moraines. Gentle undulations at the apex of the medial moraines are magnified by this differential shear on the margins (fig. 9, domain II).

Centrifuge modeling by Ramberg (1964) has produced geometrically identical sharp-pointed, arcuate folds in model moraines of slightly higher viscosity than that of the model ice. The arcuate shape of the folds reflects increasing drag toward the sides of the piedmont sheet; all movement is radial and away from the apex, but the marginal parts in domain II are retarded by frictional drag.

FOLDS IN NAMAKIERS

Namakiers are broad, thin sheets of allochthonous salt connected to extrusive topographic domes of salt. Namakiers represent large, recumbent sheath folds underlain and flanked by rigid bedrock and overlain by air. Folded layering acts as markers of the flow patterns within namakiers. The steep color layering and flow foliation of the salt dome curve into the namakier, where they parallel its sides, sole, and top. At Kuh-e-Namak, Talbot (1979, 1981) suggested that simple shear dominates in a vertical plane above bedrock obstructions and at the junction between dome and namakier and in a horizontal plane between mainstream salt and salt dammed by ridges of country rock projecting laterally into the namakier.

The namakier flows into and through zones of disturbance where folds are generated; most of these zones are steplike scarp slopes in bedrock. Immature flow folds form at the upstream end of each zone and progressively mature downstream as the salt passes

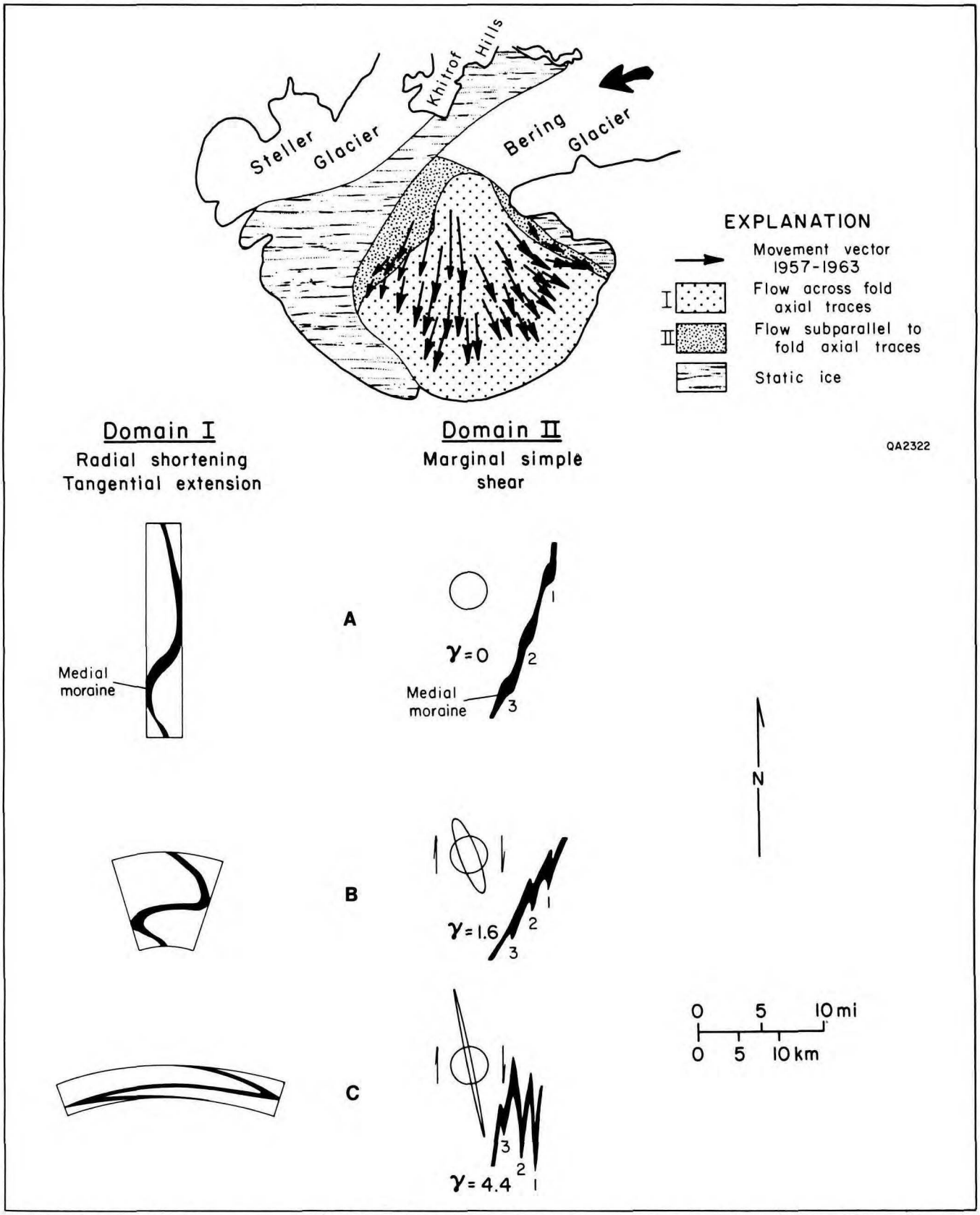

FIGURE 9. Map of the Bering piedmont glacier, southeast Alaska, showing movement vectors for surges from 1957 to 1963 (after Post, 1972). On the basis of these vectors and the orientation of mapped folds (not shown here for simplicity), two structural domains are recognized in the moving ice. The evolution of folds in medial moraines in these two domains is shown diagrammatically (stages A through C); numbers represent marker points of the moraine. (Adapted from Ramberg, 1964; Post, 1972.)

through the zone. The folds have the general shape shown in figure 4A; in cross section they are subsimilar (having a shape close to but not identical with true similar folds), but in three dimensions they are probably sheath folds elongated parallel to the length of the namakier. These flow folds are generated where flow lines diverge, thus deflecting and distorting the layering; flow lines diverge because the salt decelerates against the bedrock barrier. As salt surmounts the barrier, it accelerates and the flow lines converge; newly formed folds are tightened into recumbent isoclines. This style of recumbent folding is similar to that in glacial ice described and modeled by Hudleston (1976, 1977). Toward the base of a namakier deformation zone, the flow folds are crenulated and cut by thrusts and lags where moving salt separates from static salt at the base of the zone.

Deformation zones like these are present wherever irregular boundaries cause the flowing salt to decelerate or change direction; perhaps 20 or so exist at Kuh-e-Namak (fig. 4B). Flow carries the tightened folds and their associated slides and folded extension veins downstream into the next deformation zone. Here these structures are refolded and overprinted by a new generation of structures. In this manner, older generations become obscured beyond recognition by repeated structural overprinting, so that at any locality only the most recent episodes of deformation are recognizable. Presumably, however, many generations of folds could be recognized if they had perfect three-dimensional exposure and a robust and distinctive marker layer.

FOLDS IN SALT DIAPIRS

Fold Style

Small-scale parasitic folds in German salt mines were originally termed seismograms by Hartwig (1923); they were thought to represent "frozen" seismic tremors. This hypothesis does not have wide currency today, but no study has yet provided a plausible origin supported by quantitative data. Even the general fold geometry is disputed, largely because of imprecise terminology and lack of quantitative analysis. For example, Jefferson Island Dome (a southern dome in the Gulf Coast Basin), was described by Balk (1953) as being similar to Grand Saline Dome (a northern dome in an interior basin), apart from the presence of folds in the contact zone and a possible spine at Jefferson Island. Structural elements such as the geometry and steep orientation of isoclinal, open, and closed folds are basically alike and were therefore deduced to have similar mechanisms of formation. Conversely, Kupfer (1970) offered differences such as shear folding (in the sense of similar folding) in Grand Saline Dome and folding by "plastic flow and attenuation" in the southern domes; he thereby deduced higher temperatures of deformation in the southern domes.

I agree with Balk (1953) that such a distinction is unjustified. Part of this confusion arose from Balk's (1949, 1953) use of the term "shearfolds" to describe parasitic, lower-order folds on the limb of a larger fold. These parasitic folds were not found at Jefferson Island Dome by Balk (1953). "Shear fold" is one of the many synonyms for "similar fold," which may have led to the belief that similar folds are present in the northern domes but not in the southern domes. Even if this conclusion were correct, Kupfer's (1970) inference of higher temperatures of deformation in the southern domes on this basis would be untenable because similar folds characterize the hot, ductile core of many orogenic belts (Wynne-Edwards, 1963; Ramsay, 1967, p. 421).

Fold profiles can be geometrically classified into two ideal members: *parallel folds,* which have constant normalized orthogonal thickness throughout the fold arc, and *similar folds,* which have constant normalized thickness parallel to their axial surfaces (Ramsay, 1967, p. 359–372) (fig. 10). These folds can be further differentiated by constructing lines of equal apparent dip (dip isogons) (Elliott, 1965) connecting the inner and outer arcs of the fold (Ramsay, 1967, p. 363–366). The dip isogons of parallel folds, known as class 1B folds, converge toward the core of the fold, whereas those of similar folds, known as class 2 folds, are parallel to the axial plane (fig. 10). These are considered ideal shapes because most natural folds have intermediate shapes, chiefly in classes 1C and 3.

Fold profiles exposed in the mine roofs of Grand Saline and Avery Island Domes were analyzed using the methods of Ramsay (1967, p. 359–366) and Hudleston (1973a). These folds are so close to ideal similar folds that this type of folding is undoubtedly present in both domes (fig. 11). Published maps (Balk, 1949, 1953; Muehlberger, 1959; Hoy and others, 1962; Kupfer, 1962) indicate that similar or subsimilar folds predominate in all mapped salt domes. These profiles are compatible with other aspects of fold geometry, such as the absence of

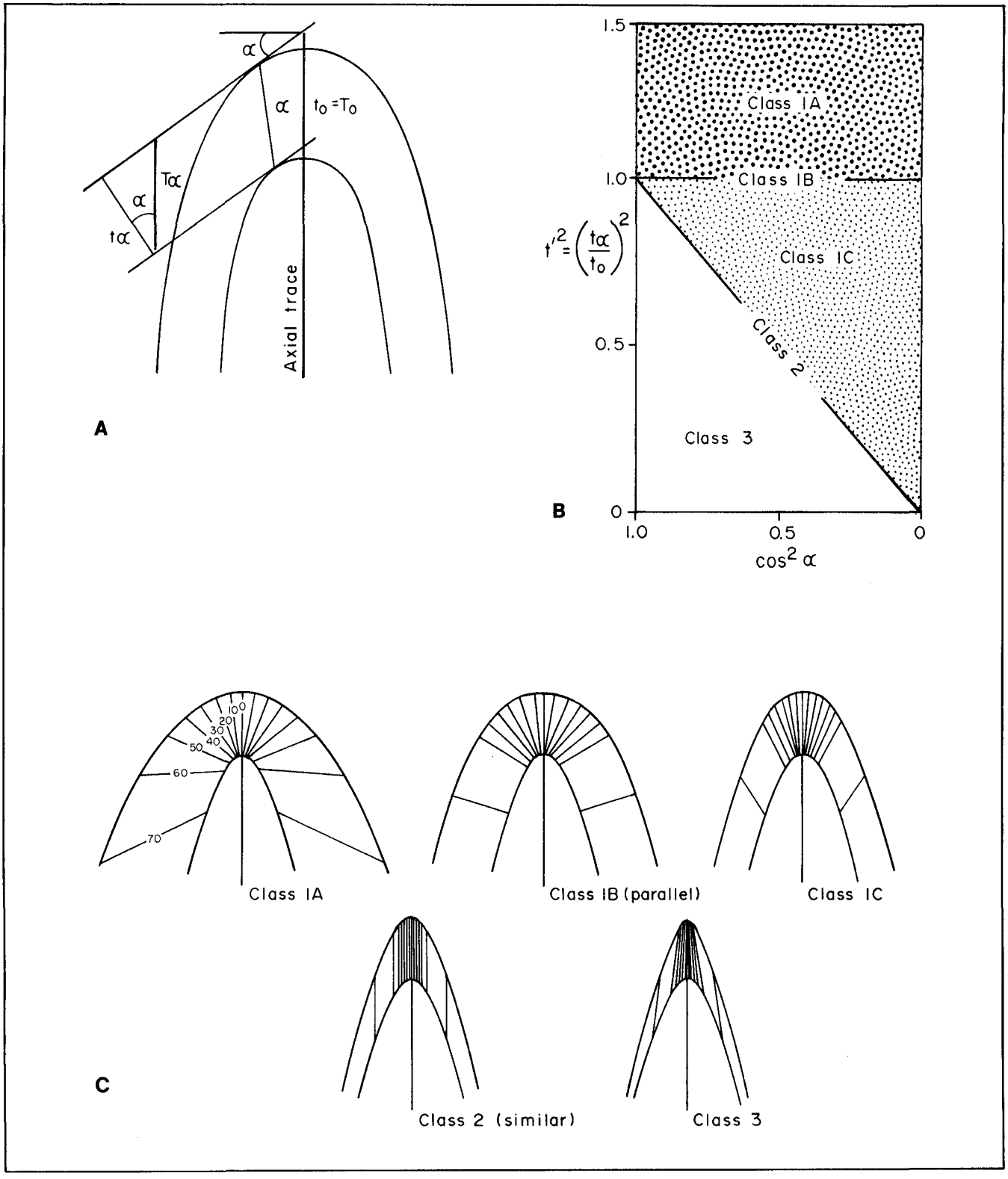

FIGURE 10. Fold-shape analysis and classification of folds. (A) Fold profile showing dip isogon (α) connecting points of equal dip, orthogonal thickness (t), and thickness parallel to the axial trace (T). Subscript refers to dip of tangents on folded surfaces measured from normal to axial trace. (B) Plot of t'^2 versus $\cos^2 \alpha$ showing classification of folds on the basis of orthogonal-thickness changes. Each quarter-wavelength fold plots as a theoretically straight line originating at the point (1,1). (C) Representative examples of each class of folds: class 1 dip isogons converge to core of fold; class 2 isogons are parallel; class 3 isogons diverge. Subclasses of class 1 are differentiated by their $t'^2/\cos^2 \alpha$ values, as in (B). (Adapted from Ramsay, 1967, his figs. 7-18, 7-24, and 7-25; Hudleston, 1973a.)

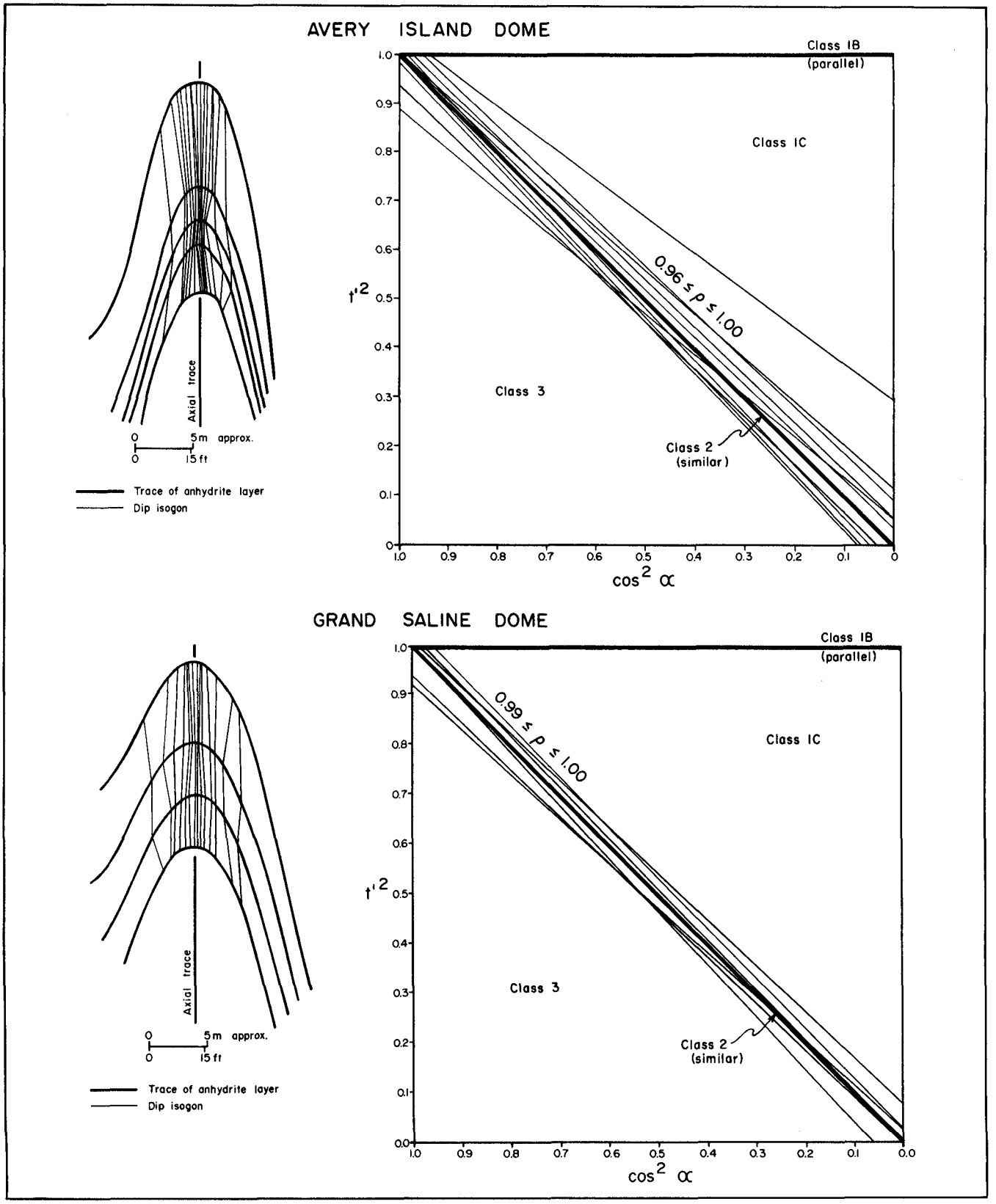

FIGURE 11. Fold-shape analysis of large folds defined by disseminated-anhydrite layers in underground salt mines in Grand Saline Dome, East Texas, and Avery Island Dome, Louisiana. Left: fold profiles showing dip isogons (Grand Saline example from Muehlberger, 1959, his pl. 5). Right: t'^2 versus $\cos^2 \alpha$ plots of 16 quarter-wavelength folds. Each plot is represented by a linear regression line. The high correlation coefficients (r) indicate close conformation to ideal folded surfaces. The positions and, more important, the slopes of these regression lines are those of similar folds.

boudinaged limbs and the prevalence of limbs having attenuated orthogonal thickness.

Deformation by similar folding also accords with the rheology of domal rock salt and interlayered disseminated anhydrite. Similar folding has been called passive because the layering is merely a marker surface having negligible mechanical control or anisotropy (Donath and Parker, 1964). Similar folding takes place in rocks that are highly ductile (such as those composed of evaporite minerals) but which have insignificant contrasts in layers of similar effective viscosity (Biot, 1965; Hudleston, 1973b). The anhydrite content of layered rock salt is generally less than 5 percent but is locally up to 30 percent (Nance and others, 1979; Nance and Wilcox, 1979; Kreitler and Muehlberger, 1981; Dix and Jackson, 1982). Thus the viscosity contrast between pure and impure rock salt in domes examined is low, so similar folding is likely on rheologic grounds alone (Schwerdtner, 1967; Ramberg, 1981). Low contrasts in viscosity also characterize glacial ice containing layers of entrained dirt and bubbles; similar folding is by far the dominant fold style in such glaciers (Wegmann, 1963; Ragan, 1969; Hudleston, 1976, 1977) and in the one namakier studied in detail (Talbot, 1979; 1981; personal communication, 1983).

Mechanics of Similar Folding

Similar folding dominates in gravity-driven structures, but how does it take place? The only satisfactory explanation for the formation of true similar folds is that differential simple shear acts across a layered structure in the rock and translates it by variable amounts, thereby inhomogeneously deforming the layers (Carey, 1962; Wynne-Edwards, 1963; Ramsay, 1967, p. 423). The shear surfaces that allow this differential translation can be infinitely close, such as viscous shear surfaces, or separated to form steplike discontinuities between microlithons, or Gleitbretter.

In similar folding by viscous shear (flow folding), the surfaces of viscous flow are termed flow surfaces; their traces in two dimensions are known as flow lines or displacement vectors (fig. 12). The geometry of similar folds was reviewed by Carey (1962) as follows:

1. The axial trace of a fold is parallel to the flow lines.
2. Provided the flow lines are parallel, the thickness of a layer measured in the direction of flow remains constant despite extreme orthogonal attenuation of layers on the fold limbs and thickening in the hinge zone.
3. The shear direction (parallel to the flow lines) is unrelated to the orientation of the layering, which acts merely as a passive marker distorted by differential shear. Consequently, fold hinges can form within the shear surface at any angle to the shear direction.
4. Similar folds only disclose differential shear that is not parallel to the layering.
5. Similar folds do not necessarily imply either shortening or extension normal to the axial surfaces. Extreme fold contortion can accompany zero bulk strain normal to the axial surface.

Similar folds defined by medial moraines and ogives in glaciers suggest that flow lines can both converge and diverge (figs. 7 and 8; Washburn, 1935; Post and LaChapelle, 1971, their figs. 53, 54, 57, 58, 59, 71). Convergence or divergence of flow lines increases or decreases, respectively, the thickness of the folding layer in the direction of flow (Ramsay, 1967, p. 430–431).

The orientation of an initially planar layer relative to the flow lines controls the final form of the fold. The simplest and most frequently cited case is that where the layer is perpendicular to the shear direction (fig. 13A). After differential shear, major axes of the ellipses define a fan that diverges toward the core of the fold. If a homogeneous flattening normal to the axial surface (that is, converging flow lines) accompanies or follows this type of folding, a similar fold having less strongly divergent strain ellipses is formed (fig. 13B). Diverging flow lines produce a similar fold having strongly divergent strain ellipses (fig. 13C). Subsimilar folds (class 1C) can form by superimposing very high flattening strains ($X:Y > 10:1$) on class 1B buckle folds (Flinn, 1962; Ramsay, 1967, p. 411–415; Hudleston, 1973a; Hudleston and Stephansson, 1973). The resulting internal strains (fig. 13D) depend on the exact mechanism of buckling but generally correspond to slightly converging strain ellipses (for example, see Dieterich, 1970; Anthony and Wickham, 1978). This mechanism for producing subsimilar folds satisfactorily explains a feature that is unaccounted for by the differential shear models outlined previously: the apparent periodicity of many similar-fold trains. This periodicity would be initiated by the buckling process. Buckling is limited in rocks that vary little in effective viscosity, such as rock salt or ice. However, intense flow-related flattening normal

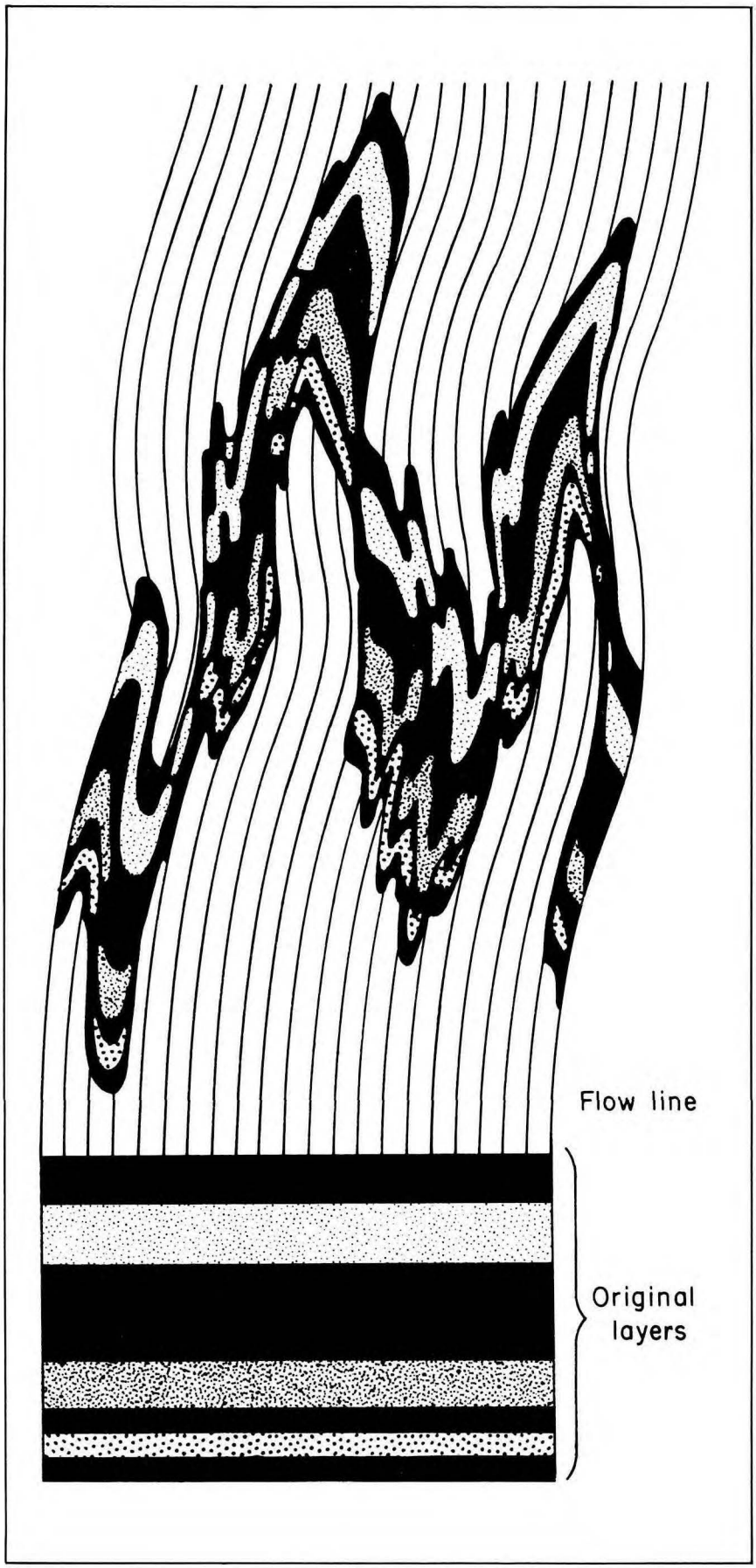

FIGURE 12. The appearance of ideal similar folds formed by differential simple shear of layers along parallel flow lines (flow surfaces in three dimensions). Layers act merely as passive markers and have no mechanical influence. Strain is zero along axial traces, which are parallel to the flow lines. Limbs are apparently attenuated, but thicknesses measured parallel to the axial traces are constant. Limbs are not boudinaged, and there is no shortening normal to the flow lines. (After Carey, 1962.)

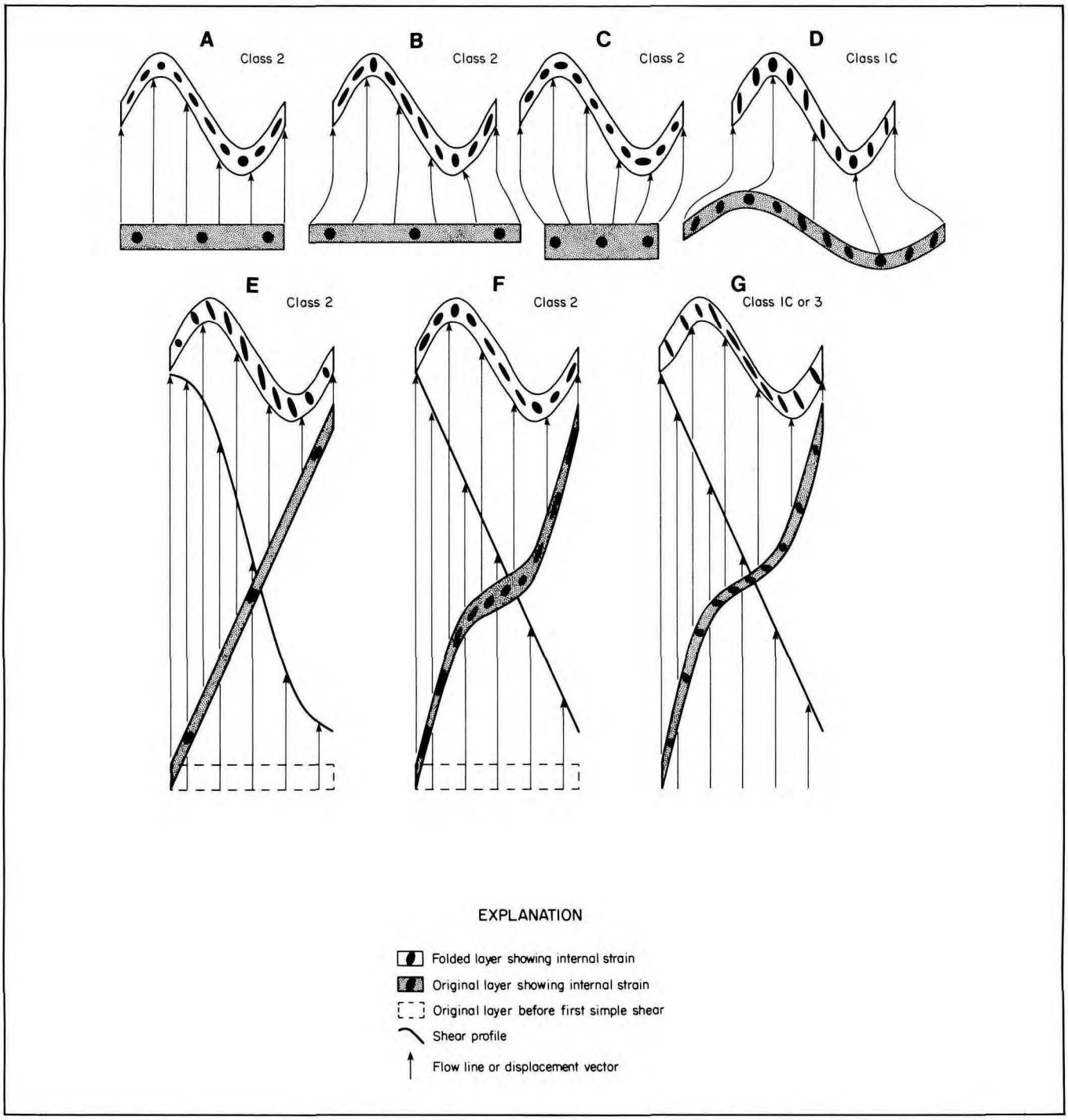

FIGURE 13. Models of the formation of similar (class 2) and subsimilar (nearly similar) folds. Folds of the same shape (for example, models A, B, C, E, and F) have different internal strains (diagrammatically shown by strain ellipses; real halite or ice grains usually recrystallize or segment before reaching the higher strains shown) because they are formed by different mechanisms. Models A, B, and C show simple shear acting on previously unstrained layers: (A) Zero tangential (parallel to original layer) elongation. (B) Tangential shortening. (C) Tangential extension. (D) Subsimilar fold formed by homogeneous tangential shortening acting on a weakly buckled flexural fold (class 1B parallel fold). Models A, B, and C require unlikely reversals of shear sense across every fold axial trace. Models E, F, and G are more realistic shear folds because they do not require reversals of shear sense. (E) Differential simple shear (curved shear profile) acting on a stippled planar layer (which may have undergone a previous episode of uniform simple shear oriented in the direction opposite to the shear profile, as shown). (F) Uniform simple shear (straight shear profile) acting on a layer whose thickness is constant parallel to the shear direction and which was previously deformed by differential simple shear of constant shear sense. (G) Uniform simple shear acting on a layer of constant orthogonal thickness previously deformed by flexural buckling. Model E adapted from Ragan (1969); F and G adapted from Hudleston (1977).

to axial surfaces can distort gentle buckles into virtually similar folds by the mechanism shown in figure 13D. The results are indistinguishable from similar-type flow folds (Ramberg, 1964).

The surge loops in glacial moraines are similar-type folds formed by the mechanisms shown in figure 13A-C. The surge acts across moraines being carried downstream by steady flow, shearing them into a loop. However, in order for a train of folds to form by these mechanisms, shear across every axial trace must systematically reverse in sense (left lateral in the left limbs of antiforms, right lateral in the right limbs). A glacial surge is confined by valley walls until it meets another branch. This confinement gives the surge its identity. No such mechanism seems to exist for producing a train of similar folds within a rock body, and it is therefore difficult to explain this train by the motions shown in figure 13A-C.

However, if a layer is initially oriented in the direction opposite to the shearing motion, heterogeneous shear having a single sense can produce a similar fold if the layering is originally planar and of constant thickness (fig. 13D) (Ragan, 1969). Homogeneous simple shear acting on a gently undulating layer oriented in the direction opposite to the shearing motion will also produce similar folds if the thickness of the undulating layer is constant parallel to the shear direction (fig. 13F) (Hudleston, 1977). Generally this thickness will not be constant (as in buckle folds), and subsimilar folds will result (fig. 13G).

Minor undulations acting as the seed in the mechanism shown in figure 13F,G can form by gentle buckling. They can also be produced as flow folds by deflection of moving ice or rock salt over bedrock irregularities in the soles of glaciers (Hudleston, 1976; Talbot, 1979, 1981). Hudleston (1976) demonstrated by mathematical modeling how very slight upward deflections of the layering across the flow surfaces of the ice become magnified by further glacial flow so that isoclinal, recumbent folds form distally. In salt domes, primary heterogeneities such as a slightly irregular floor or roof of the evaporite unit, or facies changes within the evaporite unit, could deflect flow lines sufficiently to initiate folds.

Formation of Folds and Interference Structures in Salt Stocks

Having surveyed mechanisms capable of generating similar and subsimilar folds, we can now relate the formation of these folds to the emplacement of salt diapirs. The basic flow pattern in diapirs has been known since Escher and Kuenen (1929) suggested the now popular analogy of raising several horizontal sheets through a horizontal ring. Flow circulation in a diapir has the form of a toroid: The diapir occupies the "hole in the doughnut" (Carey, 1962) or may include the "doughnut" as well if circulation is internal.

Salt flowing from bedded evaporites to the crest of a mature salt diapir passes through three distinct zones having gradational boundaries: the source layer, stem, and cap (fig. 14). During doming, convergent flow in the source layer (zone 1) toward the growing salt structure causes a unit volume of salt to be lengthened parallel to the converging flow lines and shortened normal to the flow lines in a horizontal plane; that is, radial lengthening and tangential shortening. Because the source layer thickens from the rim syncline toward the salt stock, salt must also stretch parallel to the vertical diapir axis. The bulk strain is therefore one of flattening. Viscous drag along the upper and lower boundaries of the salt layer induces additional shear strains. As salt moves inward, it is stressed by three mechanisms, each of which can cause different fold styles:

Mechanism A: shear stresses induced by upward flow (fig. 15A). As flow surfaces curve upward toward parallelism with the axis of the salt structure, simple shear acts across the bedding and progressively deflects it upward. This folding on horizontal axes, about increasingly steeper axial surfaces, forms the major structure.

Mechanism B: normal stresses induced by convergent flow (fig. 15B). These stresses act parallel to the layer, causing tangential shortening. Such stresses acting on a rheologically isotropic medium cause homogeneous shortening without folding. However, layers of sparsely disseminated anhydrite in the rock salt impart a weak planar anisotropy. This anisotropy results in the formation of gentle buckle folds of parallel style; amplitude/thickness ratios are low because of the low viscosity between the disseminated-anhydrite layers and the pure rock salt.

Mechanism C: shear stresses induced by boundary effects of the salt body (fig. 15C). As observed in salt glaciers and ice glaciers (Hudleston, 1976, 1977; Talbot, 1979, 1981), an irregular floor to the salt source layer could trigger the formation of intense, recumbent folding of similar-fold style. Such structures could also be formed by

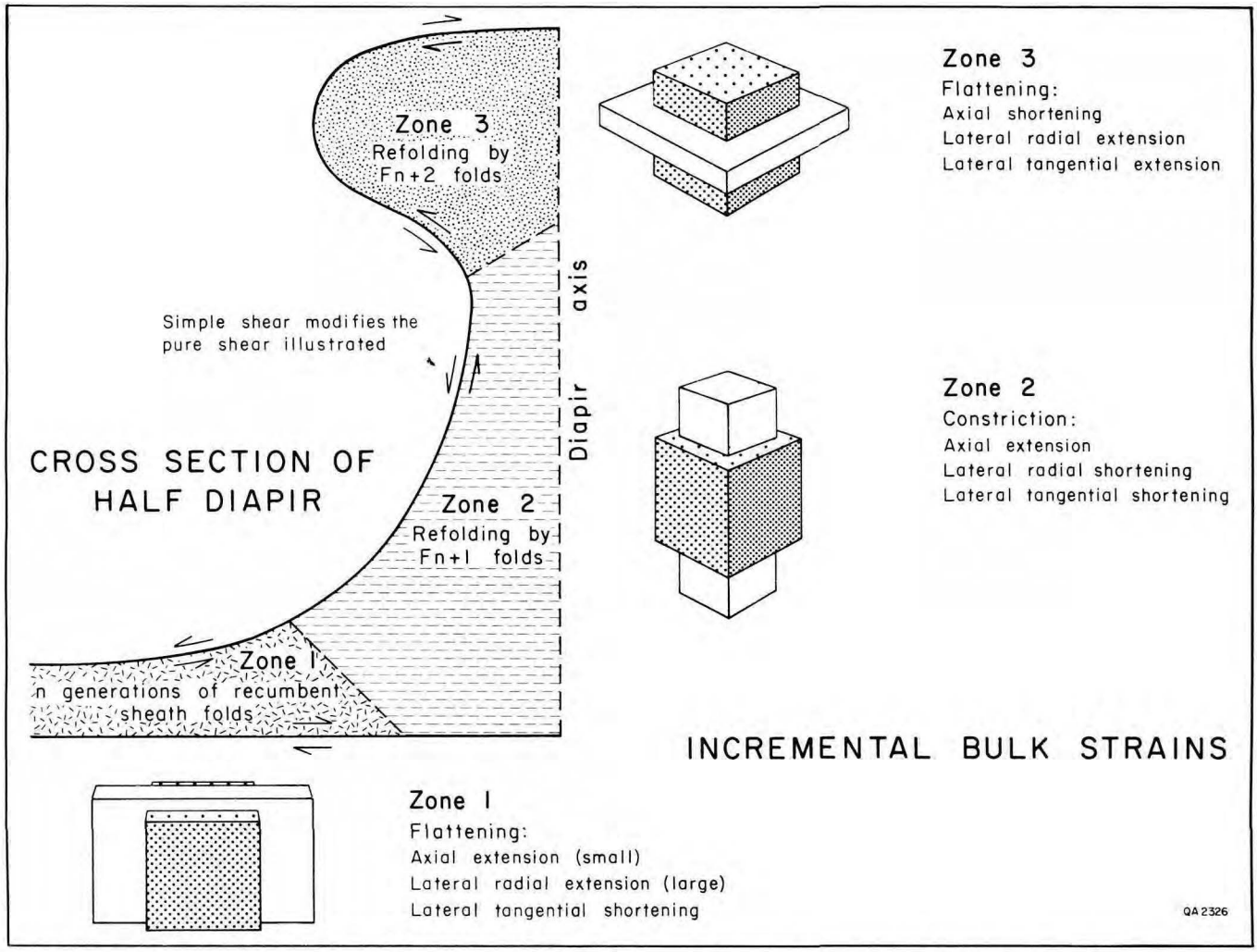

FIGURE 14. Incremental bulk strains and superposed folding in three deformation zones (source layer, stem, and cap) in a mature diapir. Boundaries between zones are approximate.

irregularities in the roof of the salt source layer or by differential flow velocities in different parts of the source layer.

Mechanism A creates the gross structure of a salt diapir and rotates minor structures formed by other mechanisms to a vertical position. Mechanisms B and C are examined to assess how this rotation affects the form and orientation of minor structures.

Convergent laminar flow superposed on weak buckling. As the gentle buckle folds formed by mechanism B are drawn toward the axis of the growing salt structure, they are modified by centripetal and upward flow (fig. 16). Converging and steepening flow paths deform the buckles by (1) rotating fold hinges to steeper plunges, (2) reducing wavelength, (3) increasing amplitude, and (4) causing extension parallel to the fold hinges. Although this convergent flow can be heterogeneous at any scale, strain is predominantly homogeneous; the parallel folds are thereby converted to sub-similar class 1C folds (Ramsay, 1967, p. 411–415; Hudleston, 1973a). These folds will become virtually similar (class 2) after considerable shear flow up the trunk of a diapir. The folds plunge near vertically at their limit, that is, with infinite convergent flow.

Refolding and rotation of upright to recumbent folds. Let F_1 represent an older generation of folds, and F_2 a younger generation, formed during deformation episodes Dl and D2, respectively. What is the result of combining the effects of convergent flow and weak F_2 buckling on preexisting recumbent F_1 folds formed by

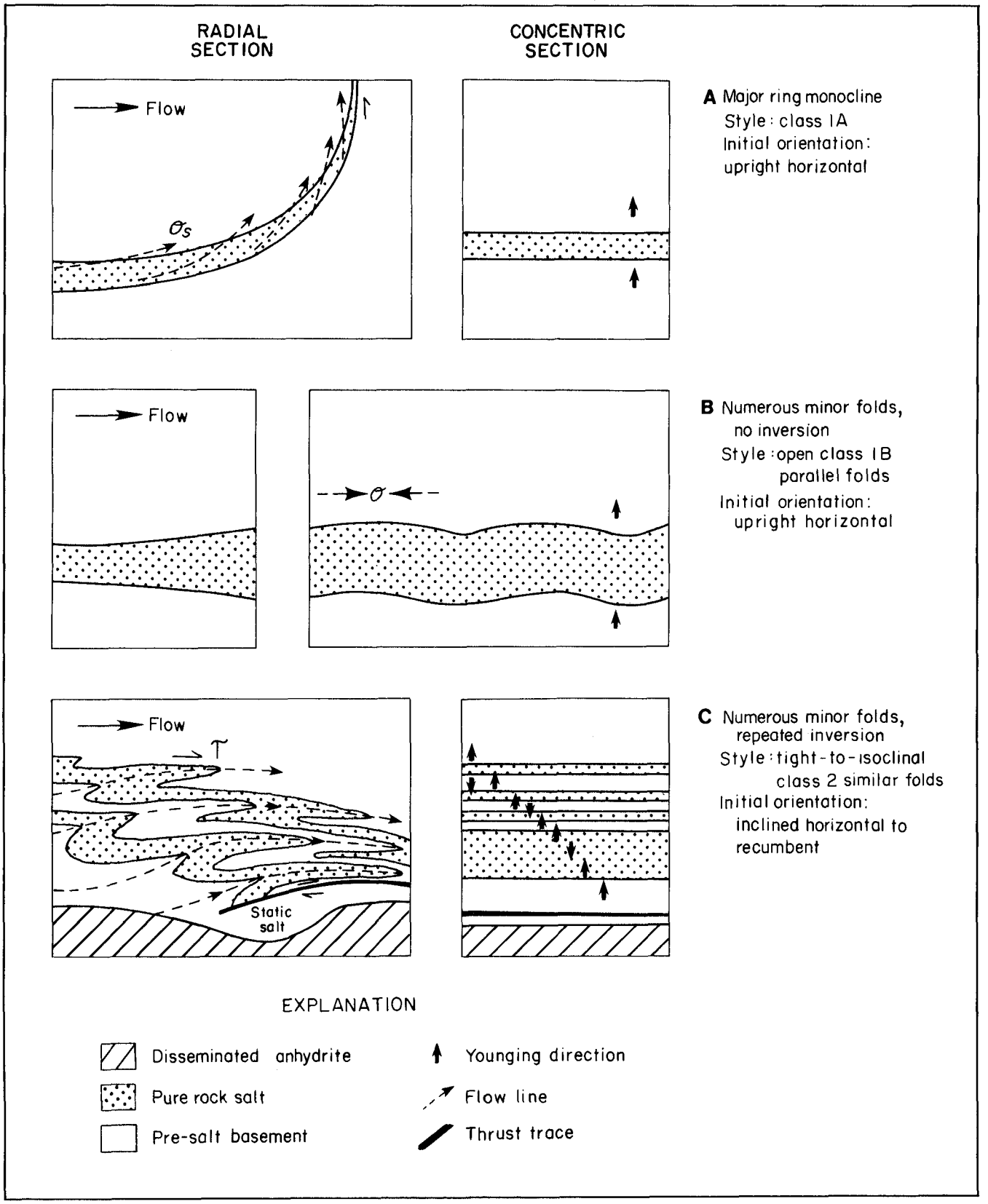

FIGURE 15. *Models for generating folds during centripetal flow of rock salt into a salt diapir. Diapir axis lies to the right of each radial section; flow in concentric section is normal to the paper. (A) Shear stresses (σ_s) induced by upward flow. (B) Normal stresses (σ_n) induced by convergent flow. (C) Shear stresses (σ_s) induced by lower boundary effects. Model C adapted from Talbot (1981), Kuh-e-Namak salt glacier, Dashti Province, southern Iran.*

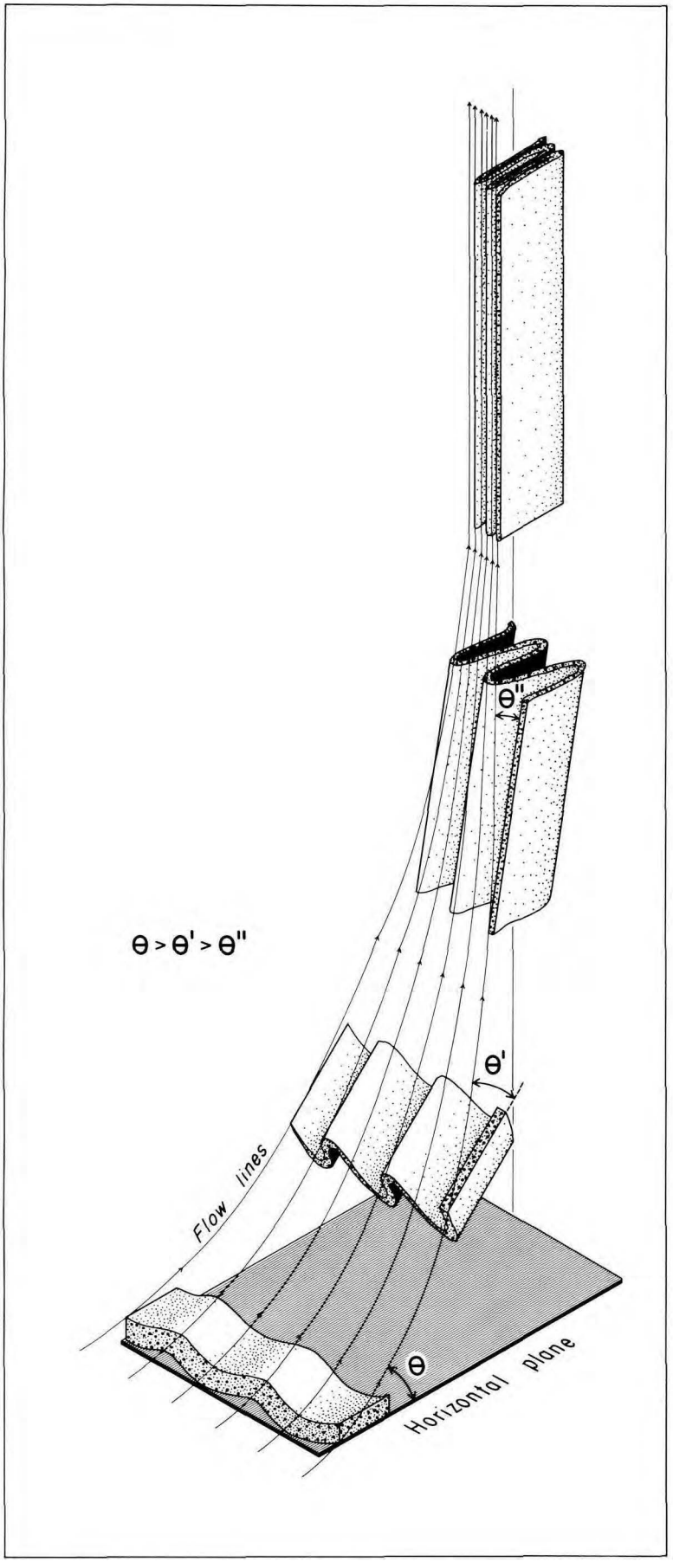

FIGURE 16. Rotation and axial constriction (by mechanism A shown in fig. 7) of initially open, upright, horizontal folds (folded by mechanism B shown in fig. 7) to form isoclinal, vertical folds by upward flow of salt into the trunk of a diapir.

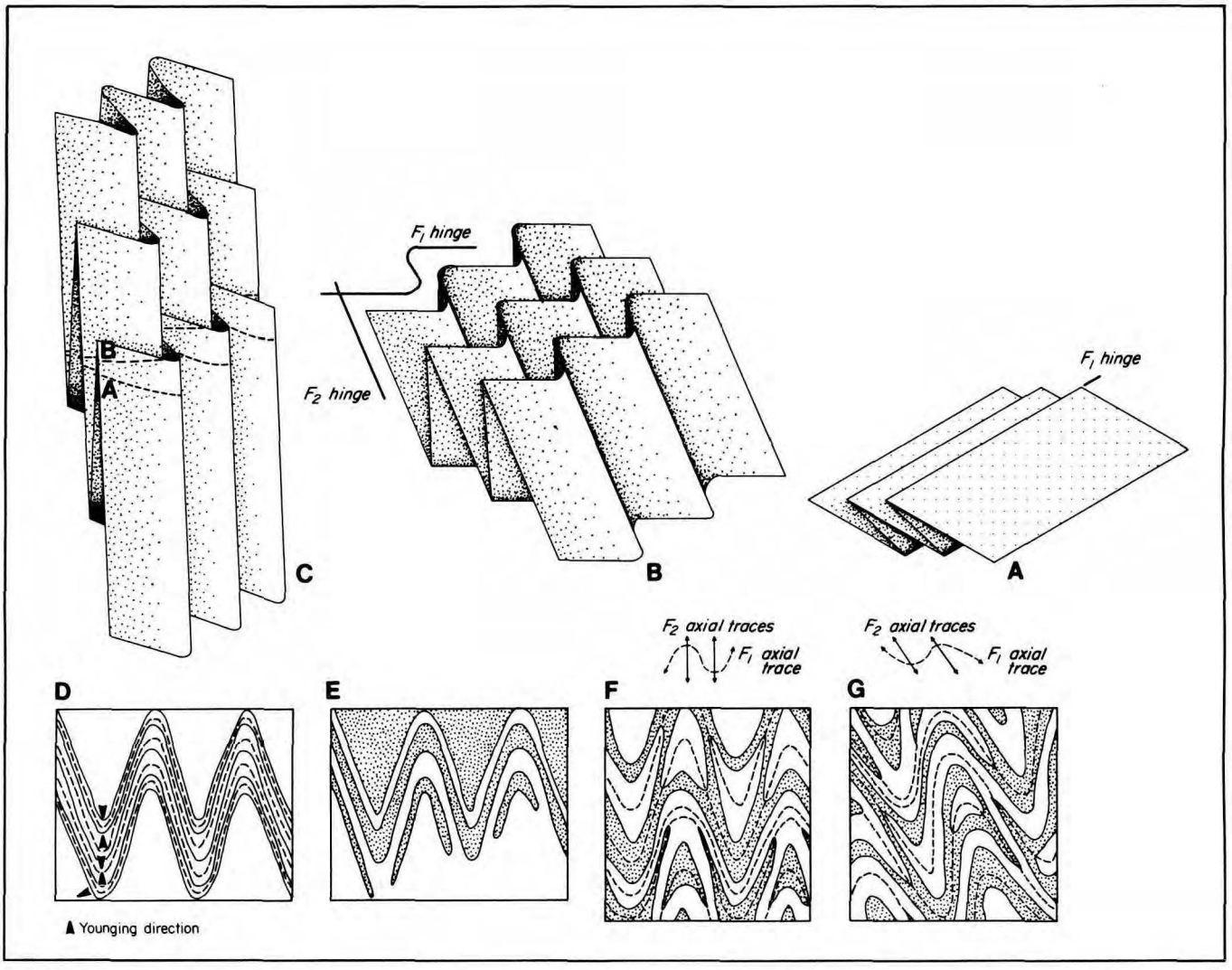

FIGURE 17. Refolding and rotation (by mechanisms A and B in fig. 15) of originally recumbent F_1 folds (formed by the mechanism in fig. 15C) during flow of salt into and up the trunk of a diapir. (A) Original F_1 folds. (B,C) Progressive F_2 refolding analogous to Ramsay's (1967) Type 2 interference. (D) No interference patterns, apart from reversal of younging directions, are visible in cross section of plane a shown in part C, normal to F_2 hinges. (E) Characteristic crescentic patterns visible in slightly oblique cross section of plane b. Younging would also be reversed. (F, G) Oblique cross sections through computer-modeled, orthogonally superposed folds (case N, Thiessen and Means, 1980) of similar geometry to those in part C. Hooks and crescents predominate.

mechanism C? The F_1 hinges and axial surfaces are deformed and rotated by the superposed strain (fig. 17B). The resulting interference structure is eventually dominated by the F_2 folds (fig. 17C). Whether F_1 folds are recognized in a horizontal cross section, such as a mine ceiling, depends on their orientation. If the F_2 folds are subvertical, so that the cross section is parallel to the F_1 fold hinges, no interference structures are visible (fig. 17D). Way-up structures such as graded anhydrite layering can reveal several F_1 axial traces, even though no F_1 fold hinges are visible. Nevertheless, in oblique sections, which are caused by nonvertical plunge of the F_2 folds, closed crescentic interference patterns are visible (Ramsay, 1967, Type 2; Thiessen and Means, 1980, Case N) (fig. 17E). Other interference patterns arise from other oblique sections through this structure (fig. 17F, G), including hook-shaped patterns.

The orientation of each fold generation during progressive rotation has been calculated and is shown in figure 18, both in stereographic form and on the dip-pitch-plunge (DPP) ternary diagram of Rickard (1971). The F_2 folds maintain their upright

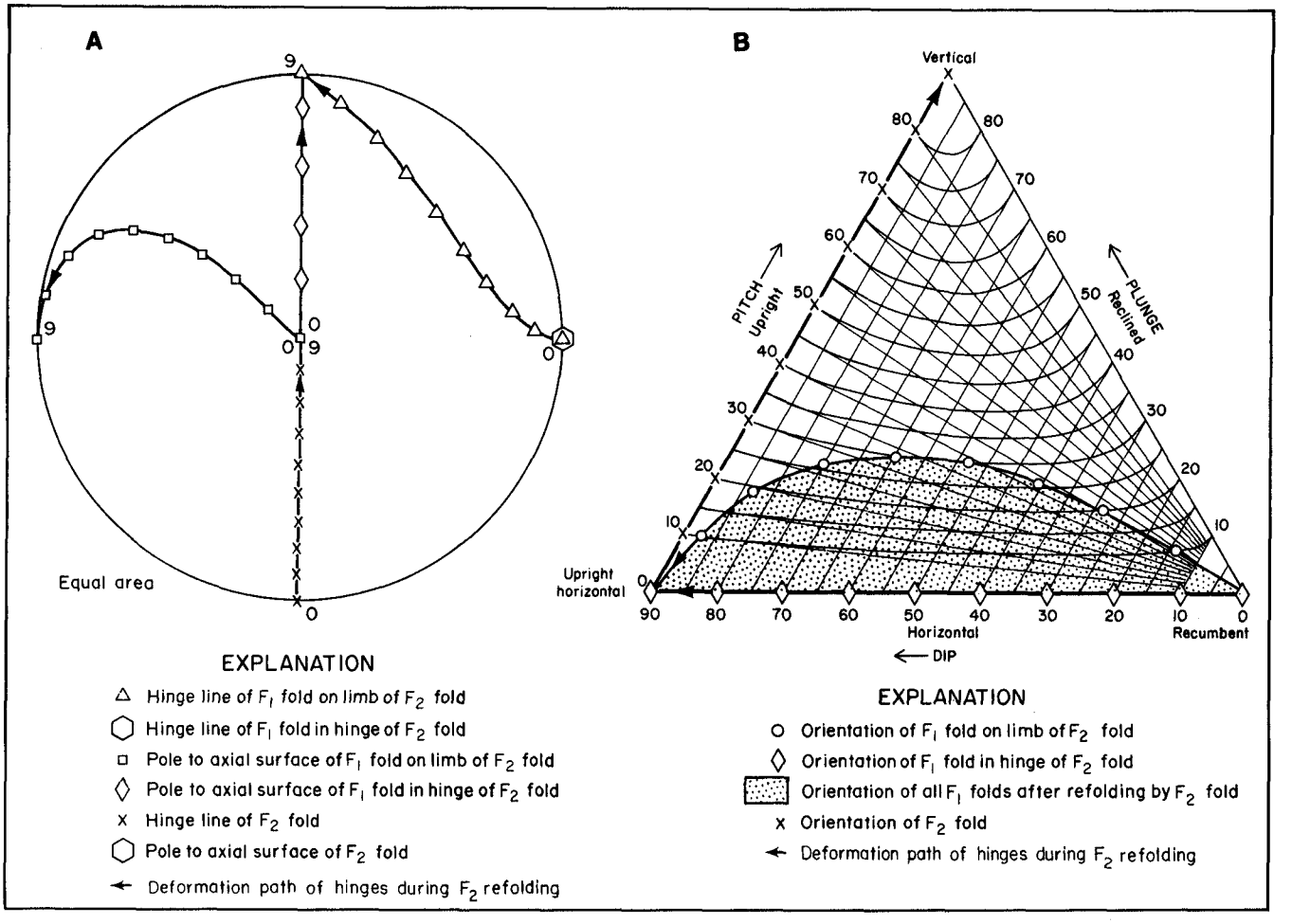

FIGURE 18. The changing orientations of F_1 and F_2 folds during F_2 refolding and rotation shown in figure 17. (A) Stereographic projection. (B) Rickard's (1971) dip-pitch-plunge diagram; curved lines in grid are for pitch. F_2 folds rotate from upright (axial planes) horizontal (hinges) to vertical along a single path with upright axial planes. F_1 folds rotate from recumbent to upright horizontal along an infinite number of paths (stippled area), ranging from horizontal (hinges) (diamond symbols) to moderately inclined (axial planes) plunging (hinges) (circle symbols). F_1 folds cannot be rotated to a vertical position in the model shown in figure 17.

attitude as they rotate from horizontal to vertical in their flow up the diapir trunk (X symbols in fig. 18). In contrast, the F_1 folds, which initially are close to recumbent, take on a wide range of attitudes during refolding and rotation, from horizontal to inclined plunging (stippled field in DPP diagram, fig. 18). But they never attain a vertical orientation. All F_1 folds tend toward an upright horizontal attitude under extreme strain. Thus, vertical folds cannot be formed by rotation of the F_1 folds shown in figure 17A.

Nevertheless, vertical folds could be formed if the F_1 folds were noncylindrical, as depicted in figure 17A, but had nonlinear fold hinges, as shown in figure 19 (left). The subtle culminations in the original F_1 folds would be greatly amplified by convergent upward laminar flow during F_2 to become tonguelike folds having circular, elliptical, crescentic, or involute cross sections and vertical fold hinges (fig. 19, right).

Inclined horizontal F_1 folds therefore probably form tangential to salt stocks by centripetal salt flow against floor or roof irregularities. Culminations in their noncylindrical fold hinges can be magnified into tonguelike vertical folds during constrictive passage up the trunk of a diapir. Accordingly, the resulting interference patterns should be visible in salt mines. They are. Closures, or eyed folds, in cavern roofs mapped by Balk (1949, 1953), Muehlberger (1959), Hoy and others (1962), and Kupfer (1962, 1968) are the cross sections through these structures. Balk and Muehlberger inferred that

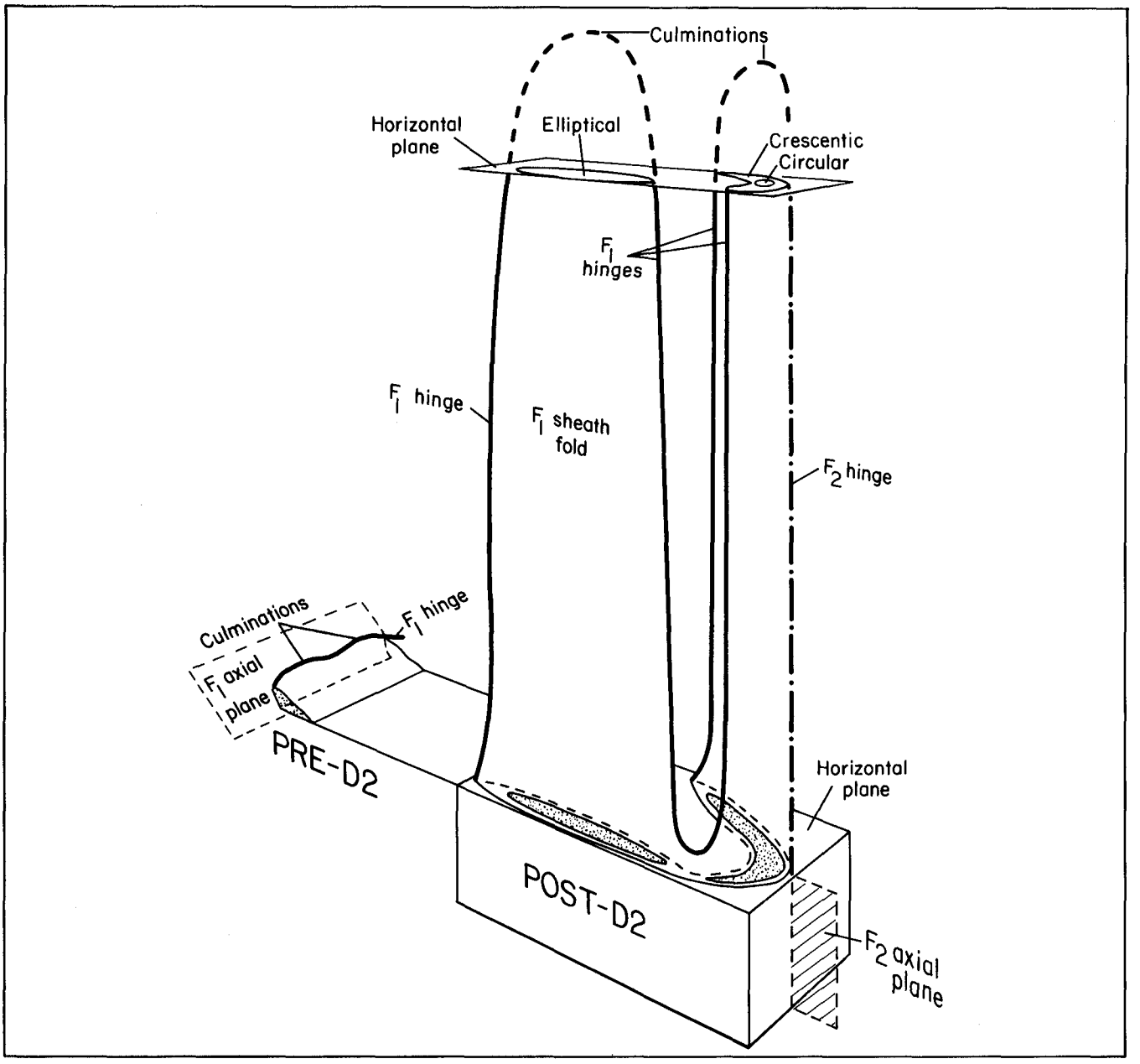

FIGURE 19. Model showing the formation of vertical and near-vertical F_2-F_1 sheath folds (right) during D2 deformation by intense constriction of originally upright or inclined, noncylindrical folds (left) during diapiric rise of rock salt. F_1 folds on the limbs of F_2 folds have elliptical cross sections, whereas F_1 folds in the hinge of F_2 folds have crescentic or circular cross sections. The F_1 sheath folds are too noncylindrical to plot on a dip-pitch-plunge diagram, but they vary from upright horizontal at the culminations to vertical down the sheath flanks.

the closures in Grand Saline Dome were cross sections through the culminations and depressions of closed interference structures that were "pipelike"; but they did not attempt to analyze how these folds were formed. A corollary of this hypothesis is that above or below these closures, the plunge of the fold hinges must locally decrease to zero. Kupfer (1962) proposed another explanation for Weeks Island Dome: namely, that the closures formed by partial fusion of isoclinal fold limbs.

Tonguelike folds, now generically called sheath folds, have been reported in blueschists, layered marbles, and mylonite (Quinquis and others, 1978; Minnigh, 1979; Mukhopadhyay and Sengupta, 1979; Cobbold and Quinquis, 1980; Henderson, 1981). The three-dimensional geometry of these

sheath folds is known from serial cross sections through hand specimens, and the formation of sheath folds has been studied by theoretical and experimental modeling. Similarities between cross sections through natural sheath folds and cross sections through salt folds are illustrated in figure 20. Note that the sheath folds in the mylonite example are about two orders of magnitude smaller than those in the salt, but their geometric similarity is striking. The most common patterns in rock salt are circles, ellipses, crescents, and hooks (fig. 20). Mushroom shapes are fairly rare. But, with the crescentic shapes, they provide the most critical evidence of all because they can only be formed by interference of folds with restricted relative orientations (Thiessen and Means, 1980). These orientations are satisfied by the model shown in figure 19.

Fold closures, mushroom shapes, and certain hook-shaped folds in horizontal sections of salt mines therefore apparently represent the distorted and rotated remains of F_1 folds (fig. 19). These folds originally formed concentrically around the base of the salt dome as a result of perturbation of laminar flow by irregularities in the upper and lower contacts of the salt source layers (fig. 15C). These F_1 folds were then carried by inward salt flow into the trunk of the diapir, where they were refolded. Most folds now exposed within salt diapirs are of F_2 age. (It should be stressed that "F2" is a label of convenience and includes all post-F_1 folding, obviously a broad category.) The F_2 folds originally must have formed as weak buckles trending toward the dome axis and resulting from tangential shortening during centripetal salt flow (figs. 15B and 16). These folds were rotated to near-vertical orientations (fig. 18) and stretched vertically; differential stretching would have encouraged the formation of ductile shear zones between tongues of salt rising at different rates. Where F_1 folds had not previously formed, the F_2 folds in the diapir trunk are inferred to have the following stratigraphic relations: Anticlines face outward and synclines face inward. Nevertheless, because of their vertical plunge, F_2 folds are structurally neutral (neither antiforms nor synforms).

ASSESSING LARGE-SCALE FLOW PATTERNS FROM LINEAR ELEMENTS

In addition to the medium-scale fold structures in salt stocks, the overall pattern of folds and other structures within a fold stock must be considered. The trunk of an active salt diapir is a regime of intense subvertical elongation caused by simple-shear viscous flow. Flow patterns within the trunk can be deduced from the theoretical behavior of linear elements. Fold hinges and mineral lineation are linear finite-strain elements. They rotate toward the shear direction as the rock enclosing them deforms by progressive simple shear, attaining parallelism in the case of infinite shear. At high shear strains, then, the orientation of lineations and fold hinges provides approximate indicators of the flow paths within salt stocks.

What is the polarity of the flow paths? Flow patterns within an intruding salt stock are largely conjectural. But because the diapir moves upward relative to the surrounding strata, a given unit of salt is more likely to move upward than downward, although downward flow is quite possible near the edges of diapirs. Thus, the trend of a linear element indicates the azimuth of the flow path, whereas the up-plunge direction (180° from the trend) indicates the probable direction of flow. In addition, however, strike directions of anhydrite layering are also flow-path indicators. Where the layering is vertical (for practical purposes, 88° to 90°), fold hinges defined by the layering must be contained within the vertical plane; thus, the trend of the fold hinge must be parallel to the strike of layer in plan view. Such strikes provide the flow path, but not the direction, or polarity, of flow; they are thus of less use than are measurements of a linear element.

To assess flow patterns of the Gulf Coast diapirs, we must rely on incomplete plan sections exposed in underground salt mines. Only three salt domes contain mines with enough field measurements of linear elements or strikes of vertical layers to enable flow directions to be estimated: the southeastern part of Grand Saline Dome (Balk, 1949), Weeks Island Dome (Kupfer, 1962), and Winnfield Dome (Hoy and others, 1962). The inferred flow directions and flow paths for these mines are shown in figure 21. Only the Carey Salt Company Mine in Winnfield Dome covers a substantial part of a dome (fig. 21A); unfortunately, this mine is now flooded and abandoned. The percentage of linear elements in the total number of control points (n) is shown as L percent for each mine; this percentage and the density of control points enable the quality of the data to be assessed.

Inferred flow directions indicate the azimuth of flow, but the vertical component of this flow is much

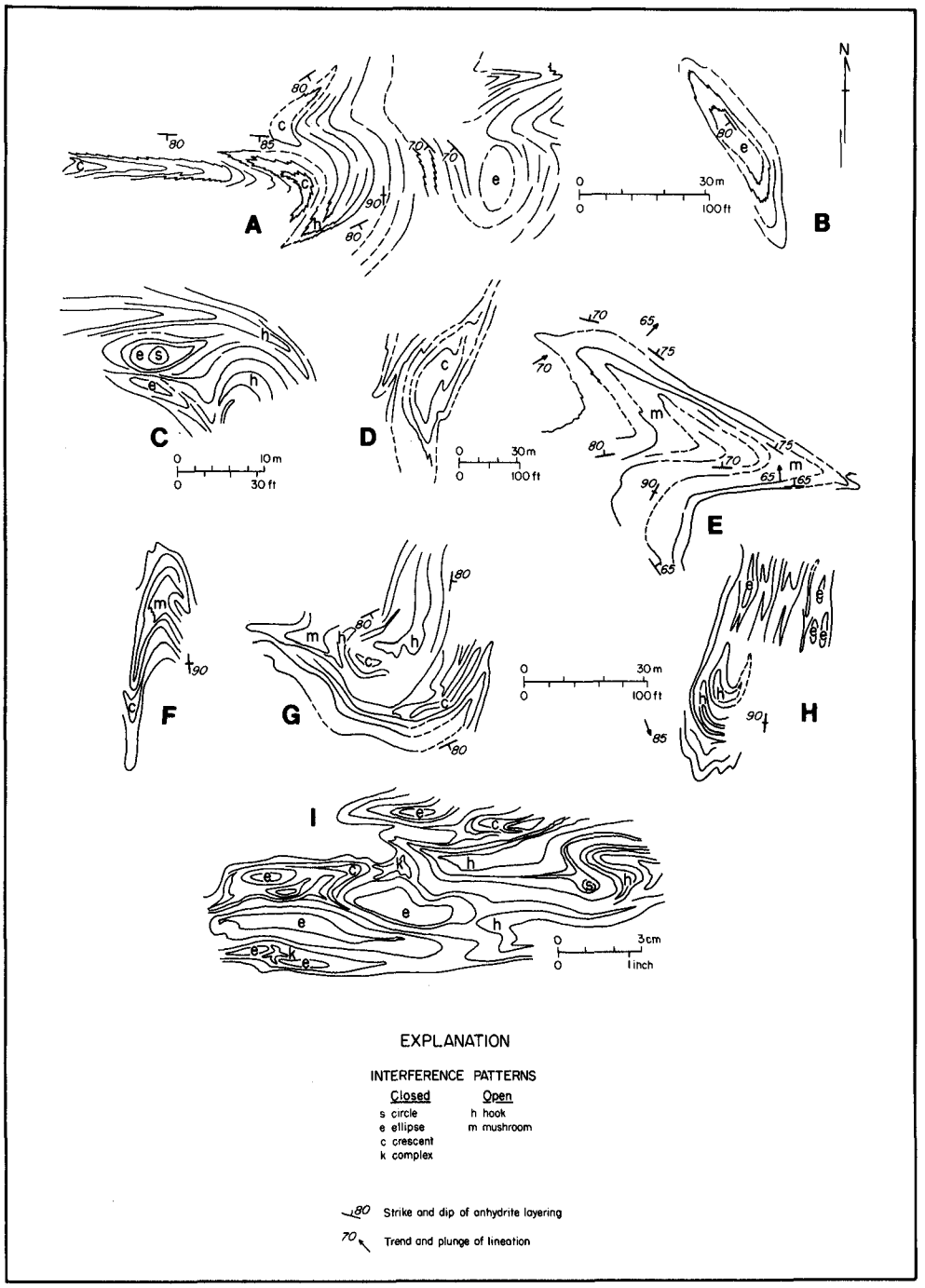

FIGURE 20. Cross sections through large fold-interference structures in the roofs of Gulf Coast salt-dome mines, illustrating six basic patterns. These patterns are postulated to be profiles of sheath folds formed by the model shown in figure 11. Except for parts C and I, all views are downward and normal to horizontal plan projections. (A, B) Grand Saline Dome, East Texas, 213-m level of Kleer Mine (after Balk, 1949). (C) Jefferson Island Dome, Louisiana, 305-m level of Jefferson Island Salt Company Mine (after Balk, 1953). Oblique view about 60° upward toward the southwest. (D, E) Winnfield Dome, Louisiana, 247-m level of Carey Salt Company Mine (after Hoy and others, 1962). (F–H) Weeks Island Dome, Louisiana, 231-m level of Morton Salt Company Mine (after Kupfer, 1962). (I) For comparison, a profile through much smaller, but similar, sheath folds in mylonitic rocks from the village of Vang, Valdres district, Norway, probably deformed by intense simple shear nearly parallel to the layers (after Cobbold and Quinquis, 1980).

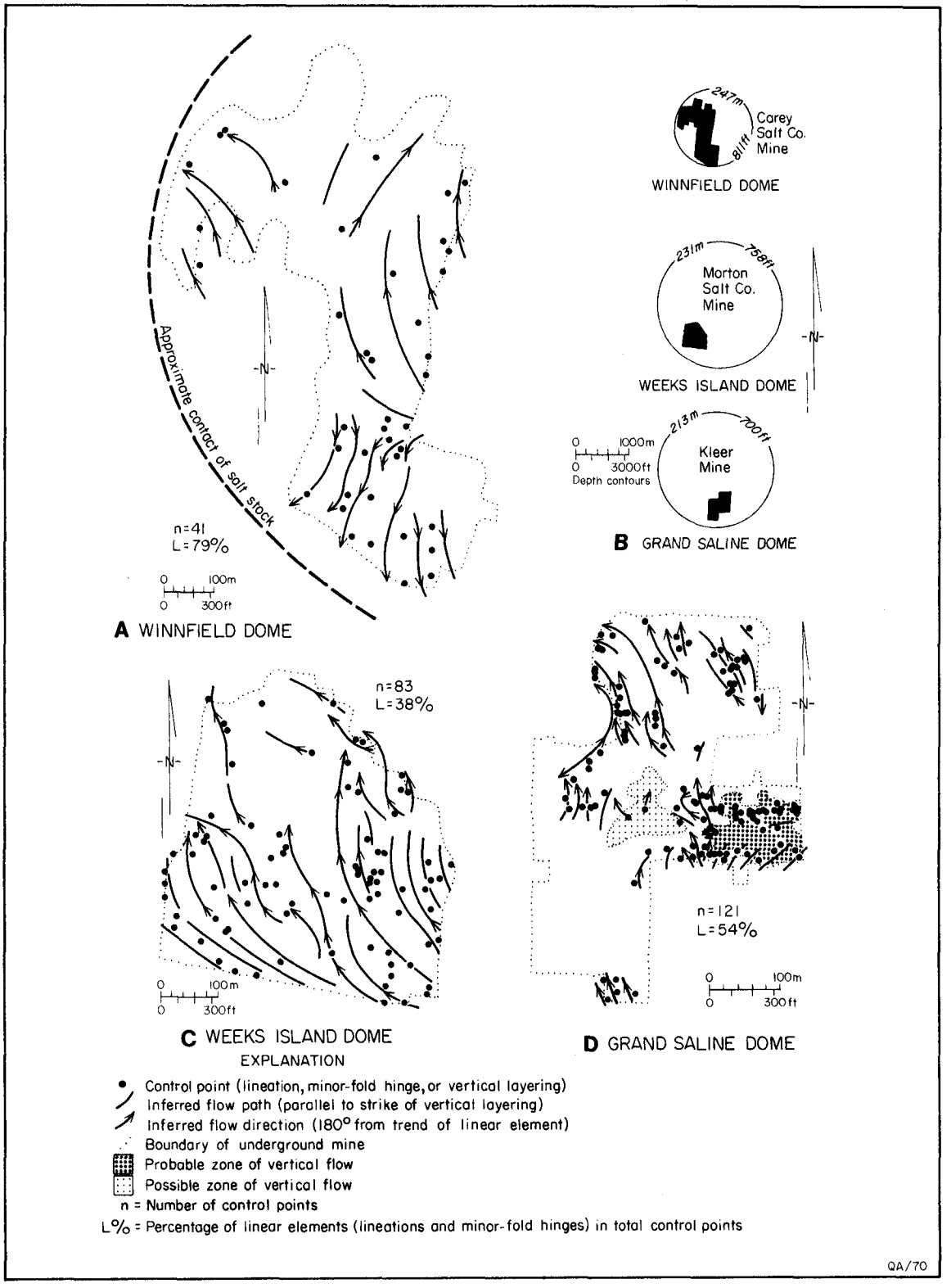

FIGURE 21. Maps showing inferred flow paths and flow directions of rock salt in three salt-dome mines. Depth contours in A delineate boundaries of salt stocks at mine level. Flow paths have much larger vertical components of movement, but only horizontal components are shown. Data compiled from Balk (1949), Hoy and others (1962), and Kupfer (1962).

greater than the horizontal component shown on the maps. Inferred flow in Winnfield Dome is outward from a zone in the southern part of the dome (fig. 21A). The inferred flow patterns in both Weeks Island and Grand Saline Domes (fig. 21C,D) suggest flow inward to the dome center; they thus appear to be opposite to that at Winnfield Dome, although the small areas sampled in Weeks Island and Grand Saline may not be representative. The probable zone of vertical flow in Grand Saline Dome is marked by vertically plunging linear elements, and the possible zone of vertical flow is marked by an absence of planar structures. All the maps in figure 21 illustrate that linear trends (and inferred flow directions) form coherent patterns that vary far less than do the seemingly chaotic strikes of layering and fold axial surfaces; the linear trends therefore simplify and unify the structure and are essential to understanding the structure and its implications for salt flow.

To assign polarity to the flow paths from the inferred flow trends in figure 21, we must assume that flow is everywhere upward; this is unproven. A more revealing way of treating the linear data is to examine the variation in plunge of these elements by means of plunge-isogon maps, which do not require this assumption. The data base is 38 to 79 percent of the size of the data base in figure 21 because vertical dips of layering, which yield trends but not plunges, are omitted. Figure 22 shows maps of plunge isogons (lines joining points of equal plunge; Elliott, 1968) drawn on the surface containing the linear elements (a surface that steeply intersects the mine roof). To filter out as many errors in the original measurements as possible—errors that would cause meaningless and confusing perturbations in the map pattern—a measuring error of ±2° was assumed. The assumed error is based on a study by Rondeel and Storbeck (1978), who found that in groups of 100 measurements of a rotatable bedding surface, 90 percent of the poles fell within an error cone of 2° half-apical angle around the mean pole under optimum conditions of measurement. Because a linear element is more difficult to measure than a planar element, especially in dim light, its measurement is likely to be considerably more error prone; thus the assumption of 2° error is unrealistically low. Even so, the plunge-isogon maps show considerable consistency and smooth variations in plunge from point to point.

How can these plunge isogons be interpreted? Inspection of the major folds in Winnfield Dome mapped by Hoy and others (1962) indicates a complex structure: Most folds have at least one overturned limb and some of the folds even face downward. The steeply plunging folds appear to be tonguelike, and older, tighter folds are deformed over antiformal crests and synformal troughs. Slide zones of simple shear divide some of the salt tongues. These fold heterogeneities can be removed by interpreting only the plunge isogons, the orientation of which is part of the large-scale strain that, in turn, is a function of the flow pattern.

The plunge-isogon maps shown in figure 22 can be converted to true-scale cross sections (fig. 23) to outline major zones of flow. The plunge isogons are interpreted using the differential-advance model shown in figure 24, which is analogous to the formation of surge loops within glaciers, to the overall flow of glaciers (Hudleston, 1980; Hudleston and Hooke, 1980) and namakiers (Talbot and Jarvis, 1984), to the lateral spreading of fold nappes (Bucher, 1956; Ramberg, 1981, his figs. 9.9 and 9.10), and to the rise of tongues in experimentally modeled diapirs (Talbot, 1974, 1977; Dixon, 1975; Ramberg, 1981, his figs. 11.25 and 15.4).

Alternative cross sections are shown across Winnfield Dome (fig. 23B,C). Because no zones of shallowly plunging structures were mapped, the cores of rising salt tongues can be inferred to be along the margin of the dome, beyond the ends of the cross-section line (fig. 23B). The junction of two tongues would be the zone of steep plunge where the sense of shear changes south of the dome center. This model is unrealistic because the two inferred tongues are placed too close to the contact zone, where frictional drag discourages any kind of rising plume, as in the glacial analogs. The alternative model places two rising tongues (marked by large arrows in fig. 23C) in the zones where Hoy and others (1962) mapped the lowest plunges (55° to 65°); this model implies that even lower plunges may be present in these zones, but these plunges have not been recorded. Some of the senses of shear in this mode are different from those in figure 23B, but the two lobes still adjoin in the zone of maximum plunge south of the dome center. This inferred flow pattern is supported by remarkably similar flow and strain patterns inside a model diapir by Dixon (1975). Measured orientations of principal extensions in this model are closely analogous to the orientations of the linear elements in Winnfield Dome. Principal extensions in the model also define two outward-

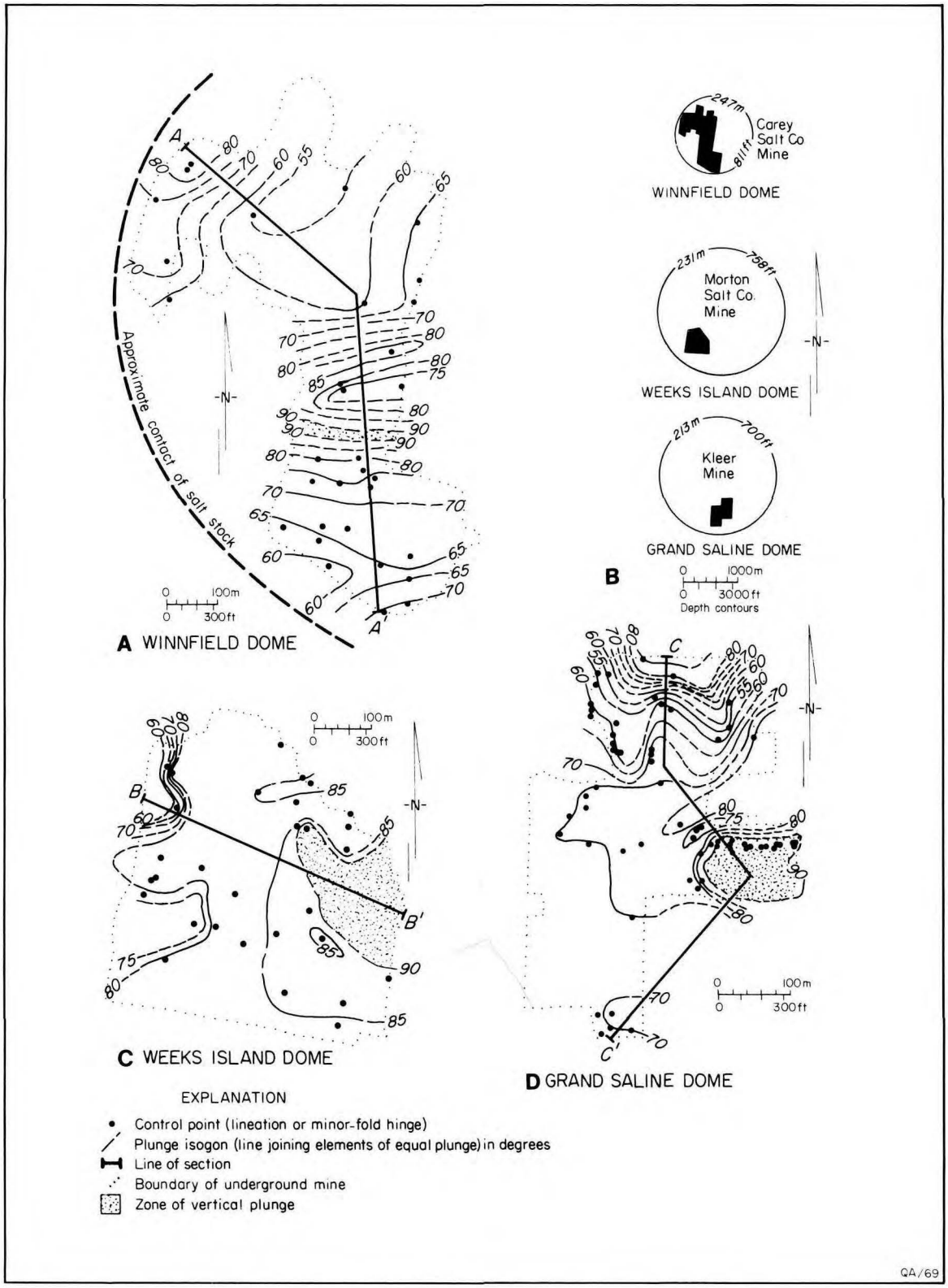

FIGURE 22. Maps showing plunge isogons for linear elements in rock salt in three salt-dome mines. Note the rarity of vertical plunges. See figure 21 for data sources. Cross sections shown in figure 23.

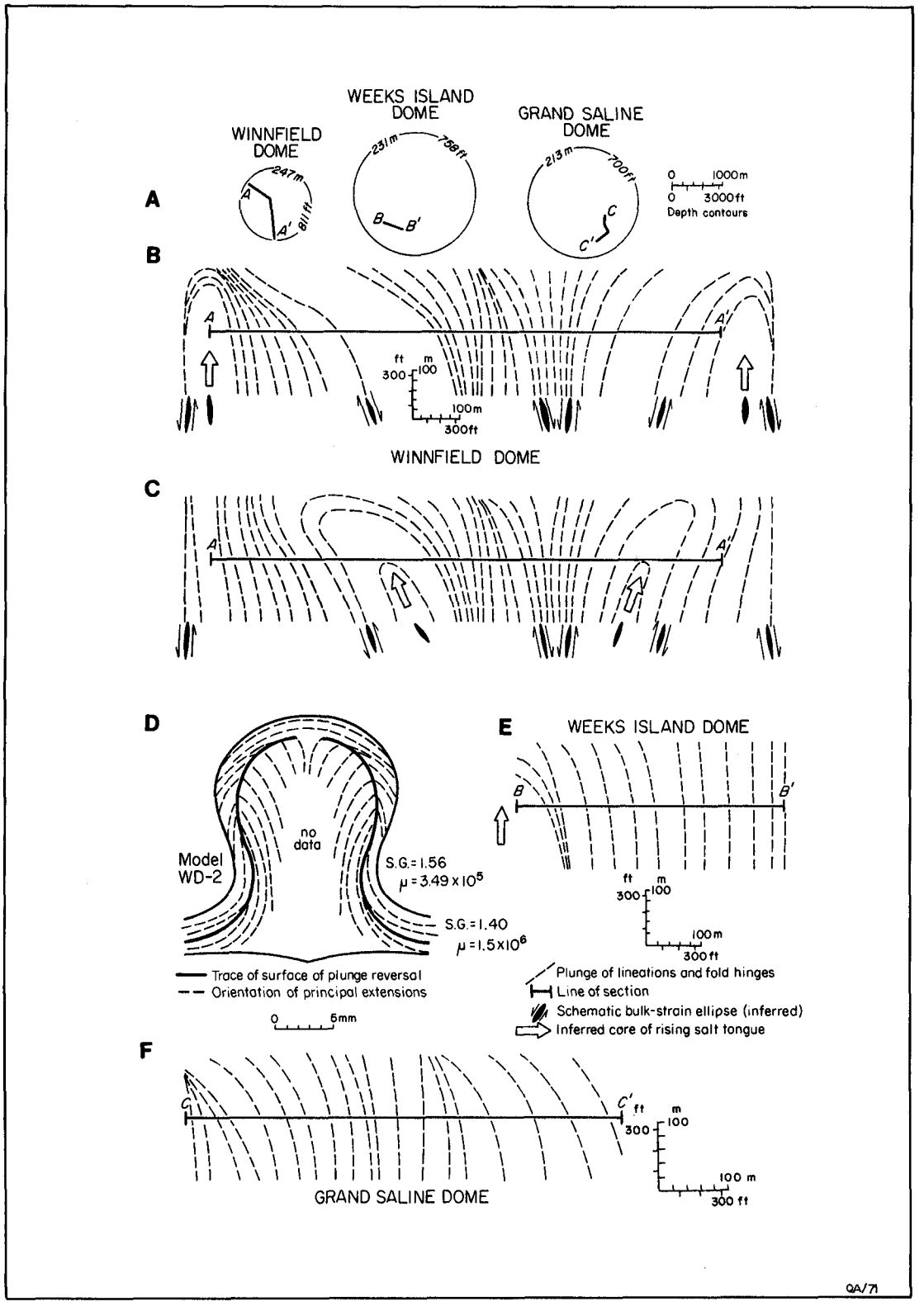

FIGURE 23. Cross sections through salt domes showing major structure and inferred salt tongues based on plunge isogons in figure 22. These tongues are defined by changes in plunge of linear elements rather than by layering. (A) Location of cross-section lines; see also figure 22. Depth contours delineate margins of salt stock at mine levels. (B, C) Alternative models for Winnfield Dome; C is more realistic and shows two major salt tongues rising symmetrically outward. (D) Structure almost identical to C in Dixon's (1975) salt-dome model WD-2, in which a surface of plunge reversal of principal extensions marks the axial surface of two symmetric tongues of diapiric material. (E, F) Cross sections for Weeks Island and Grand Saline Domes are too short to define major structures.

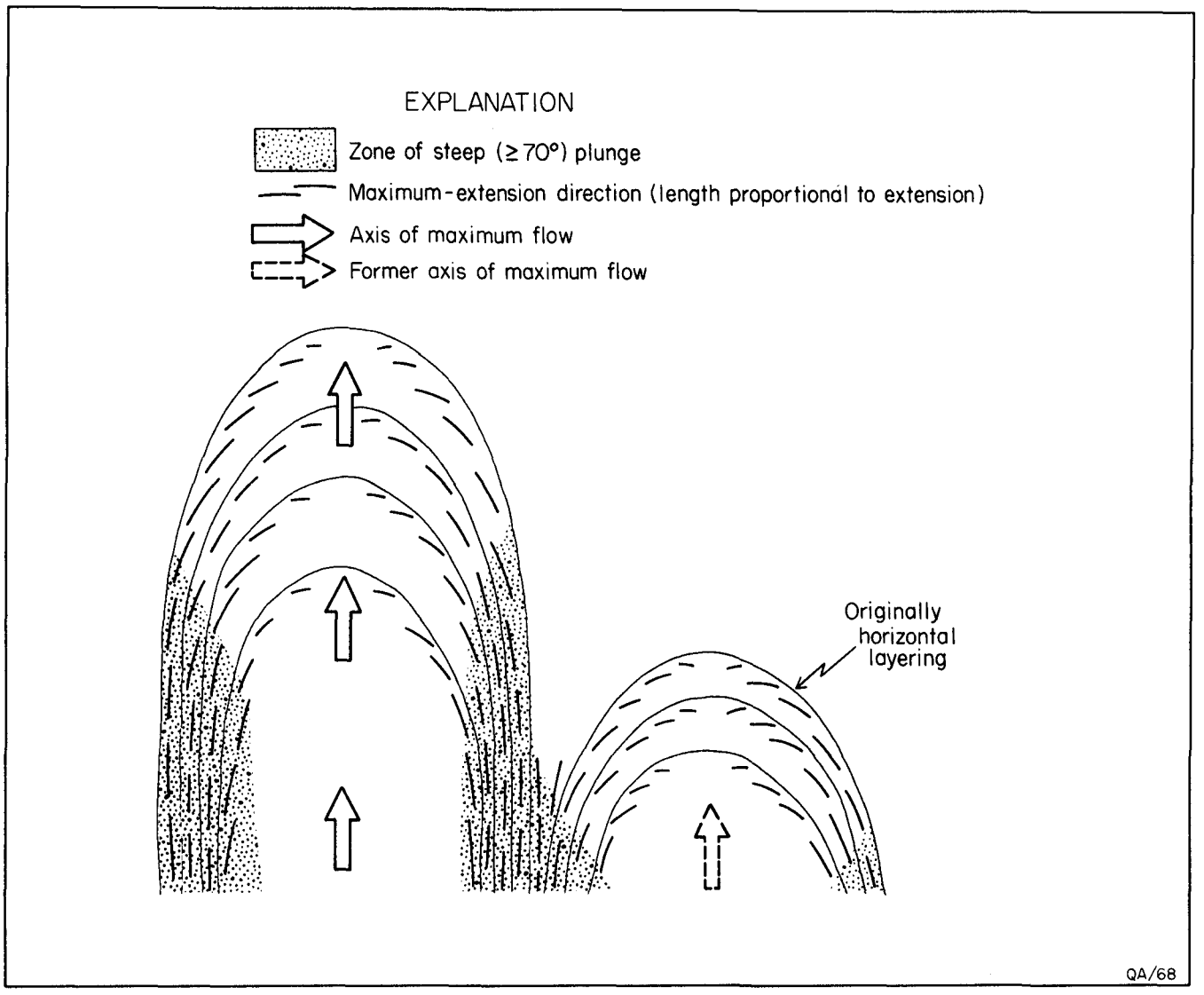

FIGURE 24. Model showing the homogeneous rise of material by differential advance. Maximum upward flow takes place beneath zones of shallow plunge; zones of steep plunge mark the borders of advancing tongues.

facing inclined lobes, as inferred for Winnfield Dome (fig. 23D). The surface of plunge reversal in figure 23D roughly corresponds to the lobes of maximum flow velocity in this model. Cross sections through Weeks Island and Grand Saline Domes are shown in figure 23E, F. Little can be deduced from them, probably because the line of section is so short in relation to the whole dome. Nonetheless, the flanks of a salt tongue are suggested just west of the area traversed by cross section B-B′.

PART II: STRUCTURE OF THE TOG-1 SALT CORE, OAKWOOD DOME

This part of the report presents new findings concerning the internal structure of Oakwood Dome, East Texas, and interprets these findings on the basis of the review of deformation structures in part I. Core from the LETCO TOG-1 borehole was the primary data source for this study. The vertical borehole was drilled just north of the axis of Oakwood Dome in Freestone County. It intersects rock salt at 354.5 m and ends at a depth of 411.8 m, yielding 57.3 m of rock-salt core. The lithology of the continuous 10-cm-wide core through salt and the base of the cap rock was studied by Dix and Jackson (1982) in transmitted and reflected light using both thick sections (1 to 10 mm thick) and thin sections (< 1 mm thick). The microstructure, fluid inclusions, and geochemistry of rock salt in this core were also studied, and a detailed lithologic log of the core was provided.

Principal conclusions of the study by Dix and Jackson (1982) were as follows: All but the upper 2 m of rock salt displays a strong deformation fabric induced by salt flow during diapirism. Recrystallization of previously foliated rock salt produced a granoblastic polygonal texture in the upper 2 m of salt core. Microstructure, fluid inclusions, and bromine concentrations in halite suggest that recrystallization was promoted by downward movement of intercrystalline brine from the lower contact of the anhydrite cap rock. Absence of a cavity at this contact indicates that the salt stock is not currently being dissolved in the zone intersected by the borehole and that previous dissolution has been compensated for by diapiric rise of rock salt. An anhydrite lamina across halite-filled extension fractures at the base of the cap rock indicates that anhydrite layers have accreted against the base of the cap rock. The 57.3 m of rock-salt core contains an average of 1.3 ± 0.7 percent anhydrite. If all the cap rock was derived by residual accumulation of such low concentrations of anhydrite, more than 6 km of rock salt would have dissolved; vertical shortening in the cap rock just above the contact was probably induced by upward force from the salt stock. This stress formed a horizontal, spaced solution cleavage by pressure solution and mass transfer of anhydrite. The solution cleavage, which is marked by a dark insoluble residue, transects older lamination that is thought to reflect cycles of accretion of anhydrite against the base of the cap rock. Further lateral extension and vertical shortening in the base of the cap rock formed halite-filled vertical extension fractures and inclined shear fractures that postdate both the cap-rock lamination and the solution cleavage (Jackson, 1981b).

This part of the report describes the results of a companion study to Dix and Jackson (1982) on natural strains in the salt core to evaluate the geologic stability of the salt. The large-scale structure of the salt intersected by the vertical drill core was delineated by geometric analysis. Strain analysis was used to estimate the orientation, type, and magnitude of finite strains at various depths and to throw light on the origin of the fabric.

GEOMETRIC ANALYSIS

Structural Elements

The form and orientation of major structures in Oakwood Dome can be deduced from minor structures in the core. The basic minor structural elements are as follows:

1. *Layering* is defined by disseminated-anhydrite inclusions in poikiloblastic halite grains. It represents the deformed remains of bedding in the original evaporite.
2. *Tectonic fabric* is defined by the shape and orientation of halite grains. A strong planar (S) component has the form of a schistosity defined by the planar preferred orientation of disc-like halite grains. A penetrative cleavage is parallel to the schistosity. A weaker linear (L) component is a mineral lineation defined by the preferred orientation of the major axes of halite grains within the plane of schistosity. Both the schistosity and the lineation can generally be recognized and delineated by eye. But in one part of the core where the fabric is weak, only strain analysis can detect the existence and orientation of these elements.

Defining Orientation in Nonoriented Core

Using the relative orientations of layering and schistosity to determine major structures in a single borehole is not straightforward. Because the TOG-1 borehole is vertical to within 2° throughout its

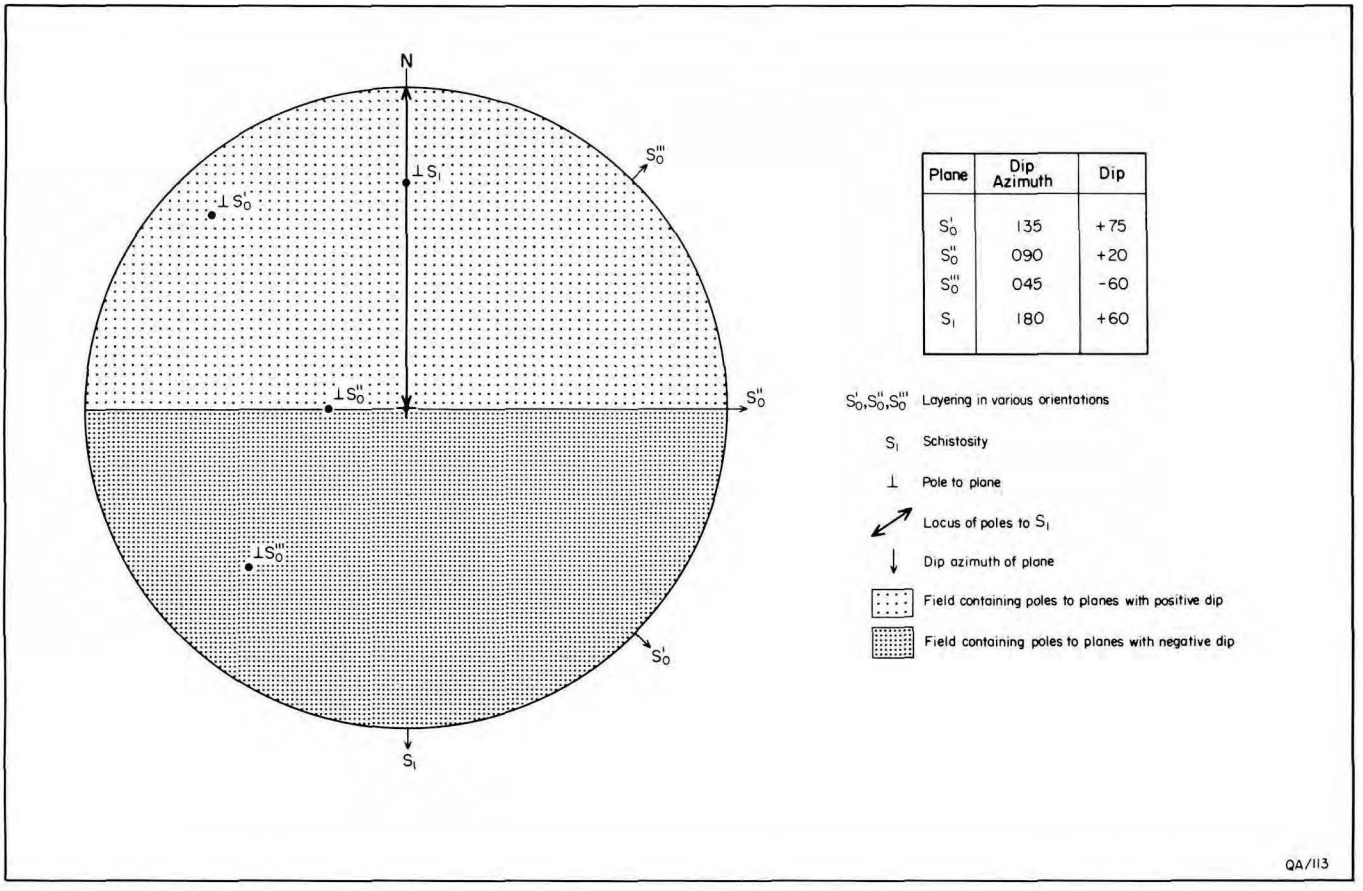

FIGURE 25. Equal-area stereographic projection showing conventions for describing orientation of structural elements relative to S_1 schistosity in the TOG-1 core.

length, all dips measured relative to the core axis represent true dips. But the core itself is nonoriented, so the directions of dip are unknown. Nevertheless, the dip of the schistosity is extremely consistent: 64 dip readings with a mean of 34° have a standard deviation of only 4°. Conceivably, the direction of dip could vary although the dip remained constant, but the resulting pattern of strain would be improbable. The most reasonable estimate of the major structure is therefore obtained by assuming a constant dip direction for the schistosity. In cross section, this dip direction is fixed toward the left; in plan view, the dip azimuth of the schistosity is to the south. The leftward direction was arbitrarily chosen. The southward direction is the most likely dip azimuth—though still speculative—because this is the direction in which the dome axis lies. Because of its consistent dip, the schistosity provides a useful reference surface with which the much more variable layering can be compared. In cross section, the schistosity is arbitrarily assigned positive dip angles. Accordingly, layering with a dip azimuth within 90° from that of the schistosity is assigned positive angles of dip (fig. 25). Conversely, layering with a dip azimuth of more than 90° from that of the schistosity is assigned negative angles of dip.

Structural Cross Section

Figure 26A was constructed to scale according to the conventions discussed in the previous paragraph. It represents a vertical cross section based on the structural elements intersected by the core. The core itself is shown as a double line down the axis of the section. The traces of layering have been projected laterally beyond the limits of the core

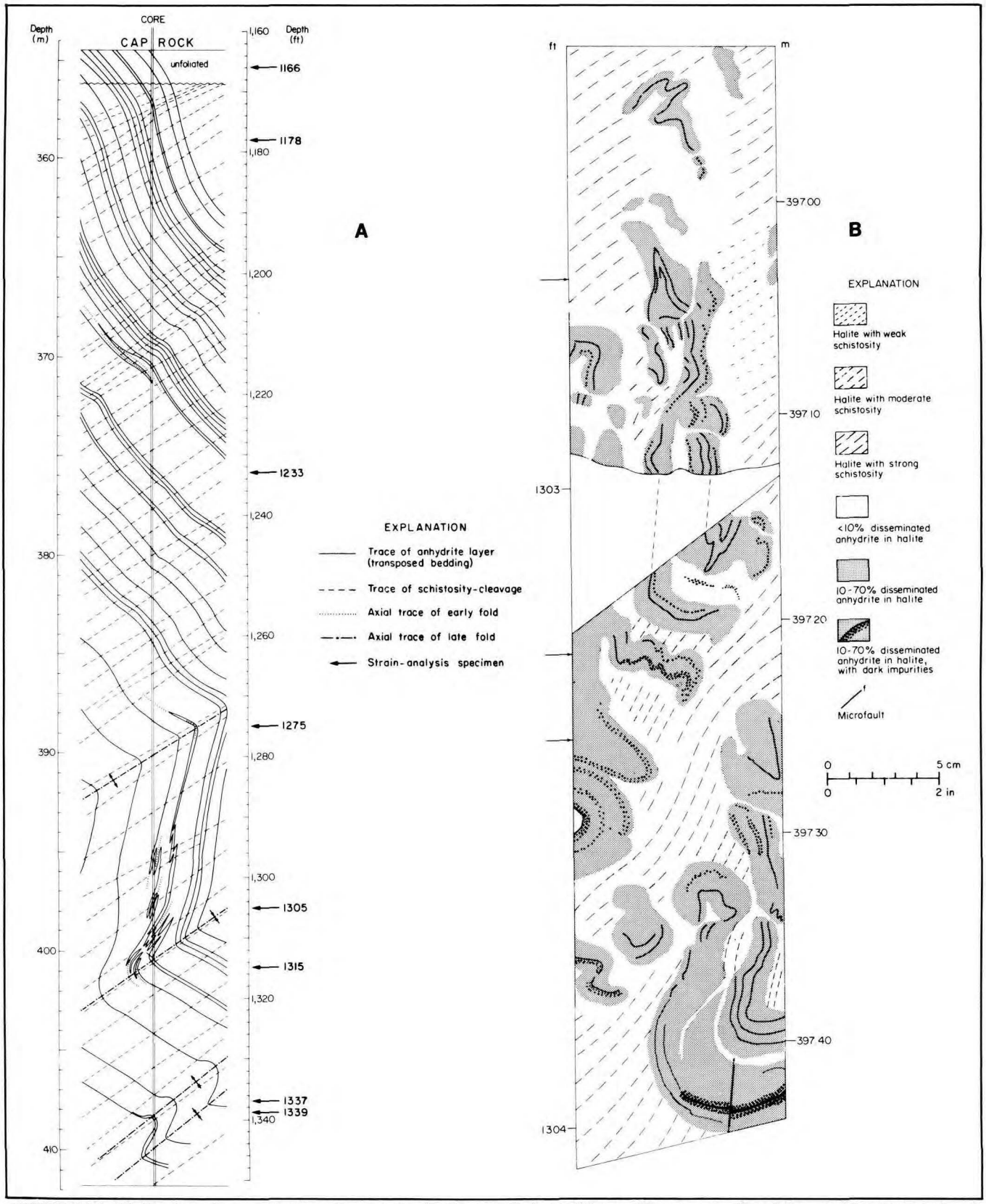

FIGURE 26. (A) Structural cross section along vertical salt core, Oakwood Dome. The core itself is delineated by the two closely spaced parallel lines. On the basis of measurements of layering and schistosity, the section was constructed to scale assuming a mechanism of similar folding and projecting elements outward from the core for better visibility. (B) Schistosity (dashed lines) in the halite transects older isoclinal folds at arrowed localities. Thin, anhydrite-rich layers containing dark laminae (each shown as a solid line) have been boudinaged in several places. Traced from contiguous thick sections. (From Dix and Jackson, 1982.)

into the adjacent areas to display the large-scale structure clearly without distortion, such as exaggerating the horizontal scale. The projection assumes similar-type folding for reasons discussed in the section titled "Fold Style" (p. 20). The traces of layering were projected with fixed orientation along the schistosity trace. In similar folds, the schistosity trace represents a direction of high geometric stability, along which changes in layering orientation are small.

In the upper two-thirds of the salt core, the schistosity and the layering dip in opposite directions, separated by a dihedral angle of about 90°. This geometric relation indicates the hinge zone of a first-order inclined antiform. The axial surface of this fold dips leftward. The lower third of the core represents the lower limb of the first-order antiform, in which four second-order major folds have formed. Their axial traces are shown in figure 26. These first-order and second-order flexures can be termed younger folds because they fold an older generation of isoclines. The axial traces of these older isoclines are subparallel to the layering. Examples can be seen at depths of 370 m and 394 to 401 m in figure 26A and in detail in figure 26B. The minor isoclines are transected by the schistosity. These older folds may be prediapiric, having formed by diagenetic volume changes in the evaporite unit. Or they may be syndiapiric, having formed during centripetal salt flow toward the base of Oakwood Dome by either of the two mechanisms (convergent flow superposed on weak buckling, or refolding and rotation of recumbent folds) discussed in the section titled "Formation of Folds and Interference Structures in Salt Stocks" (p. 26).

The mutual orientations of schistosity and layering allow determination of the orientation of the fold axes relative to the schistosity. As explained previously, schistosity is assumed to dip southward. In the core, the trace of the disseminated-anhydrite layering is visible on the schistosity surface as a fuzzy band 1 to 5 cm wide. The broad width and vague delineation of this layering trace make precise measurement difficult. But where recognized, this trace is approximately parallel to the strike of the schistosity (fig. 27). Using Laing's (1977) method for interpreting bedding-cleavage intersections on cleavage surfaces, the axes of the major folds intersected by the drill were determined to trend east-west with negligible plunge (fig. 27). These inclined horizontal folds therefore appear to be concentric about the axis of Oakwood Dome, assuming that the schistosity dips toward this axis.

The large-scale structure of a first-order inclined antiform with second-order folds on its lower limb is illustrated in figure 28. The inferred form of the major structure above and below the core is shown by dashed lines. Three hypothetical fold forms, marked a, b, and c, show possible upward continuations of the structure in the past. However, this zone is now occupied by cap rock, indicating that the inferred salt structures have been removed during truncation of the dome crest. The most obvious agent for truncation of the salt stock is ground-water dissolution. The minimum thickness of salt removed can be estimated, as shown in figure 28. These estimates vary from 30 m upward, according to the model selected for the former shape of the upper part of the structure, shown as a, b, or c.

Because of this inferred truncation, the horizontal base of the cap rock is discordant across the inclined layering and schistosity (fig. 26). On a broad scale, therefore, this contact has the geometry of an angular unconformity. Nevertheless, detailed study of the microstructure of the uppermost zone of rock salt, which is unfoliated and very coarsely grained, shows that this salt recrystallized and was partly dissolved during accretion of the lowermost layer of the anhydrite cap rock (Dix and Jackson, 1982). A high degree of discordance between the cap-rock contact and layering in rock salt has also been reported from Tatum Dome in Mississippi (Eargle, 1962), and from Rayburn's and Vacherie Domes in Louisiana (Nance and Wilcox, 1979; Nance and others, 1979). A contact such as this is exposed at surface in the Mount Sedom salt diapir in the Dead Sea rift valley (Zak and Freund, 1980).

Implications for Internal Structure

Although the forms of major structures in salt stocks can be delineated on the basis of a single core, despite the absence of either recognizable stratigraphy or known orientation of core, we cannot confidently extrapolate beyond the zone penetrated by the borehole. We can only speculate on the gross structure of Oakwood Dome by analogy with the models described in part I. The intersected inclined antiform is most probably a sheath fold formed by the mechanism shown in figure 19. Emplacement of the sheath fold as a tongue of salt may have been by the mechanism shown in figure 24. We can only guess as to the distribution and attitude of these tongues. Figure 29 is one such guess. Each tongue flows at different velocities and times. Differential vertical movement

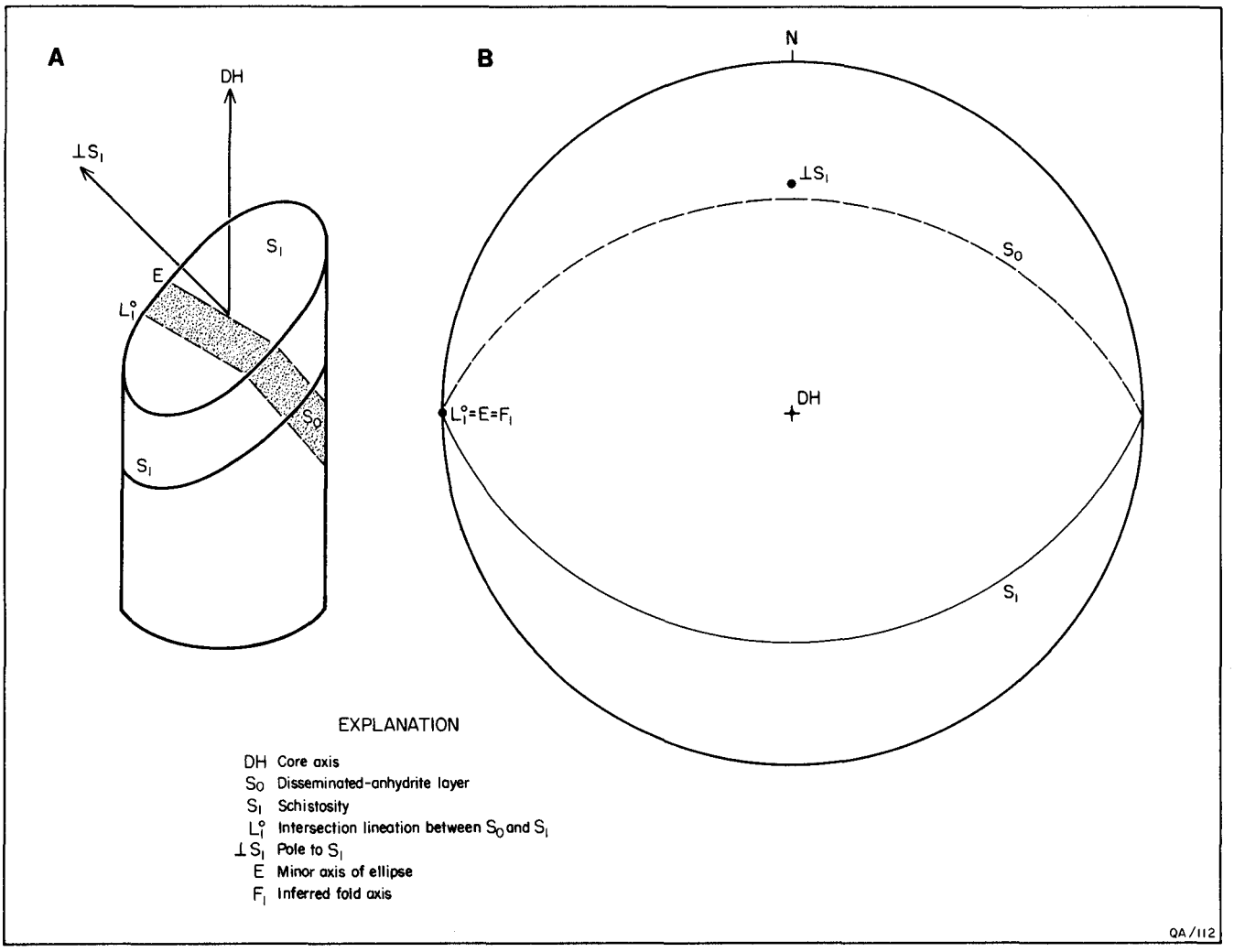

FIGURE 27. Deducing the orientation of a fold axis (F_1) from the trace of layering in a schistosity plane. Fold axis trends subhorizontally, parallel to strikes of S_0 and S_1. (A) Diagrammatic view of vertical core. (B) Equal-area stereographic projection.

of salt tongues has been previously inferred for other salt domes (Balk, 1949; Lotze, 1957; Muehlberger, 1959; Kupfer, 1974, 1976) but was not postulated for lateral flow as well. The salt tongues emerge from the stem of the diapir as vertically plunging folds and become progressively refolded by lateral flow to form recumbent overthrust folds. The geometry of the oakwood salt core suggests that it passed through the hinge zone of one of the younger, higher Overthrust antiforms within the dome. Almost certainly, however, the internal structure is more complicated than this, and extrapolation based on a single core is unreliable.

STRAIN ANALYSIS

Strain analysis—the determination of the magnitude, orientation, and type of strains in a given sample—has progressed so that any rock, including ice, may be investigated. Petrofabric studies, which represent a microscopic approach to geometric analysis, have been carried out on halite (for example, Balk, 1949; Schwerdtner, 1967; Muehlberger and Clabaugh, 1968), but these studies did not attempt to quantify strains.

The raw materials for strain analysis consist of discrete objects in deformed rock, such as initially subspherical ooids, spherulites, pisolites, oncolites, reduction spots, and vesicles and nonspherical mineral grains, clasts, lapilli, body and trace fossils, stromatolites, folds, or igneous and sedimentary veins. Only objects whose initial shape, size, or orientation can be reasonably inferred can be used as strain markers.

Not all aspects of deformation can be computed by strain analysis of natural rocks. The translation,

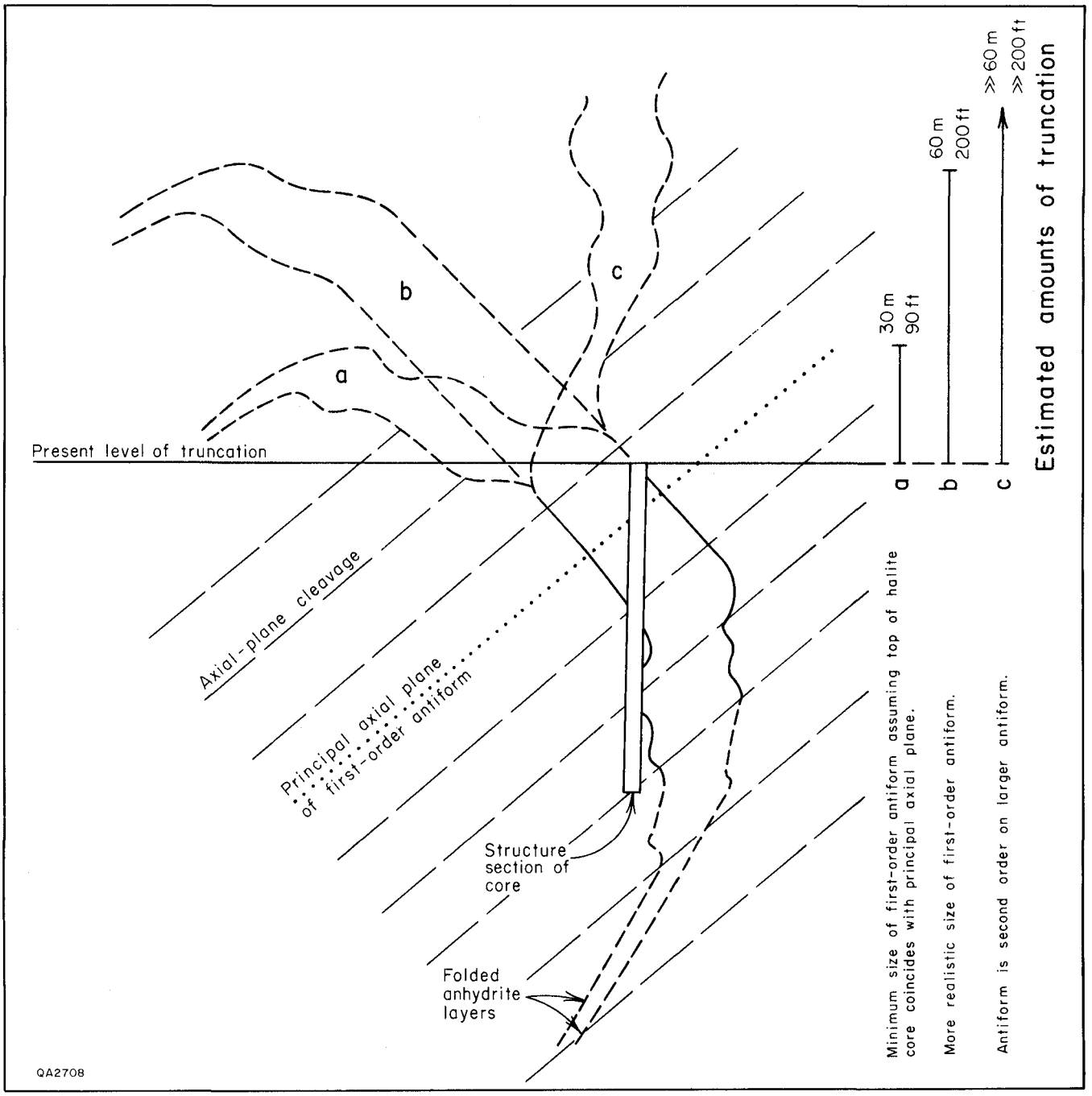

FIGURE 28. Medium-scale structure within Oakwood Dome, extrapolated upward on the basis of figure 26A. Three hypothetical structures (a, b, and c) may have existed. Each allows a different estimate of the amount of structural truncation. (Adapted from Jackson and Dix, 1981.)

or direction and amount of movement of the entire rock mass from its place of origin, can rarely be determined. Similarly, strain analysis rarely allows determination of the rotational component of strain, that is, the angle of rotation of a line that has become the direction of maximum elongation. Strain analysis is best used to determine the distortional component of strain, which describes the change of shape during deformation. Most strain markers yield only the proportional ratio of the principal strains and not the actual elongations.

Because the shapes of halite grains in the deformed rock salt of Oakwood Dome can be approximated closely by ellipsoids, we need

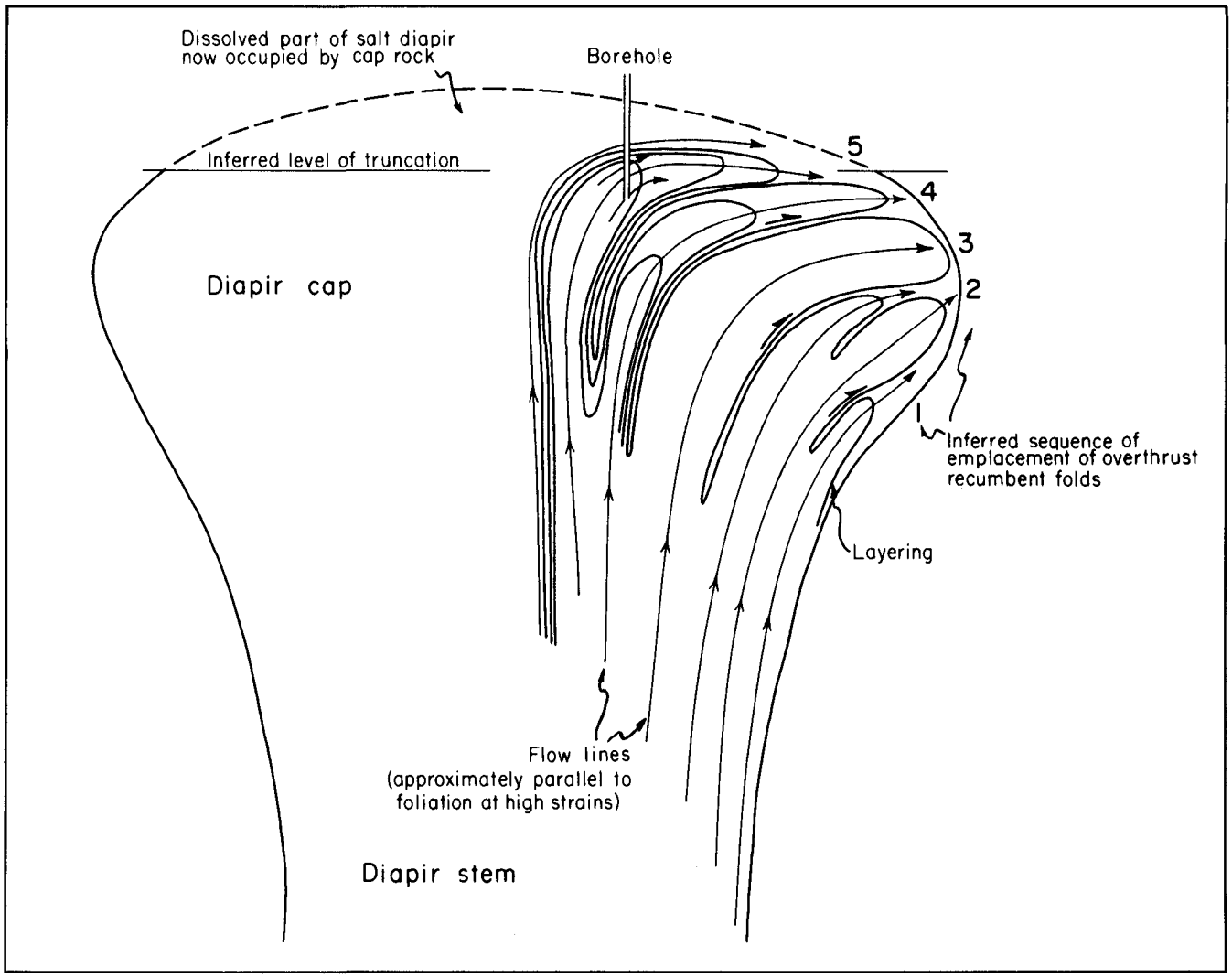

FIGURE 29. One model, based on figures 26 and 28, showing flow patterns within Oakwood Dome. Tongues of salt are sequentially overthrust as vertical folds refolded to recumbent folds. The TOG-1 borehole has pierced the lower part of tongue 5. The upper part of this tongue has been removed by truncation of the dome crest. This model assumes that the structure penetrated by the borehole is representative of the stock as a whole, an assumption that can only be evaluated by further exploration. (From Jackson and Dix, 1981.)

consider only those methods of strain analysis applicable to ellipsoidal objects. Most objects in sedimentary rocks can be mathematically treated as ellipsoids because two-dimensional sections through them yield elliptical shapes. Critical examination of unstrained, natural fabrics in undeformed rocks has shown that truly spherical particles are extremely rare, even in rocks such as oolitic limestone (Boulter, 1976; Ramsay, 1976; Sarkar and others, 1982). Accordingly, the deformation fabric shown in figure 30A is rare in natural examples. The initial distribution in figure 30B is also unrealistic. Even if a rock were composed of ellipsoidal particles of uniform shape and size, elliptical sections through them would vary in size because not all of them would pass through the centers of grains. Most sedimentary rocks contain elliptical markers that initially had variable axial ratios and are commonly in random orientation. Figure 30C, therefore, represents a common and realistic sedimentary fabric.

In contrast to these isotropic initial fabrics, many tectonically undeformed rocks contain anisotropic fabrics caused by depositional currents, mass flow, or compaction. This anisotropy is manifested in linear or planar preferred orientation of clasts. Initial anisotropy is difficult to detect after the rock has been naturally deformed (fig. 30D, E), and most methods of strain analysis are not equal to the task. Although the initial fabric in figure 30E is

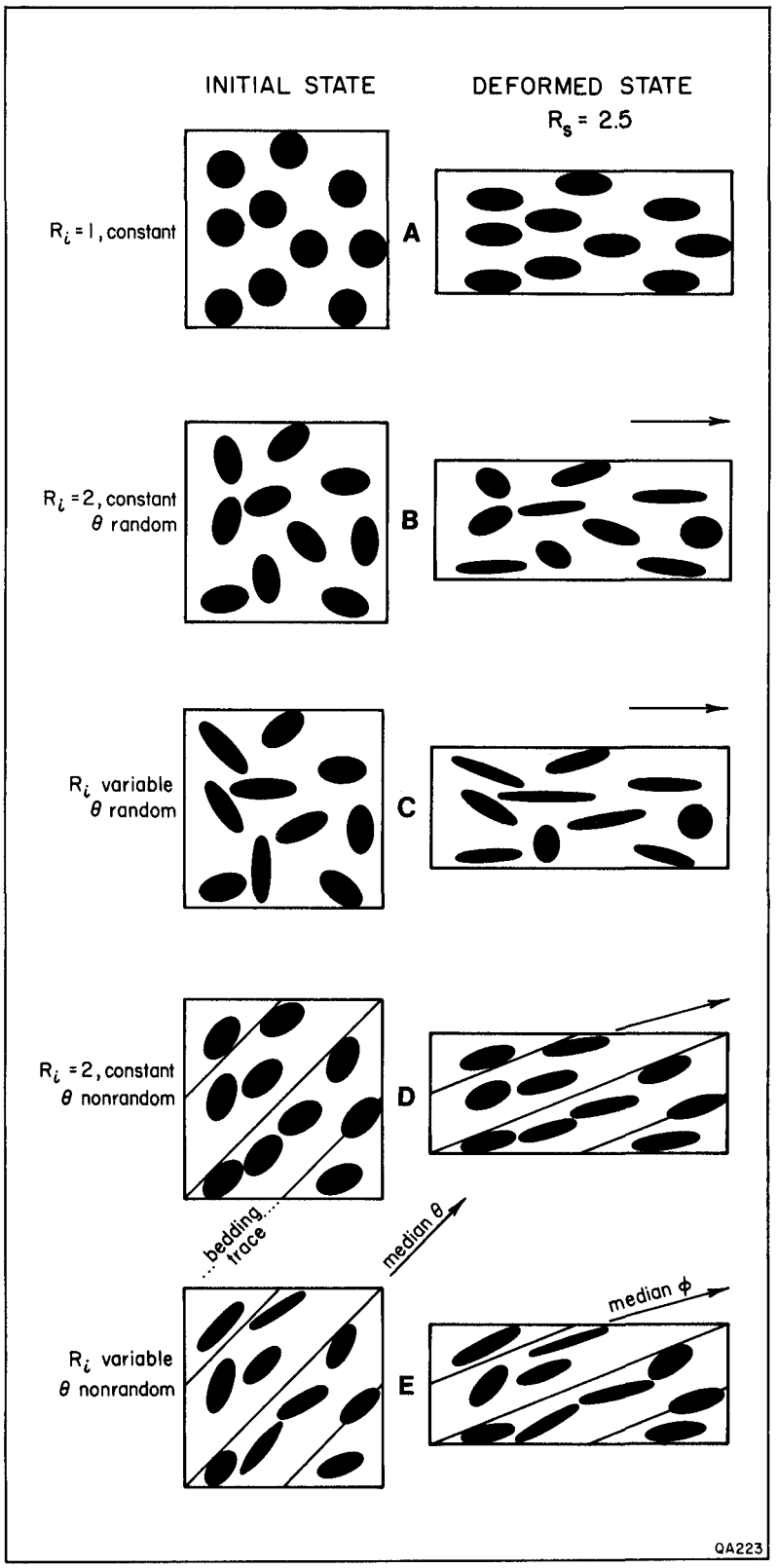

FIGURE 30. Model deformation fabrics produced by homogeneous, plane-strain, pure shear (R_S = 2.5) of ideal populations of circular and elliptical particles (black dots). Initial axial ratios and orientations, designated R_i and θ, respectively, are shown at left. Circular particles (A) each act as strain ellipses. For random initial distributions (B,C), median ϕorientations after strain (shown by arrows) are parallel to principal-extension directions (long side of right rectangles). For nonrandom initial distribution where the particles show bedding-preferred orientation (D,E), the median ϕ, the principal-extension direction, and the bedding trace are not parallel after strain. (A–D adapted from Ramsay, 1976.)

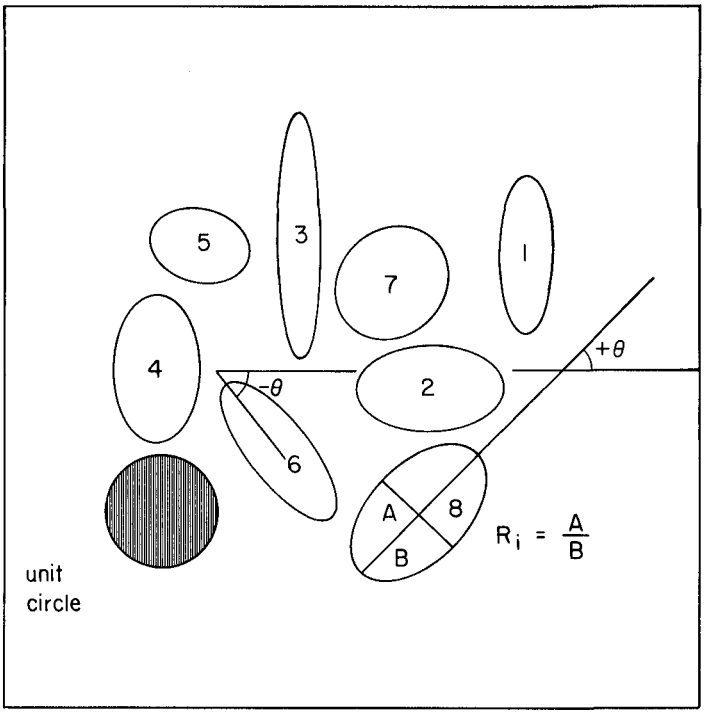

FIGURE 31. Unstrained elliptical particles, numbered arbitrarily for reference, and a unit circle, showing initial axial ratios (R) and θ angles measured from a reference line. Note the sign convention for θ angles. (From Jackson, 1981a.)

probably common in clastic rocks because of compaction, the anisotropy does not always pose problems because either the rock is such that compaction is negligible (as in chemical precipitates and most igneous rocks) or the compactional strain is dwarfed by the tectonic strain.

Ideally, methods of strain analysis should allow one to (1) determine whether strain was homogeneous (where sets of planes that were parallel before deformation remained parallel after deformation) within the scale of the sample, (2) apply the method to particles that were of variable shape and orientation before deformation, and (3) recognize or analyze fabrics that were anisotropic before deformation, such as those containing imbricate clasts.

Methods of strain analysis use data from deformed rocks concerning grain shape and, commonly, grain orientation. The data are mathematically or graphically unstrained to the point where the fabrics are closest to what is assumed to be the original undeformed state—typically ellipses of variable axial ratio and random orientation. The reciprocal of this "unstrain" is inferred to be the amount of finite strain undergone by the rock since its initial undeformed state. Most methods of strain analysis study two-dimensional strains recorded in planes through rock samples. Three-dimensional strains can be estimated by integrating strains calculated in two or more of these planes, as described in the section titled "Three-Dimensional Strains" (p. 60).

The theoretical behavior of elliptical particles during homogeneous strain is well understood (for example, see Ramsay, 1967, p. 202–221; Dunnet, 1969; Elliott, 1970; Dunnet and Siddans, 1971; Matthews and others, 1974; Shimamoto and Ikeda, 1976). In any group of elliptical particles, the shape and orientation of each ellipse can be specified by its axial ratio (R_i) and the angle (θ) between its major axis and an arbitrary direction (fig. 31); note the sign convention for θ angles, proposed by Elliott (1970). After a homogeneous strain of $R_s = 3$, represented by the strain ellipse in figure 32, each ellipse takes on a new shape (R_f) and orientation (ϕ), depending on its initial shape and orientation and the imposed strain (fig. 32).

Particles whose major or minor axes are parallel to the principal extension direction, or X direction, can be divided into four types (Elliott, 1970), whose names are those applied to distorted fossils by Breddin (1956). Particles, such as ellipse 1 in

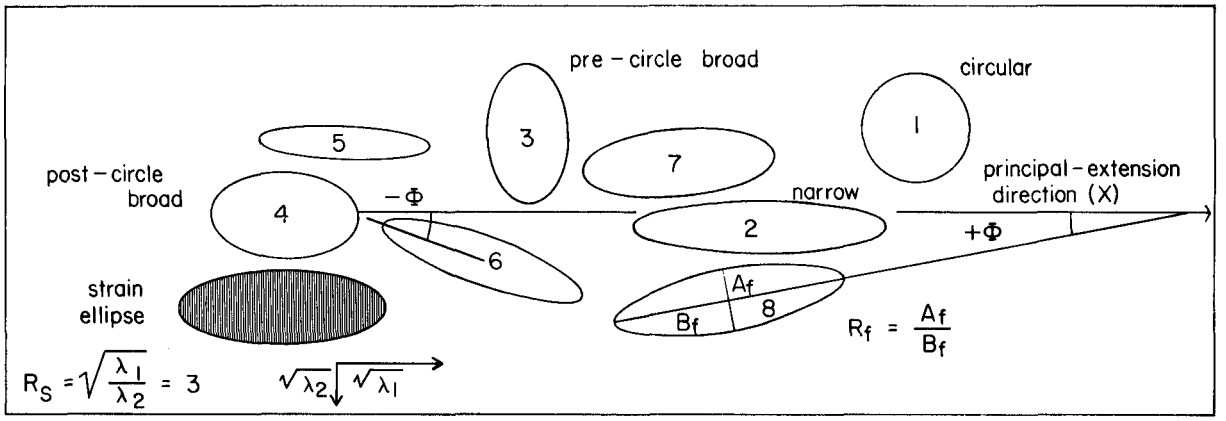

FIGURE 32. The particles of figure 31 after homogeneous pure shear (R_s = 3, illustrated by the strain ellipse), showing finite axial ratios (R_f) and ϕ angles measured from a reference line (here, parallel to the principal-extension direction, X). Note the sign convention for ϕ. Most particles have become thinner and have rotated toward the X direction. But particle 3 has become fatter, particle 1 has become circular, and particle 4 is little changed in shape although its orientation has changed by 90°. (From Jackson, 1981a.)

figure 31, can be distorted to a *circular* form if their initial shape and orientation is an exact reciprocal of the imposed strain (fig. 32). Particles that are "unstrained" to less elliptical shapes are known as *pre-circle broad* (Elliott, 1970), such as ellipse 3. Particles that are "unstrained" to the point where they pass through the circular form and switch the orientation of their major axis, like ellipse 4, are known as *post-circle broad.* Particles that simply become progressively more elliptical because they were originally elongated in the principal-extension direction, like ellipse 2, are known as *narrow*. Apart from these four forms, most particles become more elliptical and rotate toward the X direction with increasing homogeneous strain. As a result, the fluctuation, or range of ϕ angles, invariably decreases with increasing strain, a characteristic exploited by some methods of strain analysis.

Two-Dimensional Strains

Eight sample locations were chosen along the salt core; seven are in the foliated section (termed R-1 by Dix and Jackson, 1982) and one is in the unfoliated (R-2) section (fig. 26). Sample numbers are equivalent to depths in feet. Sample sites were chosen to (1) avoid rock salt of very coarse grain size and, consequently, few grains per specimen, (2) avoid concentrations of disseminated-anhydrite grains, which obscure halite grain boundaries and induce inhomogeneous deformation, and (3) study particular structural positions like hinge zones. From each sample site, three mutually perpendicular planes were cut parallel to the principal planes of strain. The orientation of the foliation (XY) plane was estimated visually, and the first cut was made parallel to it. The orientation of the principal extension (X direction) was determined by strain analysis. Planes parallel to the XZ and YZ planes could then be accurately cut and analyzed. From these analyses, closeness in orientation of the initial cut to the XY plane could be determined, and the results adjusted algebraically or on a Mohr diagram (see "Three-Dimensional Strains," p. 60).

Rock-salt specimens must be prepared with special techniques because of high solubility and very coarse grain size. The effects of high solubility were countered by lubricating the cutting saw with mineral oil rather than water. Grain size varies from an average of 23 × 7 mm in foliated pure rock salt to an average of 11 × 3 mm in foliated rock salt containing more than 5 percent disseminated anhydrite; in the unfoliated (R-2) zone, the mean grain size is 5 to 10 mm (Dix and Jackson, 1982). The coarse grain size was accommodated by using large specimens, either 250 × 100 × 9 mm thick sections or 250 × 100 x >10 mm etched slabs. Thick sections were constructed by polishing a slabbed surface on a grinding wheel with mineral oil; removing the oil with acetone or by heating at least 14 hr at 80° C; mounting on Plexiglas with polyester resin; planing by slow, dry sawing, polishing, and cleaning with acetone; and covering with a thin layer of polyester overlain by a sheet of mylar to ensure smoothness of the upper surface of the polyester. Etched slabs were prepared by lightly hand-rubbing the sawed surface with water to smooth out saw

Table 2. Some methods of strain analysis applied to elliptical particles.*

Method	Principles	Advantages	Disadvantages	References
Harmonic mean (H)	$H = \frac{n}{\sum \frac{1}{R_f}}$	Fast, simple, objective. Accurate to within 10 percent with $R_s > 2.5$ and $R_i < 2.2$, or $R_s > 1.5$ and $R_i < 1.5$. Accuracy increases at high strains and low fluctuation. Measurements of ϕ not required.	Valid only for isotropic initial fabrics. Greatly overestimates R_s in cases of low R_s or high R_i.	Lisle (1977b) Lisle (1979)
Shape-factor grid	Polar graph of 2ϕ against $\frac{1}{2}\log_e R_f$. Qualitative identification of initial fabric from Mellis contoured pattern on graph. Strain estimate based on identification of initial circle point (ICP).	Suitable for isotropic, bedding-parallel, or imbricate initial fabrics. Does not require bedding or cleavage trace.	Serious errors result from misidentification of initial fabric. Less accurate at high R_s and low ϕ.	Elliott (1970) Boulter (1976)
Theta curve (θ)	Rectangular graph of ϕ against $\log R_f$ compared with sets of θ curves, which are loci of equal initial orientation, for different R_s values. Set resulting in most uniform distribution is taken as actual R_s. Computerized method provides unstraining facilities, χ^2 tests for goodness-of-fit.	Objective. Can test data for anisotropy in initial fabrics. Checks for ductility contrast or pressure solution. Does not require bedding or cleavage trace.	Valid only for isotropic initial fabrics. Less accurate at high R_s and low ϕ.	Lisle (1977a) Peach and Lisle (1979)
R_f/ϕ	Rectangular graph of ϕ against $\log_{10} R_f$ compared with sets of R_f/ϕ curves and curves based on 50 percent of data. Computerized methods check symmetry.	Enables R_s to be estimated from initially anistropic fabrics in some cases. Valid for noncoaxial strain.	Later versions designed for some anisotropic initial fabrics, but not necessarily valid. Matching of R_f/ϕ curves is subjective. Data are not used to test method. Less accurate at high R_s and low ϕ. Most versions require bedding or cleavage trace.	Ramsay (1967) Dunnet (1969) Dunnet and Siddans (1971) Roberts and Siddans (1971) Le Theoff (1979) De Paor (1980) Siddans (1980)
Random-point distribution	Produces all-object-separations plot corresponding to strain ellipse. Computerized or entirely graphical methods available.	Records total strain in rock. Method unaffected by pressure solution. Does not require bedding or cleavage trace.	Not suitable for Poisson, or truly random, initial distributions. Valid only for isotropic initial distributions.	Fry (1979) Hanna and Fry (1979)

*After Jackson (1981a).

marks, air-drying to frost the surface by hydrous etching, and coating with a thin layer of 1:1 glycerin-water mixture; the resulting surfaces are transparent but can be marked with fine pencil lines.

On each of the three principal planes at the eight sample sites, the maximum and minimum lengths and the orientation with respect to the side of the slab or section of 100 halite grains were measured, using the conventions shown in figure 32. A total of 2,400 grains were measured. Large grains were preferentially selected in order to omit less deformed subgrains, which record less of the deformation history. Grain boundaries were distinguished from fractures and other surfaces by a combination of the following features: (a) different cleavage directions on opposite sides of the boundary, (b) concentrations of small anhydrite crystals along them; (c) irregular geometry and air bubbles at intersections; and (d) an etched-induced depression along them, commonly rimmed with salt efflorescence.

Many methods of strain analysis are available for the study of elliptical particles. The principal groups of methods, their sources, and their advantages and disadvantages are summarized in table 2. Because no one method is flawless, three

different methods were employed to allow comparisons: the harmonic mean method, the theta curve method, and the shape-factor grid method. The results of these three methods for an XY (little-deformed) section and an XZ (highly deformed) section are compared in figure 33. Only the third method is valid for initially anisotropic fabrics (fig. 30D, E) and was included mainly for this reason. However, as described on p. 60, no evidence for initial anisotropy was found.

The harmonic mean (table 2) of the axial ratios of a set of elliptical particles provides an approximate measure of the strain ratio (R_s). The accuracy of this measure increases with increasing strain ratios and decreasing initial axial ratios (R_i) and fluctuation; it is invariably more accurate than either the arithmetic mean or the geometric mean (Lisle, 1977b). Unlike the other methods, it does not require measurement of grain orientations (ϕ), so both data collection and processing are much faster.

The theta curve method (Lisle, 1977a) is an accurate and completely objective means of determining strain. Its efficiency was greatly improved by the computer program THETA developed by Peach and Lisle (1979). As well as calculating the harmonic mean, the program sequentially unstrains the R_f/ϕ data in small increments by superimposing a coaxial strain whose extension direction is normal to the preferred orientation of the grain distribution. The program calculates the vector mean and the median ϕ angle to check for skewness of data and to find the correct unstraining angle. At each unstraining increment, the distribution is tested for randomness by the χ^2 test until the point of maximum randomness (lowest χ^2 value) is reached. The reciprocal of the unstraining amount is taken to be the amount of finite strain undergone by the analyzed specimen. The lowest χ^2 value also serves as an objective test for the appropriateness of the method. If strain or initial preferred orientation is inhomogeneous, specified χ^2 levels are exceeded, indicating that results should be treated with caution.

Unlike the two previously mentioned methods, Elliott's (1970) shape-factor grid method is largely graphical. It uses exactly the same R_f/ϕ data as the theta curve method. The data are plotted on a special polar grid, the coordinates of each point corresponding to a radius proportional to half the natural log of the R_f ratio and an angle of 2ϕ. After contouring the data by the Mellis method (Mellis, 1942), the initial circle point (ICP) is located, corresponding to an imaginary grain of circular section before deformation. The subjectivity inherent in this locating process is minimized by (1) assuming an initial random distribution unless the pattern of points diverges markedly from a circular or elliptical distribution field; (2) knowing that the ICP must lie along the schistosity trace on the grid; and (3) locating the ICP slightly farther away from the graph's origin than the present center. Heart-shaped or delta-shaped contour patterns would indicate an initial preferred orientation in clastic rocks; here the ICP would again be on a plane of mirror symmetry but on the edge of the field.

The two-dimensional strains obtained by these three methods are summarized in table 3; figures 34 through 37 show the measured data in graphical form. To test the hypothesis that smaller grains in each data sample may represent less deformed subgrains, program THETA was modified slightly to order each sample of 100 grains by size and divide them into two groups of 50 grains separated by the median value; these groups are termed large grains and small grains, whereas the full sample is termed all grains. All strain ratios shown have been corrected by internal checks, described in the section on three-dimensional strains (p. 60).

The harmonic mean invariably overestimates the strain ratio (Lisle, 1977b, 1979). If the strain ratio (R_s) and the initial grain shape (R_i) are known, the error can be calculated. Figure 38A shows the maximum, minimum, and median axial ratio in each data sample before the grains were deformed (referred to as initial grains), as calculated by program THETA. Although the maximum initial grain axial ratio varies widely in each of the principal strain planes (XY, YZ, and XZ), the median value is remarkably constant at $Ri \approx 1.5$. Using estimates of strain ratios from the theta curve method, the expected percentage error, or overestimate of the harmonic mean, can be obtained for each of the principal-strain planes using Lisle's (1979) figure 2. Histograms of these errors are shown in figure 38B. Predictably, because the median value of the initial grain shape is uniform, the error is almost entirely controlled by the strain ratio. Thus, the more highly strained YZ and XZ sections have much lower errors than does the XY foliation plane. This characteristic was exploited in the integration of the results into three dimensions (discussed in the following section, p. 60). These expected errors are similar to the actual discrepancies of the YZ and XZ strain ratios obtained by the harmonic mean and theta curve

Table 3. Two-dimensional strain ratios (R_f) from Oakwood Dome salt core obtained by three different methods (adjusted for internal consistency).

Sample number	Sample depth	Principal plane	Harmonic Mean			Theta Curve			Shape-Factor Grid
			All grains	Large grains	Small grains	All grains	Large grains	Small grains	
	m								
1166	355.4	XY	1.02	1.03	1.07	1.00	1.38	1.03	1.16
		YZ	1.71	1.63	1.74	1.40	1.12	1.33	1.31
		XZ	1.74	1.69	1.87	1.40	1.54	1.37	1.51
1178	359.1	XY	1.14	1.10	1.19	1.00	1.02	1.00	1.18
		YZ	2.08	2.09	2.07	2.00	2.08	1.89	1.96
		XZ	2.38	2.31	2.45	2.00	2.12	1.89	2.31
1233	375.8	XY	1.11	1.06	1.16	1.18	1.20	1.13	1.30
		YZ	2.25	2.26	2.23	1.97	1.94	2.36	2.06
		XZ	2.49	2.41	2.58	2.33	2.33	2.09	2.67
1275	388.6	XY	1.42	1.46	1.37	1.30	1.28	1.21	1.30
		YZ	2.24	2.16	2.33	2.24	2.14	2.18	2.28
		XZ	3.17	3.15	3.19	2.91	2.75	2.63	2.97
1305	397.8	XY	1.42	1.33	1.51	1.15	1.08	1.44	1.20
		YZ	2.13	2.28	1.99	2.12	2.39	1.74	2.29
		XZ	3.02	3.03	3.00	2.44	2.58	2.50	2.75
1315	400.8	XY	1.29	1.34	1.24	1.41	1.47	1.29	1.47
		YZ	2.32	2.21	2.46	2.00	1.97	2.20	2.20
		XZ	3.00	2.95	3.05	2.81	2.89	2.83	3.23
1337	407.5	XY	1.39	1.56	1.21	1.25	1.40	1.13	1.37
		YZ	2.23	2.04	2.48	2.23	2.15	2.40	2.25
		XZ	3.10	3.17	3.00	2.79	3.01	2.72	3.08
1339	408.1	XY	1.25	1.19	1.19	1.23	1.32	1.29	1.31
		YZ	2.53	2.62	2.54	2.43	2.41	2.23	2.62
		XZ	3.16	3.11	3.02	2.99	3.18	2.87	3.44

methods (table 3). Confidence in both methods is therefore increased.

The theta curve method (Lisle, 1977a; Peach and Lisle, 1979) allows the reliability of the unstraining procedure to be statistically tested by the χ^2 test for randomness. Figure 38C summarizes the results of these tests. At least half the unstrained all-grains population exceeds the specified χ^2 limit of 15.5 (for 8 degrees of freedom, 10 classes); the orientation of the grains is not statistically random. This nonrandomness could have two causes: either the grains were not randomly oriented before strain or strain was inhomogeneous at the scale of the specimens. It is demonstrated in the next paragraph that the grains were randomly oriented originally. What about inhomogeneity? After the all-grains population is split into equal numbers of large grains and small grains, almost all the χ^2 values fall below the limit of 15.5 (fig. 38C), indicating the validity of the test. Thus, if treated as separate populations, the large and small grains strained homogeneously. But combined into a single population, the strain is inhomogeneous in half the cases (fig. 38C). Because the finite strains calculated for the all-grains, large-grains, and small-grains populations are similar (table 3), the results obtained for the all-grains populations can be accepted as substantially correct, particularly as they are similar to the results obtained by the shape-factor grid method.

The shape-factor grid method was designed to test for the existence of preferred orientation (nonrandomness) in initial fabrics. Elliott (1970) demonstrated that a clastic rock having an initially unimodal fabric would yield delta-shaped or heart-shaped distributions on the shape-factor grid; such distributions are recognizable after superimposed tectonic strain. These distributions arise because thin ellipses (large axial ratios) are better oriented

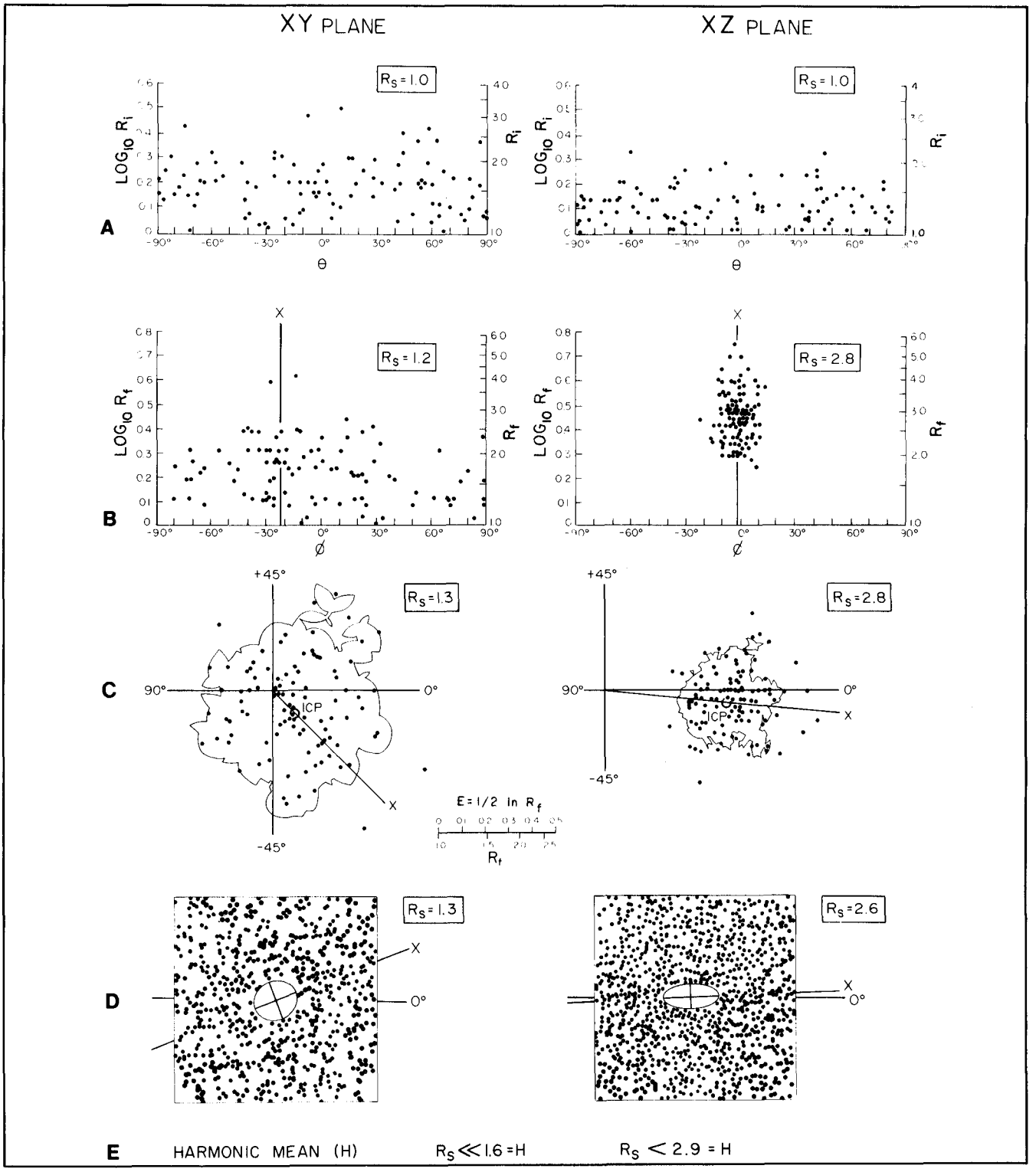

FIGURE 33. Comparison of strain-analysis methods of perpendicular sections (principal planes of strain) through the same specimen (1339) of rock salt in core from Oakwood Dome, showing minimum strain (R_S = 1.2 in XY plane) and maximum strain (R_s = 2.8 in XZ plane). (A) One hundred mathematically unstrained grains on a log R_f/ϕ plot, showing estimated initial fabrics in salt before deformation. (B) One hundred strained grains on a log R_f/ϕ plot, showing the present strains in the salt. (C) One hundred strained grains on the shape-factor grid. The initial circle point (ICP) lies on the X direction and defines the finite strain for the whole sample of grains. (D) Random-point distributions that define ellipses representing whole-rock strain. In these particular distributions, the ellipses are fairly well defined and the strain magnitudes agree with those of the other methods. But in general this method does not define strain ellipses with sufficient accuracy and was not used. (E) Harmonic means provide reasonably accurate strain ratios at high strains (XZ plane) but overestimate strain ratios at low strains (XY plane). (From Jackson, 1981a.)

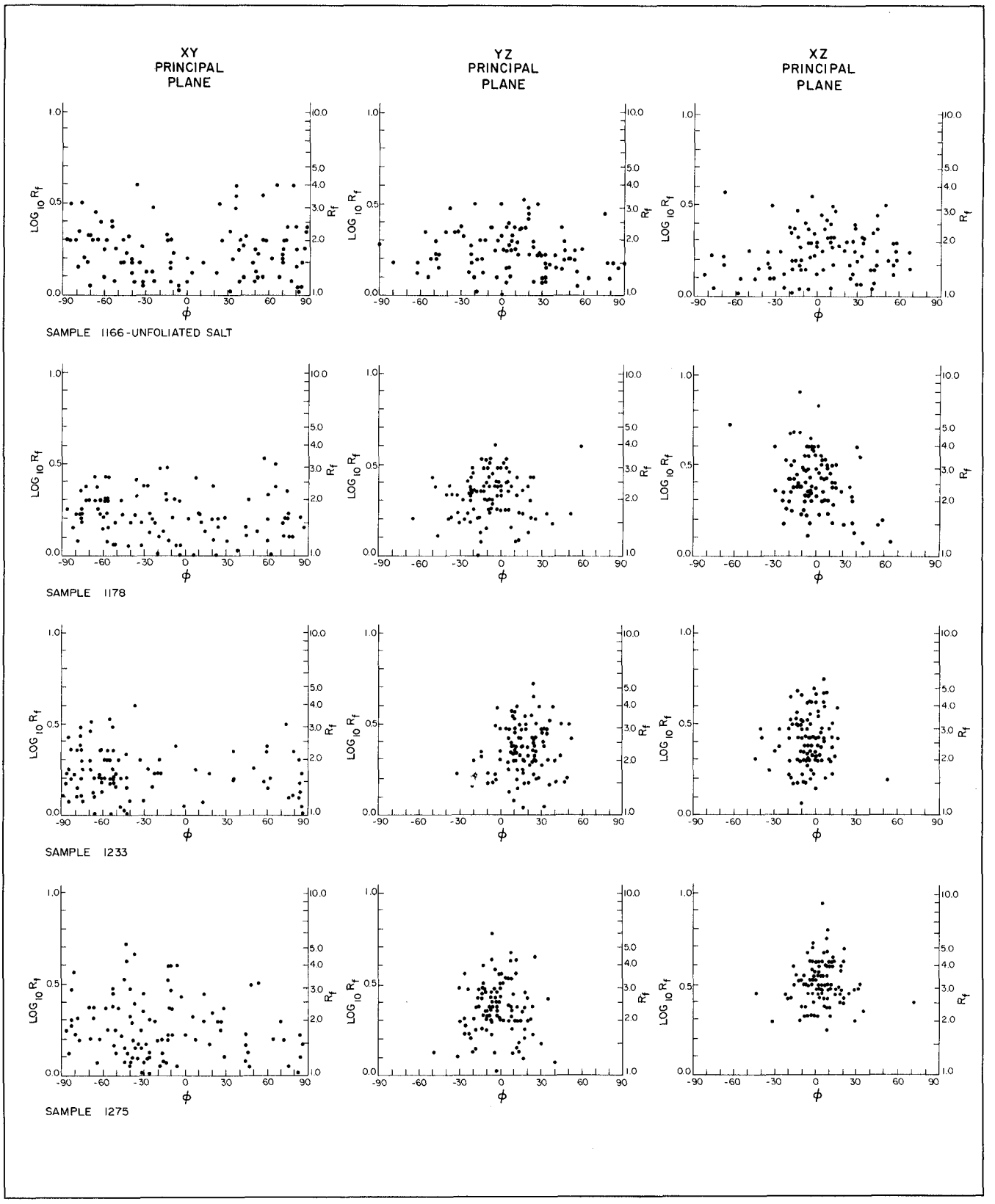

FIGURE 34. Strain states in rock-salt specimens 1166, 1178, 1233, and 1275 on R_f/ϕ plots. Note the increased degree of preferred orientation in the most strained (XZ) sections.

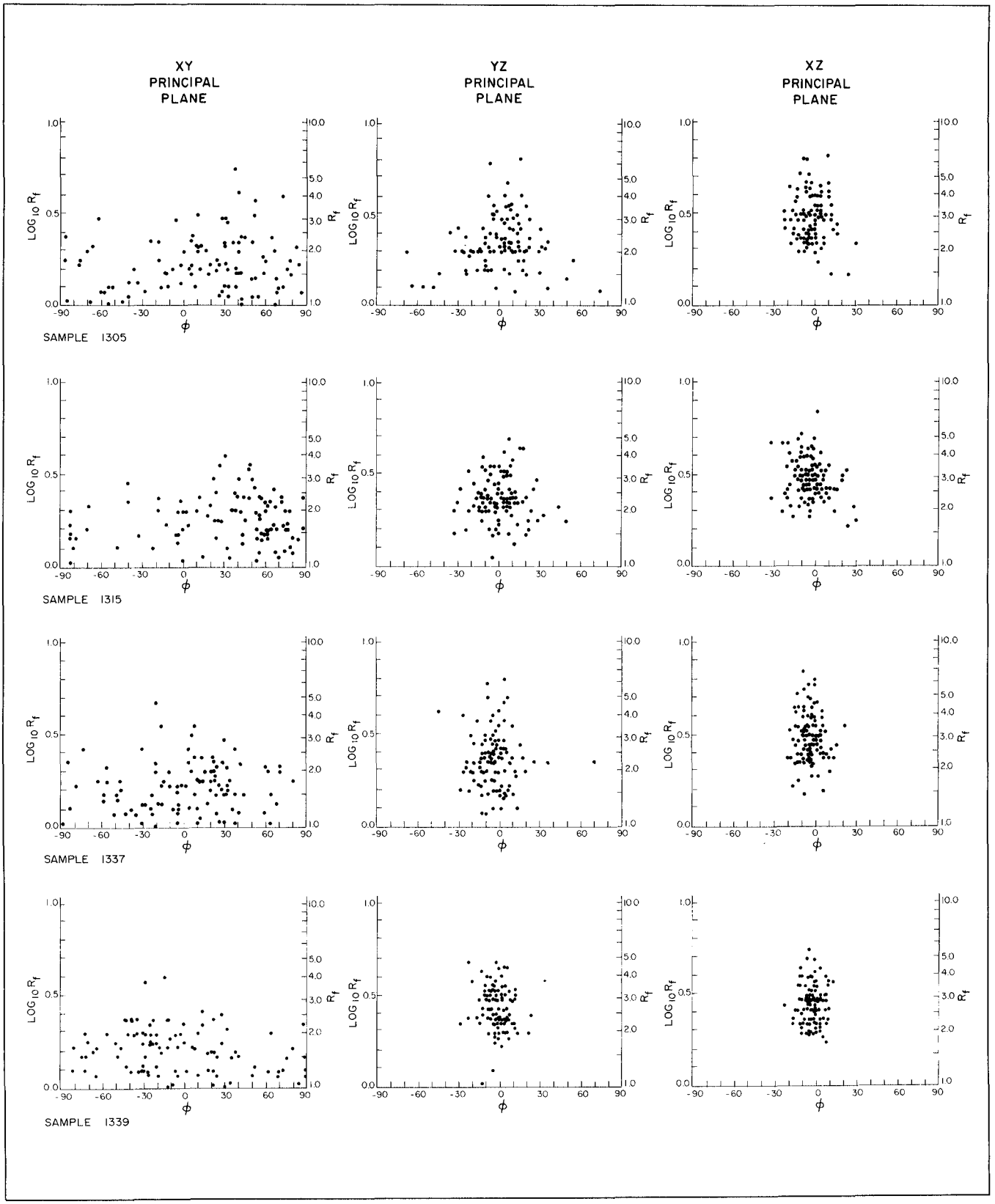

FIGURE 35. Strain states in rock-salt specimens 1305, 1315, 1337, and 1339 on R_f/ϕ plots. Note the increased degree of preferred orientation in the most strained (XZ) sections.

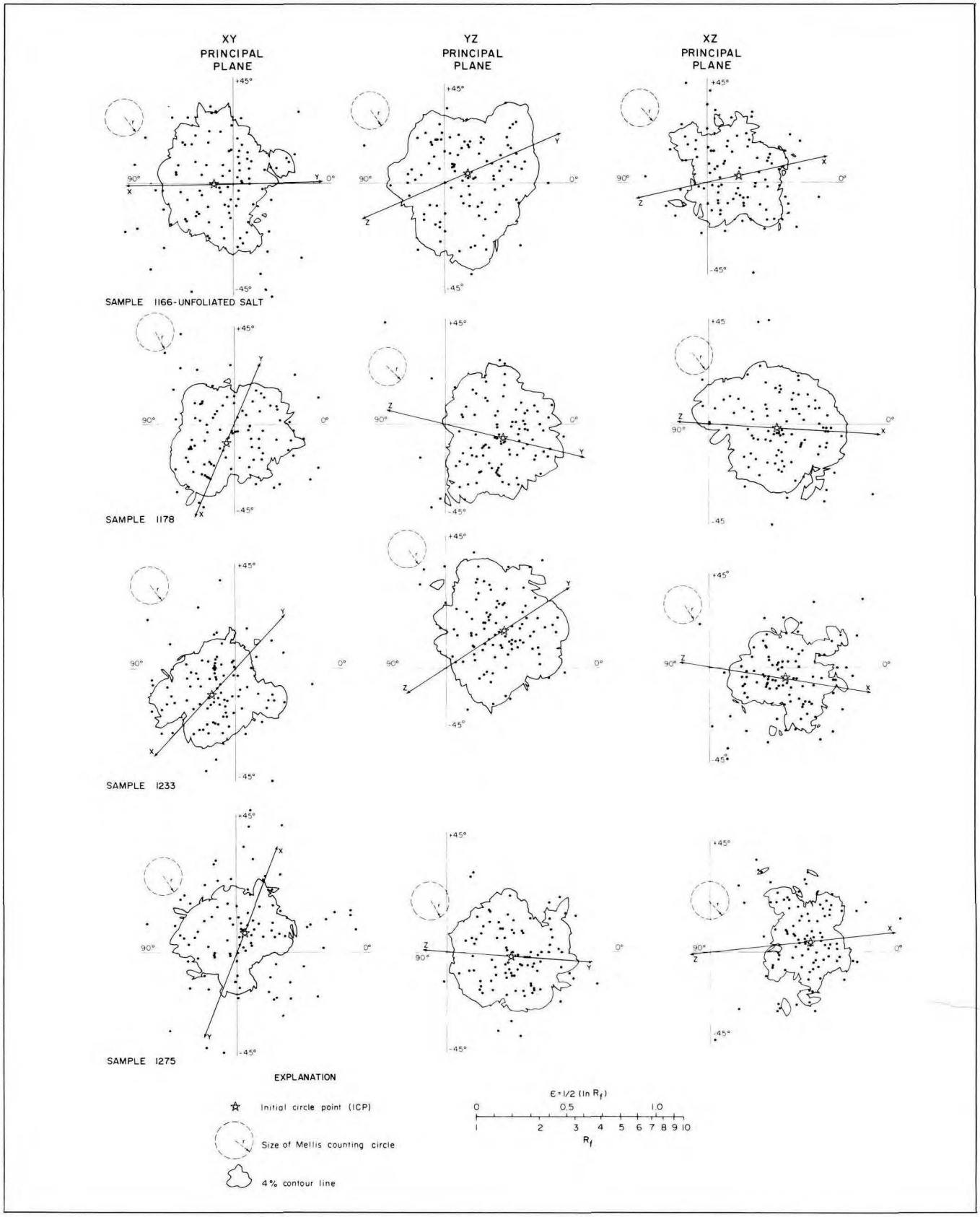

FIGURE 36. Strain states in rock-salt specimens 1166, 1178, 1233, and 1275 on the shape-factor grid.

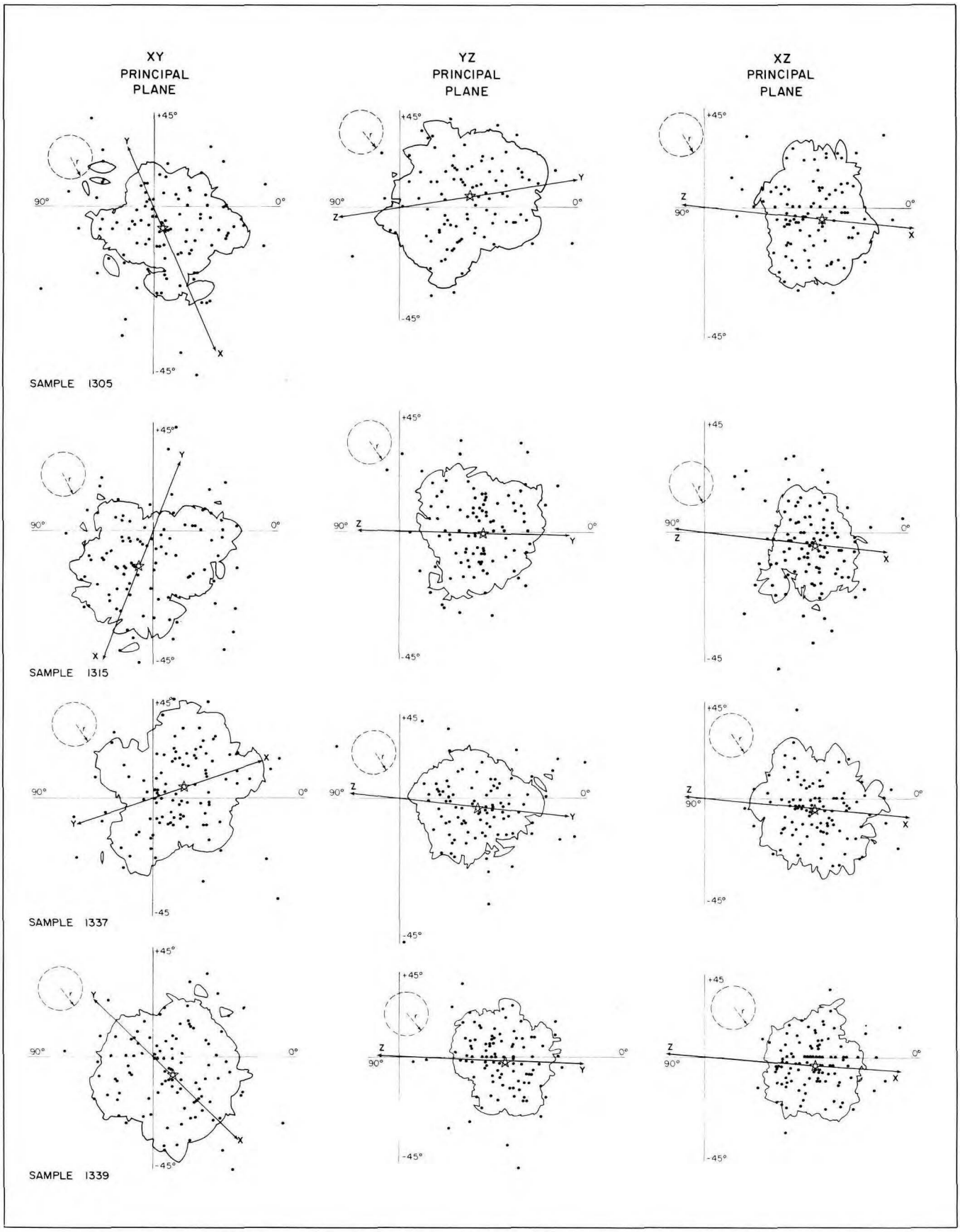

FIGURE 37. Strain states in rock-salt specimens 1305, 1315, 1337, and 1339 on the shape-factor grid. See figure 36 for key and scale.

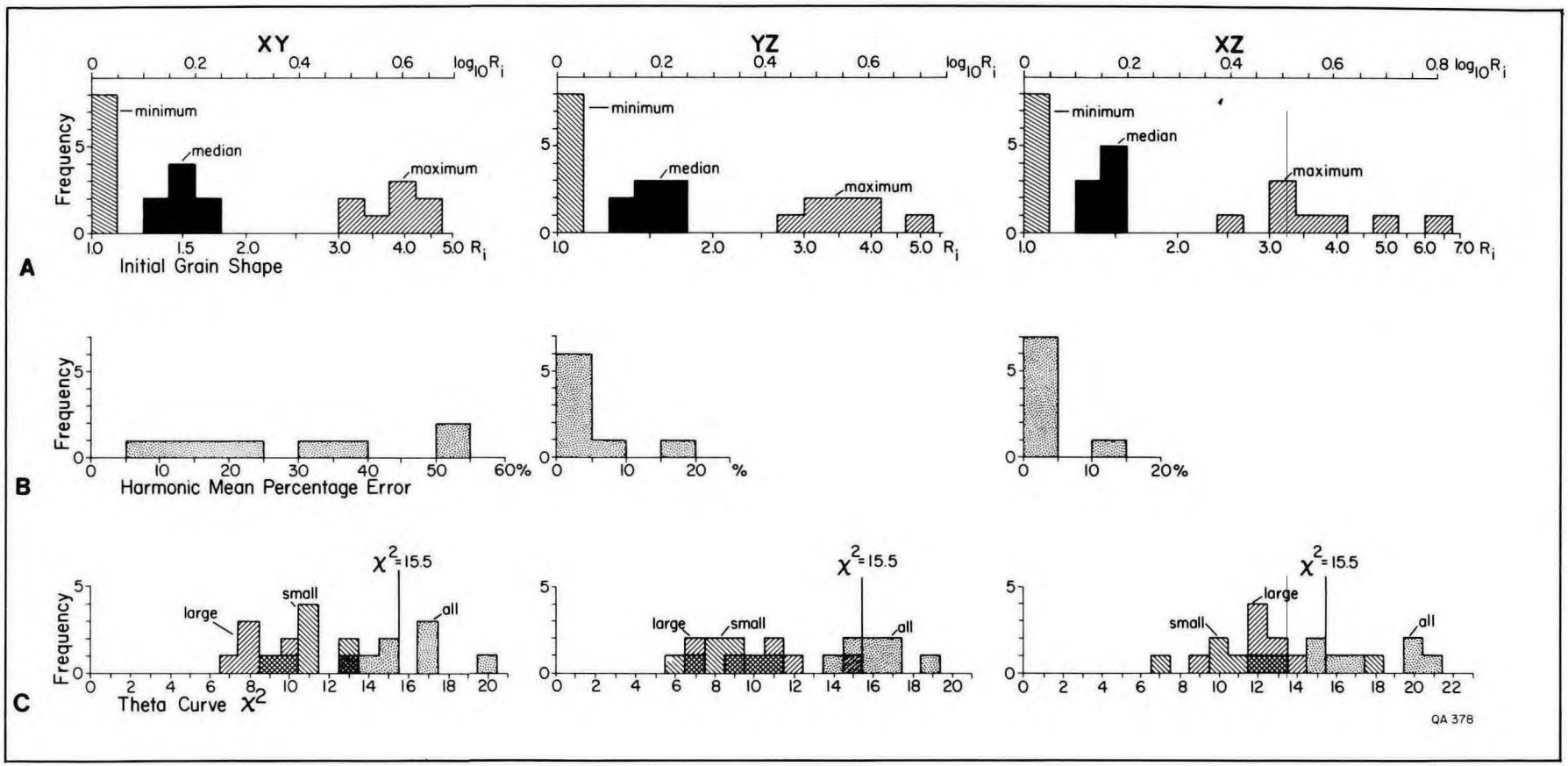

FIGURE 38. Error-analysis histograms of strain data of 2,400 grains in the eight rock-salt specimens. (A) Initial grain shapes calculated by program THETA. The median initial axial ratio was 1.5 in all three principal planes of strain. (B) Percentage overestimate of strain by the harmonic mean method. The error increases with increase of initial grain axial ratios (R_i) and decreases with increase of imposed strain (R_s). (C) χ^2 tests for randomness by program THETA. Half of the all-grains samples exceed the χ^2 limit of 15.5. But if separated into large grains and small grains, almost all samples fall below the χ^2 limit.

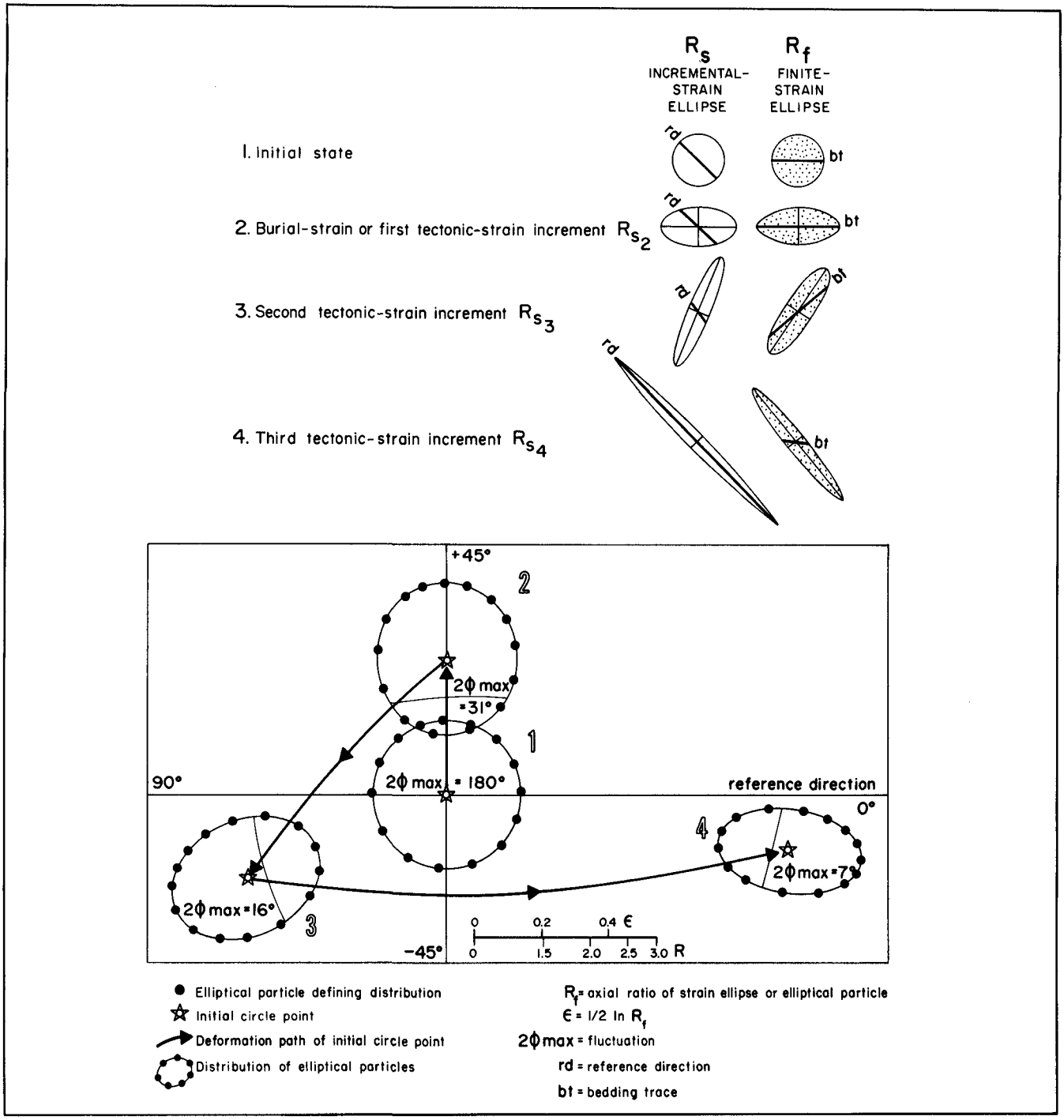

FIGURE 39. Theoretical fabrics produced by homogeneous strains of a model sample of elliptical particles on the shape-factor grid. An initially random distribution, defining a circular field at the graph's origin, is deformed into an elliptical field by burial or tectonic strain. Subsequently, superimposed strains produce only elliptical fields. Strain ellipses show that a finite, or total, strain can be less than even one of the incremental strains that built up the finite strain.

(lower φ range) by currents or mass flow than are fat ellipses (small axial ratios). However, these distributions are produced in clastic sediments rather than in chemical precipitates like rock salt (though they may also be common in igneous rocks that have undergone viscous flow before cooling). Thus, this distribution is inapplicable to rock salt, even though some of the plots suggest deltas (for example, sample 1315 XY in fig. 37). Nor can deltoid distributions result from the effects of either compactional strain or superimposed tectonic strain, or both. Figure 39 shows that an initially

random distribution, which is circular, can only produce elliptical distributions, no matter how many times the rock is homogeneously strained and regardless of whether the rock had a pretectonic burial strain. Thus, only elliptical distributions are possible in evaporites, and it was on this basis that strain values were obtained from the shape-factor grid. The absence of initial preferred orientation is also indicated by the close similarities between the calculated initial grain shapes for differently oriented XY, YZ, and XZ sections (all have median axial ratios of 1.5) and analogous similarities between χ^2 values (fig. 38A,C). Differently oriented sections would be expected to yield different initial grain shapes and different χ^2 values if there were initial anisotropy. For these reasons, the possibility of predeformational nonrandomness in initial fabrics can be discounted in this strain analysis.

Three-Dimensional Strains

For each of the eight samples, two-dimensional strains were calculated for three mutually perpendicular surfaces by the methods discussed in the previous section (p. 49). Each trio was combined to yield three-dimensional strains for each sample. Because each surface was parallel, or nearly parallel, to a principal plane of strain, the mathematical procedure was simple. The strains estimated in misaligned surfaces were adjusted to conform to principal planes, either graphically by using a Mohr diagram (Ramsay, 1967, p. 69–74) or mathematically by using equation 3-49 of Ramsay (1967, p. 69).

Because the measured surfaces are parallel to principal planes of strain, internal checks on the errors are available, according to the relations X.Y.Z. = 1 and X/Y.Y/Z = X/Z (where X, Y, and Z are the lengths of the maximum, intermediate, and minimum principal axes of the strain ellipsoid). The measured strains were adjusted to conform to these relations by exploiting the strengths of each method. The harmonic mean method is known to be more accurate at higher R_s values (Lisle, 1977a, 1979). Thus, the XY ratio was adjusted to conform to the higher strain ratios, so that XY = XZ/ YZ. The other two methods are more accurate at low R_s values, where the fluctuation is high. Thus, both XZ and YZ values were adjusted by the same proportion, so that XZ/YZ = XY. Table 3 shows two-dimensional strain values after adjustment.

Three-dimensional strain values are shown in table 4, which also defines strain parameters. These results are graphically summarized in a deformation plot, the Flinn diagram (fig. 40; compare Flinn, 1978), which shows the average strains measured by all three methods for the all-grains population.

All the strains lie in the flattening field of deformation, in which both the large and intermediate principal axes of strain, X and Y, have extended. Figure 41 compares the results obtained by the three different methods; each method forms an apex for each of the eight triangles. The areas of the triangles (a measure of the discrepancy between methods) decrease with increasing strain, or distance away from the origin of the graph. This is probably due to the logarithmic nature of the two coordinates. In general the shape-factor grid method yields strains having higher k values (ln a/ ln b). The harmonic mean value for unfoliated salt 355.4 m deep (specimen 1166) can be ignored because of severe overestimation by this method at low levels of R_s strain. In general, the methods show reasonable agreement and yield the same trend.

Figure 42 compares the strains measured by the harmonic mean method for the three sample groups of different-sized grains: all, large, and small grains. For ease of comparison, strain is given as natural strain (E_s). Natural strain provides a measure of the overall strain magnitude in all three dimensions, unlike, say, maximum percentage shortening parallel to Z. Here, again, there is good agreement between groups. Each trio of values, except for the lowest strain (nearest origin of graph), is spread out roughly parallel to contours of equal natural strain. Thus, the smaller grains show magnitudes of strain similar to those of the larger grains in any one specimen (except the least deformed). This indicates that contrary to expectation, the smaller grains are not subgrains formed by recovery of larger, more deformed grains. They are simply smaller grains, with no evidence of a different strain history. Nevertheless, subgrains may be present at a scale smaller than that of the measured halite grains.

Variations in strain magnitude with depth are shown in figure 43. The three straight lines obtained by linear regression indicate the general trend for each method. The goodness-of-fit to a straight line was examined using the correlation coefficients (r values) for different levels of significance (Fisher and Yates, 1963, their table 8). The significance of the slope of the regression line was examined by the F test and by techniques for analysis of variance (Draper and Smith, 1967, p. 24–32; Davis, 1973, p. 106–114, p. 192–217). With regard to shortening parallel to Z (fig. 43A), all seven specimens of

Table 4. Three-dimensional strain parameters from Oakwood Dome salt core obtained by three different methods.

Sample number		1166	1178	1233	1275	1305	1315	1337	1339
THETA CURVE	All grains								
	ln a	0.000	0.000	0.166	0.262	0.140	0.344	0.223	0.207
	ln b	0.336	0.693	0.678	0.806	0.751	0.693	0.802	0.888
	k	0.000	0.000	0.244	0.325	0.186	0.500	0.278	0.233
	%Z	10.6	37.0	39.8	46.5	42.2	43.8	45.6	48.4
	ν	1.000	1.000	0.608	0.509	0.686	0.333	0.565	0.622
	E_3	-0.112	-0.462	-0.507	-0.625	-0.548	-0.576	-0.609	-0.662
	E_s	0.274	0.566	0.632	0.787	0.678	0.747	0.762	0.823
THETA CURVE	Large grains								
	ln a	0.322	0.020	0.182	0.247	0.079	0.385	0.337	0.278
	ln b	0.113	0.732	0.663	0.763	0.870	0.677	0.765	0.878
	k	2.84	0.027	0.275	0.323	0.091	0.569	0.441	0.317
	%Z	16.7	39.0	39.5	44.6	45.5	44.0	46.3	49.2
	ν	-0.479	0.947	0.569	0.512	0.833	0.275	0.388	0.519
	E_3	-0.183	-0.494	-0.503	-0.591	-0.607	-0.580	-0.622	-0.677
	E_s	0.319	0.606	0.629	0.745	0.745	0.760	0.799	0.853
THETA CURVE	Small grains								
	ln a	0.030	0.000	0.122	0.191	0.367	0.254	0.125	0.251
	ln b	0.285	0.639	0.737	0.777	0.551	0.787	0.875	0.804
	k	0.104	0.000	0.166	0.245	0.665	0.323	0.143	0.312
	%Z	18.1	34.6	41.3	44.1	38.7	45.6	46.5	46.2
	ν	0.812	1.000	0.715	0.606	0.201	0.512	0.750	0.524
	E_3	-0.200	-0.425	-0.533	-0.582	-0.489	-0.609	-0.625	-0.620
	E_s	0.246	0.522	0.657	0.725	0.653	0.768	0.771	0.779
HARMONIC MEAN	All grains								
	ln a	0.017	0.135	0.105	0.349	0.350	0.255	0.329	0.222
	ln b	0.538	0.732	0.809	0.806	0.754	0.844	0.802	0.928
	k	0.032	0.184	0.129	0.432	0.464	0.302	0.411	0.240
	%Z	30.6	41.3	43.7	48.0	46.17	47.7	47.5	50.0
	ν	0.938	0.689	0.771	0.397	0.366	0.536	0.417	0.613
	E_3	-0.365	-0.533	-0.574	-0.654	-0.620	-0.648	-0.644	-0.693
	E^s	0.446	0.660	0.707	0.838	0.806	0.813	0.823	0.863
HARMONIC MEAN	Large grains								
	ln a	0.034	0.100	0.062	0.381	0.283	0.291	0.442	0.172
	ln b	0.490	0.738	0.818	0.768	0.825	0.791	0.713	0.963
	k	0.069	0.135	0.076	0.496	0.343	0.368	0.619	0.179
	%Z	28.7	40.9	43.2	47.2	47.5	46.4	46.3	50.3
	ν	0.871	0.762	0.859	0.337	0.489	0.462	0.235	0.696
	E_3	-0.338	-0.526	-0.566	-0.639	-0.644	-0.624	-0.622	-0.699
	E_s	0.415	0.647	0.695	0.828	0.814	0.792	0.824	0.865
HARMONIC MEAN	Small grains								
	ln a	0.072	0.171	0.149	0.314	0.411	0.217	0.190	0.174
	ln b	0.553	0.726	0.801	0.847	0.688	0.899	0.909	0.932
	k	0.129	0.236	0.186	0.371	0.598	0.241	0.209	0.186
	%Z	32.5	41.8	44.2	48.8	44.9	48.9	48.8	37.5
	ν	0.771	0.618	0.686	0.459	0.252	0.612	0.654	0.686
	E_3	-0.393	-0.541	-0.583	-0.669	-0.596	-0.671	-0.669	-0.470
	E_s	0.484	0.674	0.723	0.849	0.785	0.837	0.831	0.841

(Continued on next page)

Sample number		1166	1178	1233	1275	1305	1315	1337	1339
SHAPE-FACTOR GRID	ln a	0.145	0.163	0.262	0.262	0.185	0.384	0.312	0.273
	ln b	0.267	0.673	0.720	0.825	0.828	0.788	0.811	0.962
	k	0.544	0.243	0.364	0.318	0.224	0.487	0.384	0.284
	%Z	20.2	39.5	43.3	47.2	45.9	48.0	47.5	51.9
	ν	0.295	0.609	0.466	0.517	0.634	0.345	0.445	0.558
	E_3	-0.226	-0.503	0.567	-0.637	-0.614	-0.654	-0.644	-0.732
	E_s	0.296	0.627	0.719	0.802	0.763	0.845	0.820	0.917

e_1, e_2, e_3 = elongations parallel to X, Y, Z
ln a and ln b = natural logs of $a = (1 + e_1)/(1 + e_2)$ and $b = (1 + e_2)/(1 + e_3)$
$k = \ln a / \ln b$ = Flinn parameter
$\%Z = -e_3 \cdot 100$ = percentage shortening parallel to Z
$\nu = (1 - k)/(1 + k) = (2E_2 - E_1 - E_3)/(E_1 - E_3) = (\ln b - \ln a)/(\ln b + \ln a)$ = lode factor, where E_1, E_2, and E_3 are logarithmic strains equal to $\ln(1 + e_1)$, $\ln(1 + e_2)$, and $\ln(1 + e_3)$
$E_s = {}^{2/3}[(\ln a)^2 + (\ln b)^2 + (\ln a \cdot \ln b)]^{-1/2}$ = natural strain

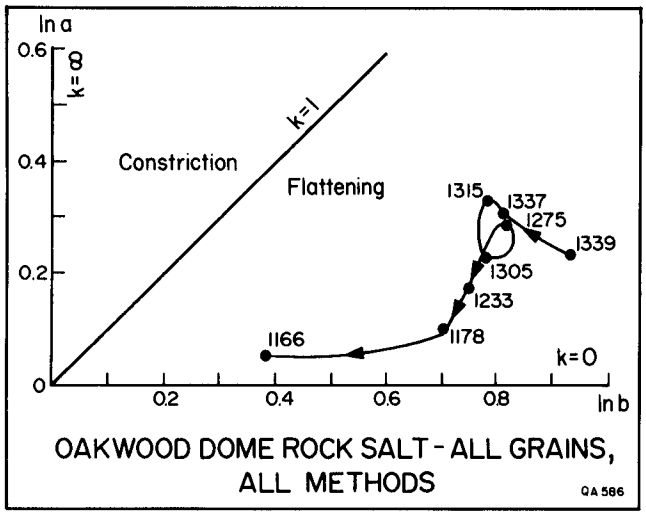

FIGURE 40. Flinn diagram showing the mean strain in the all-grains samples of halite recorded by all three methods of strain analysis. Numbers refer to specimen numbers, equivalent to depth in feet. Line connecting points indicates upward trend in strain states. All samples lie in the flattening field of strain.

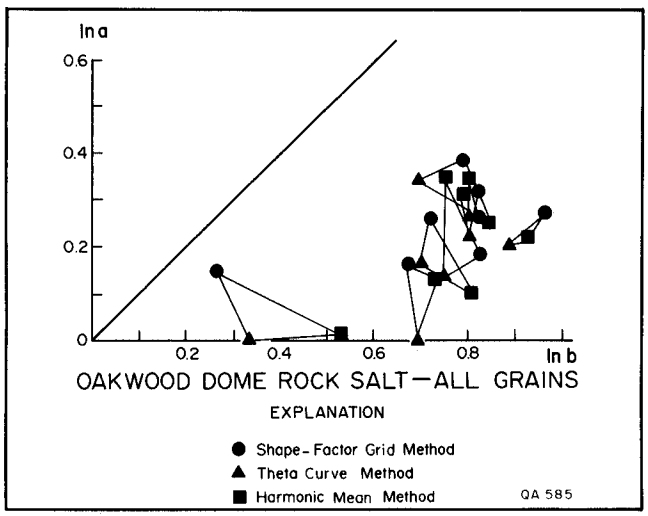

FIGURE 41. Flinn diagram showing triangles of discrepancy between results obtained by different methods of strain analysis on the same specimen. The lowermost harmonic mean value can be ignored because strain in this specimen is too low for accurate results by this method.

foliated rock salt yield strains that show a significant decrease in shortening with decreasing depth using each of the three methods. Both the linearity and slope of the regression lines are significant. Mean shortening decreases from around 50 percent in the deepest foliated salt to around 35 percent in the shallowest foliated salt. The unfoliated salt has low strains, averaging 15 percent (ignoring the unrealistic harmonic mean value). These strains in the rock fabric are too weak to be visible to the eye. Strain magnitude, as expressed by natural strain (E_s), gives virtually identical results (fig. 43B).

The parameters k and ν are alternative measures of the relative dominance of flattening (oblate strain ellipsoids with $k = 0$, $\nu = +1$) versus constriction (prolate strain ellipsoids with $k = \infty$, $\nu = -1$). Figure 40 shows that all strains fall within the flattening field, where $0 < k < 1$ and $1 > \nu > 0$. Do k and ν vary systematically with depth? Figure 43C shows the statistically tested regression lines for each of the three methods. Two methods show significant trends of decreasing k values with decreasing depth; the third method shows no correlation between depth and k value. These results suggest

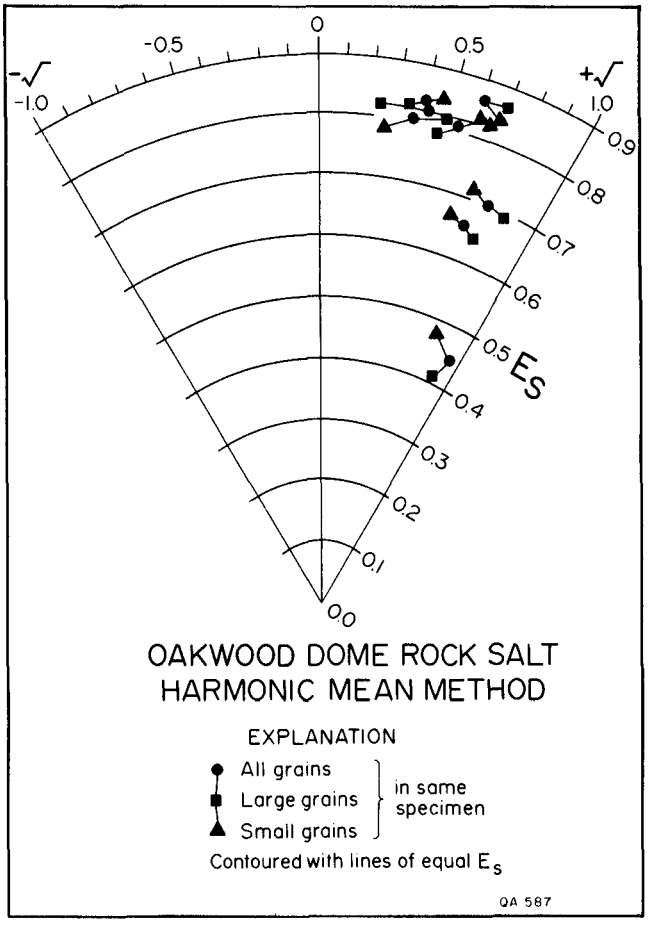

FIGURE 42. Hsu diagram (compare Hossack, 1968) showing strain states in the three different grain-size populations: all grains, large grains, and small grains. Natural-strain intensity (E_S) increases outward from origin of plot. Among the moderately to strongly deformed specimens, all three grain-size populations show similar levels of strain.

that the shallower strains were characterized by more flattening and less constriction than were the deeper strains. The significance of these trends is discussed in the next section.

Orientations of the principal strains at various depths in the foliated-salt core are shown in figure 44. According to the conventions described in the section titled "Defining Orientation in Nonoriented Core" (p. 40), the XY foliation plane has been assumed to dip south toward the axis of Oakwood Dome. The uniform dip of the foliation plane is indicated by the small variation in plunge of its pole, the Z axis. The XY foliation plane steepens with depth down to 400.8 m (specimen 1315) below which it is progressively less steep with depth. The depth of 400.8 m (specimen 1315) corresponds to the axial surface of an overturned, inclined synform (fig. 26). No significance is placed on this coincidence for two reasons. First, examination of about 65 more-closely-spaced, direct readings of the foliation dip in the core (appendix to Dix and Jackson, 1982), show no such trend. Second, the overlying antiform shown in figure 26 indicates no analogous change in dip of foliation at a depth of 389.5 m (specimen 1278). Within the foliation plane, the principal extension axis (X), which marks the mineral lineation direction, ranges from downdip at a depth of 407.8 m (specimen 1338) to strongly oblique at depths of 375.8 m (specimen 1233) and 400.8 m (specimen 1315) (fig. 44). Below 400.8 m, the foliation plane becomes less steep with depth. The predominantly downdip orientation of the lineation within the foliation plane is compatible with the hypothesis that tongues of rock salt rise predominantly updip and, presumably, outward from a central core. The oblique lineation at some points (for example, 375.8 m [specimen 1233] and 400.8 m [specimen 1315]) suggests that a significant component of oblique flow has also occurred, as was noted in Winnfield, Weeks Island, and Grand Saline Domes in the section titled "Assessing Large-Scale Flow Patterns from Linear Elements" (p. 33).

SIGNIFICANCE OF MEASURED STRAINS

Actual Strains and Measured Strains

The measured strains in Oakwood rock salt are also almost certainly smaller than the actual strains that affected the rock. The three methods employed all yield the minimum finite strain. As shown in figure 39, the finite strain, or end result of superimposing several strain increments, is less than the sum of the incremental strains, apart from cases where the superimposed strains are coaxial. The actual strain can only be determined if the deformation path can be deduced, as from synkinematic fiber growths, for instance.

A second reason for lower strains is the probability of hot working or synkinematic recrystallization. The buildup of dislocations within crystals undergoing plastic strain causes strain hardening. Several strain-softening mechanisms counteract this buildup: (1) faster dislocation climb relative to dislocation buildup, promoted by high temperatures and low strain rates; (2) recovery by subgrain polygonization; and (3) recrystallization, or formation of new grains. Recrystallization can be divided into synkinematic recrystallization, which

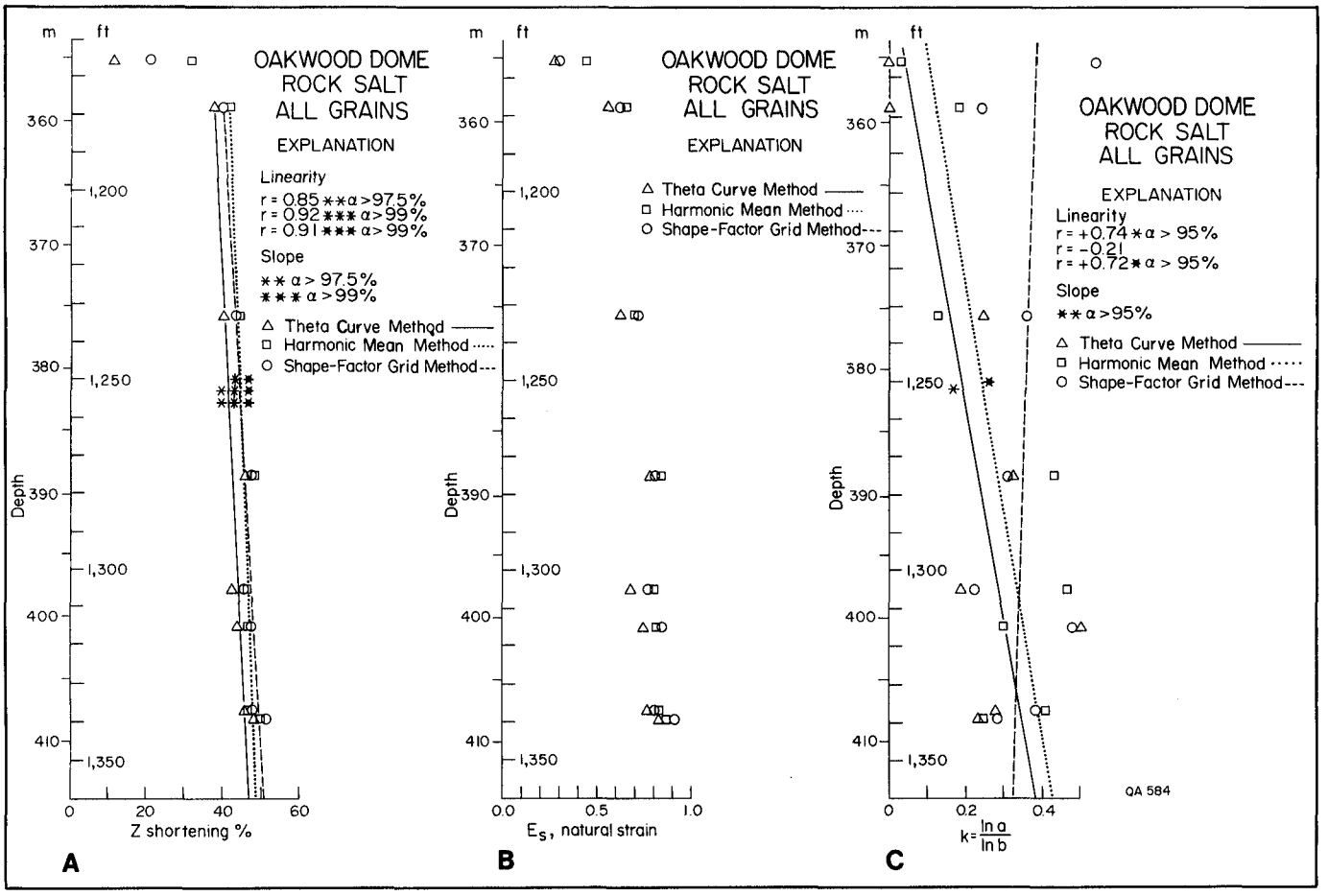

FIGURE 43. Variations in strain magnitude and type with depth. Regression lines for foliated rock salt have been statistically tested for linear fit to data and slope of line. Uppermost data points are from unfoliated rock salt. (A) Percentage shortening parallel to Z. (B) Natural strain. (C) Ratio of constriction to flattening, or k value. Strain magnitudes and k values decrease upward significantly.

takes place during deformation under directed stress, and annealing recrystallization under non-directed stress.

Recrystallization generally occurs at higher temperatures than recovery, at homologous temperatures of 0.3 to 0.7; this range corresponds to an actual temperature range of 50°C to 480°C for recrystallization of halite. The crest of Oakwood salt stock is currently at a temperature of about 42°C; a temperature of 50°C is unlikely to prevail at depths shallower than 630 m, some 220 m deeper than the borehole (table 5). Temperature at the base of the Oakwood salt stock is estimated to be about 200°C. Thus, whereas the crestal rock salt is now too cool to recrystallize, it is likely to have been hot enough for syntectonic recrystallization during most of its rise up the diapir stem. Because folds provide ample evidence for the existence of geologically effective differential stress, the Oakwood rock salt has almost certainly recrystallized synkinematically.

A mechanism for forming preferred orientation by this type of recrystallization in equant minerals like pyroxene and quartz—and halite—has been identified by observations of experimental deformation (Etheridge and Kirby, 1977; Kern, 1977; Tullis, 1977; Ross and Nielsen, 1978) and natural deformation (Marjoribanks, 1976; Rousell, 1976). The syntectonic new grains formed preferentially from more-highly-strained grains, which tend to be less randomly oriented (Vernon, 1975; White, 1976). The probability of synkinematic recrystallization in Oakwood Dome implies that the existing grains have lost the memory of earlier deformation. In contrast, structures such as bedding and desiccation cracks have extremely long memories because they cannot be destroyed by recrystallization. For example, paleoshrinkage cracks in gneissose halite from a ramp shear zone in the Boulby potash mine, England, (Talbot and others, 1982), show distortions equivalent to strain

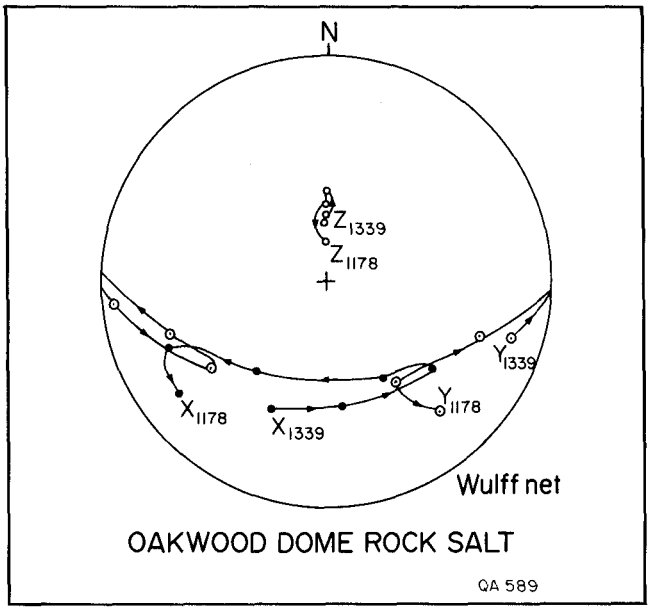

FIGURE 44. Equal-angle stereographic projection of the orientations of the principal axes of strain (X, Y, and Z), assuming a southward dip of the XY foliation plane. Arrows connecting points indicate upward trend of orientations. The X direction of maximum extension varies widely, although the XY plane containing X dips uniformly.

ratios of about 12 to 1 (C. J. Talbot, personal communication, 1983). Yet the maximum axial ratio of these halite grains is only 4 to 1. This is because once a grain reached this ratio, it recrystallized into smaller, more equant grains. These smaller grains also eventually formed another generation after sufficient strain. About four generations of successively smaller grains are inferred. The mineral grains only record the last few increments of strain. Similar observations have been made at Kuh-e-Namak namakier, Dashti Province, Iran (Talbot, 1979, 1981).

The present analysis, therefore, is based on minimum finite strains in the rock salt, which record only the late deformation history of salt emplacement.

Model Strains and Measured Strains

Oakwood rock salt shows two upward trends through the foliated section (96 percent of the salt core): (1) decreasing natural strain and maximum shortening and (2) decreasing k values, or increasing flattening/constriction ratios. How do these trends compare with those observed in experimentally modeled diapirs?

The only quantified internal strains in diapir models known to the writer are those in models by Dixon (1975). His models were of circular or elliptical salt diapirs and ridgelike gneiss diapirs. Both types are qualitatively similar, apart from higher strains in the less viscous model salt. But only the ridgelike geometry lends itself to quantification of the internal strains. Dixon's models of gneiss domes were studied as two-dimensional plane-strain structures from which qualitative three-dimensional strains during radial flow can be deduced. Constriction strains in the diapir trunk result from radial tangential shortening; they were replaced upward by flattening strains in the diapir crest, which extended tangentially beneath the crest's uplifted overburden. Plotted on a graph of depth versus k value, these strain states would show a trend of decreasing k values upward. This same trend was observed in Oakwood Dome (fig. 43C).

The upward trend of decreasing strain with decreasing depth toward the crest of Oakwood Dome (fig. 43A,B) has no counterpart in experimental models. But the crest of Oakwood Dome is unlike that of the experimental models in at least one respect. Structural evidence for truncation of the salt stock was given in the section on geometric analysis (p. 40). Fluid-inclusion studies and the microstructure of the rock-salt/cap-rock contact (Dix and Jackson, 1982) suggest that ground-water dissolution was the agent for this truncation. Thus, we should compare the present crest of Oakwood Dome not with the crests of Dixon's diapirs but with lower zones in his models. In Dixon's models WD-2 and WD-8, whose overhangs were smaller and larger, respectively, than that of Oakwood Dome, a neutral-strain zone was situated at depths of 17 to 48 percent of diapir height, where strains were minimal ($1+e < 1.1$). Below and above this neutral-strain zone, the strains increased downward and upward, respectively. By approximate analogy with this model, therefore, the Oakwood crest would have truncated to a present level *below* this neutral-strain zone.

It should be stressed that this comparison can only be approximate because (1) the model structure is ridgelike, (2) the viscosity of the buoyant layer is modeled after gneiss, which is stiffer than its overburden (probably unlike salt), and (3) internal strains in Oakwood Dome are much less homogeneous, as evidenced by the existence of salt tongues. Nevertheless, this model is the nearest analogy we have to the combined trends of upward decrease in both strain magnitude and k value.

Table 5. Probable physical conditions existing during Oakwood Dome diapirism.

Depth		Lithostatic pressure[a]	Temperature[b]	Pressure difference[c]
	m	MPa	°C	MPa
Crest	355[d]	7.2	42	negative buoyancy
Neutral buoyancy level	890	18.7	57	0
Base	5,500[e]	113.0	197	9.0

[a] Based on mean overburden shale density of 2,075 kg/m^3 at depth of 355 m and mean salt density of 2,200 kg/m^3 (Gussow, 1968).

[b] Based on geothermal data from 73 wells around Oakwood Dome (Law Engineering and Testing Company, 1983) and on mean surface temperature of 19.5°C (Kier and others, 1977).

[c] Between top of stock and depth listed (due to buoyancy), based on mean salt density of 2,200 kg/m^3 and mean shale densities of 2,200 kg/m^3 at 890 m depth and 2,400 kg/m^3 at 5,500 m depth. Carbonate units interbedded with shale around dome cause actual pressure difference to be somewhat higher than these values, which are based on an all-shale sequence.

[d] From borehole log.

[e] From depth-corrected seismic section.

Recrystallization and Measured Strains

The sequence of events during halite recrystallization and anhydrite cap-rock formation deduced by Dix and Jackson (1982) is summarized in figure 45. This sequence portrays the most recent cycle of, perhaps, many thousands of cycles. Each cycle is speculated to have formed a lamina in the laminated anhydrite cap rock.

Stage 1. Vertical shortening (under vertical compressive stress greater than confining stress) resulted from rise of the diapiric rock salt. The shortening produced horizontal pressure stripes and vertical dilation veins in the anhydrite cap rock. The medium-grained unfoliated salt, containing inclusions of disseminated anhydrite, formed in the previous cycle of dissolution.

Stage 2. A further influx of water dissolved rock salt to form a cavity below the cap-rock contact, as at Gyp Hill, Winnfield, Jefferson Island, and Lake Washington Domes (O'Donnell, 1935; Taylor, 1938, p. 53–54; Hoy and others, 1962; Kreitler and Dutton, 1983). Active flow of ground water has been documented within some of these cavities (Huner, 1939, p. 221; Hoy and others, 1962). Water penetrated the underlying Oakwood rock salt along halite grain boundaries, causing secondary recrystallization just below the cavity (forming the coarse-grained R-3 zone of unfoliated salt having abundant intracrystalline fluid inclusions) and primary recrystallization slightly deeper (forming a new zone of medium-grained unfoliated salt, the R-2 zone).

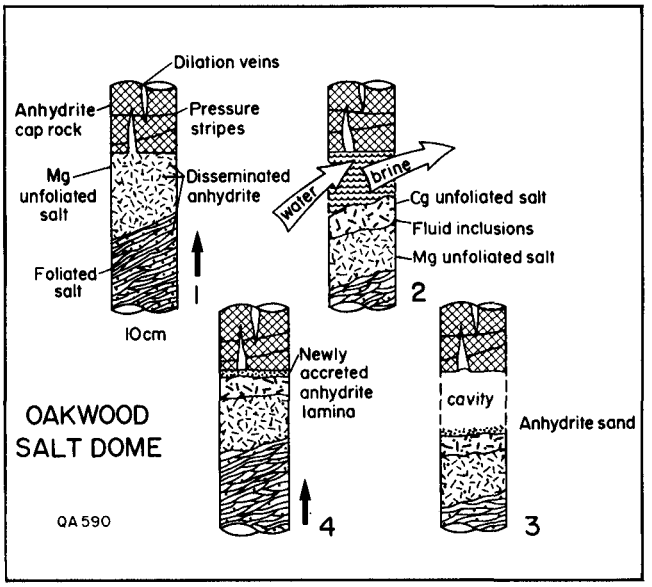

FIGURE 45. Schematic illustration of the model proposed by Dix and Jackson (1982) for basal accretion of anhydrite cap rock, formation and closure of a dissolution cavity, and superimposed strains in rock salt and cap rock of Oakwood Dome.

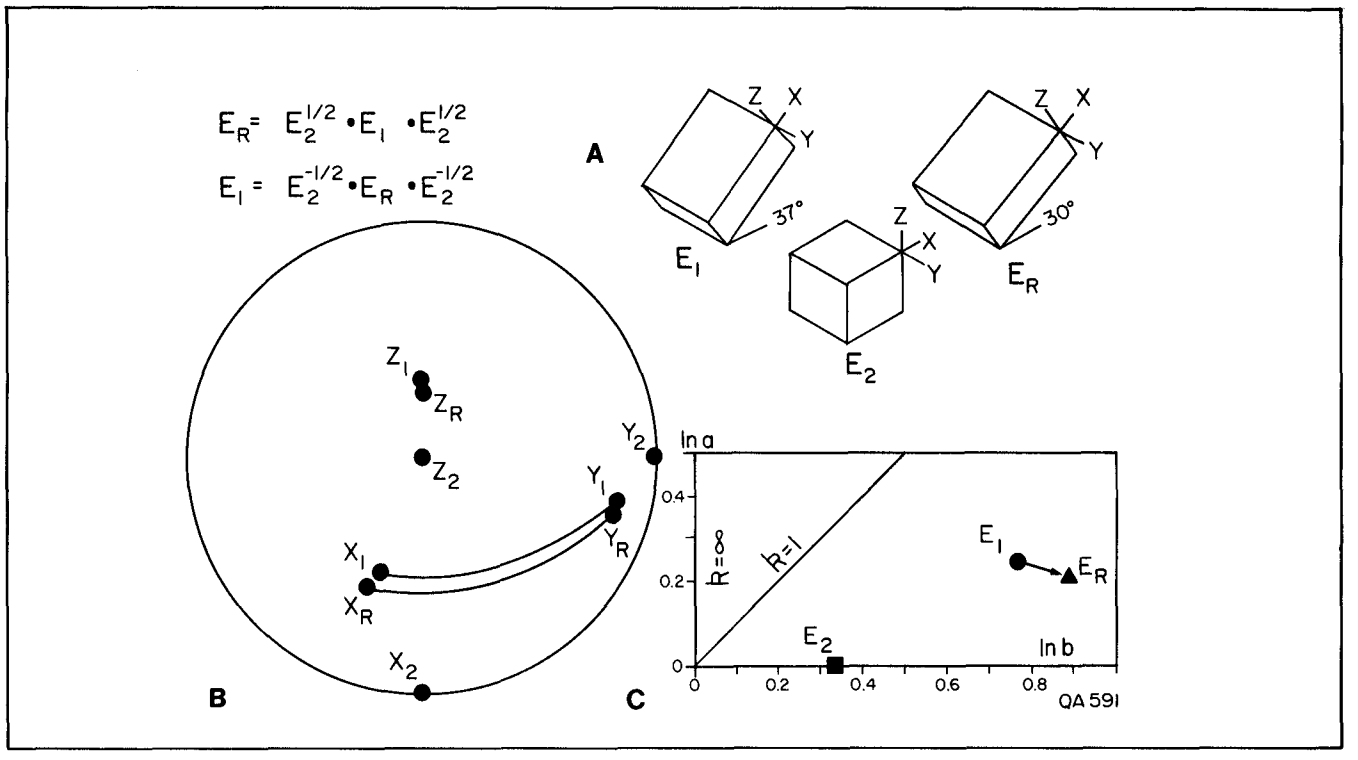

FIGURE 46. Quantitative modeling of superimposed strains in the crest of Oakwood Dome. E_1 is initial-strain ellipsoid; E_2 is incremental-strain ellipsoid; E_R is resultant-strain, or final-strain, ellipsoid. (A) Strains drawn to scale as blocks in true orientation. (B) Equal-area stereographic projection (Schmidt net) showing orientation of principal-strain axes of the three strain ellipsoids. (C) Flinn diagram showing deformation path of E_1-strain ellipsoid being converted to E_R-strain ellipsoid by addition of E_2-strain increment.

Stage 3. Anhydrite sand accumulated on the floor of the cavity as a residue from the dissolution of halite.

Stage 4. The cavity closed by diapiric rise of the salt. (There is no evidence for collapse of the cap rock, nor would such collapse result in vertical principal compressive stresses.) The anhydrite sand was accreted against the base of the cap rock. Forceful closure of the cavity is indicated by a tightly sealed halite-anhydrite contact, inclined shear fractures that offset the horizontal pressure stripes, and buckled vertical dilation veins.

The final-strain increment (strain ellipsoid E_2), induced by vertical uniaxial compression as the dissolution cavity closed, is recorded in the recrystallized unfoliated salt (specimen 1166). The total strain (strain ellipsoid E_R), which comprises both this final-strain increment and the previous strain increments, is recorded in the foliated salt (specimen 1178 and lower specimens). Knowing the strain in E_2 and E_R, represented by 3 × 3 symmetric matrices, the state of strain at the top of the R-1 zone *before* the final-strain increment can be calculated by means of the equation

$$E_R = E_2^{1/2} \cdot Ei \cdot E_2^{1/2} \quad \text{(Flinn, 1978, eq. 13a)}$$

which may be rewritten

$$E_1 = E_2^{-1/2} \cdot E_R \cdot E_2^{-1/2}$$

to solve for E_1 by matrix multiplication. This procedure allows the final part of the salt deformation path to be calculated. The strain ellipsoids E_1, E_2, and E_R are schematically illustrated in block form in figure 46A, and their orientations are shown in stereographic projection in figure 46B. During the final-strain increment (E_2), the XY foliation plane in the uppermost foliated R-1 salt rotated from a dip of 37° to 30°. Figure 46C shows the deformation path on a Flinn diagram. Addition of the final-strain increment (E_2) changed E_1 to E_R by increased flattening. This increased flattening (decreasing k value) is similar to that recorded in Dixon's (1975) model diapirs.

CONCLUSIONS

Findings of this study, which support the complementary study by Dix and Jackson (1982), include both generic conclusions on the internal structure of salt domes and specific conclusions on the internal structure of Oakwood Dome.

1. Direct and indirect measurement of strain rates in Iranian namakiers (salt glaciers) indicates that salt flows under tiny differential stress much faster and more readily than is predicted by laboratory experiments. The presence of water is essential for rapid flow, perhaps allowing flow by liquid diffusion. By inference, the concentration of water in repository rock salt plays a critical role in determining rate of salt creep around mined cavities.

2. Contrary to widespread generalization, a review of published maps shows that little of the interior of Gulf Coast salt mines consists of vertical or near-vertical structural elements; rather, most dips and plunges are steep. This inclined fabric anisotropy has an important bearing on fluid flow paths and on the flow paths of salt during creep.

3. There is no evidence of fundamental differences between the internal structures of salt stocks in Gulf interior basins and those in the Gulf Coast, as has been proposed in the literature. All salt stocks studied share certain characteristics. A broad range of dissimilarities also exists.

4. Folding in salt domes closely follows the similar-fold model (shear folding), though many folds appear to have been initiated by buckling. The closed interference structures are sheath folds formed by intense constriction of originally gentle fold culminations and depressions.

5. The flow directions of diapiric salt can be crudely deduced by construction of plunge-isogon maps from linear structural elements mapped in salt mines. Winnfield Dome, for example, appears to have been fed by two massive tongues of rising salt, showing geometric similarity with ice lobes in piedmont glaciers, with recumbent sheath folds in namakiers, and with certain model diapirs. In some salt mines, few linear structural elements have been measured, so the data base is too sparse to analyze some domes by plunge isogons.

6. Strain rates estimated for natural deformation of rock salt range from 10^{-8}/s to 10^{-16}/s. The slowest rates characterize average uplift rates of salt diapirs over millions of years.

7. The Oakwood Dome salt core has penetrated the hinge zone and lower limb of an inclined, overturned antiform. This is inferred to represent one of several salt tongues that have fed the diapir, rising upward and outward and changing in orientation from steeply plunging folds to recumbent, overthrust folds.

8. Geometric and strain analyses of Oakwood Dome salt core indicate profound truncation of the diapir crest, so that fold structures originally situated deep in the cap—or even the trunk—have now been bared and juxtaposed against the base of the cap rock. This truncation, almost certainly by ground-water dissolution, is an integral part of cap-rock formation, in which anhydrite sand is concentrated by dissolution of halite and repeatedly accreted against the base of the cap rock by diapiric rise of salt.

9. The uppermost part of the Oakwood Dome salt stock is now too shallow and cool to undergo conventional recrystallization (formation of new grains). But at depths greater than about 630 m, the salt would have been able to recrystallize during its rise to the diapir crest. Homologous temperatures suggest that the water-facilitated recrystallization of the upper 2 m of rock salt took place when the crest of the diapir was at least 275 m deeper than it is at present. At current maximum erosion rates, based on suspended-sediment data collected in the area (Collins, 1982), this would have occurred at least 2 Ma ago. Bearing in mind the uncertainties of extrapolating these erosion rates backward, active recrystallization is now unlikely in shallow parts of salt stocks. Nevertheless, recent experimental work on another evaporite chloride, bischofite (Urai, 1983), has shown that the presence of minute amounts of intercrystalline water (0.1 weight percent) greatly promotes recrystallization in a manner analogous to rise of temperature with increasing burial. Until we know more about the effects of water on halite recrystallization, we should neither presume that homologous temperatures of 0.3 (50°C for halite) represent the lower temperature limit for recrystallization nor rely on calculations of required depth of burial. Regardless of the conditions of its formation, the resultant coarse-grained isotropic rock has great significance to rock mechanics during mining because its properties are probably radically different from those of foliated rock salt.

10. There is no evidence that smaller halite grains in Oakwood Dome represent subgrains that have

undergone less deformation than have larger halite grains.

11. All the strains recorded from Oakwood Dome are of the flattening type and the ratio of flattening to constriction increases upward, whereas the strain intensity decreases upward. This upward decrease in strain intensity may mark the transition to an originally neutral-strain zone in the diapir, since removed by dissolution during diapir truncation.

12. The orientations of maximum-extension directions in the rock-salt samples vary widely, even though the foliation plane, which contains these directions, dips uniformly. Thus, the preferred directions of salt creep or intergranular fluid flow are also likely to vary widely.

ACKNOWLEDGMENTS

This study is part of the East Texas Nuclear Waste Isolation Feasibility project, which was funded by the National Waste Terminal Storage (NWTS) program of the U.S. Department of Energy under Contract No. DE-AC97-80ET46617 (formerly Contract No. DE-AC97-79ET-46605). The LETCO TOG-1 core was supplied by Law Engineering and Testing Company under the NWTS program.

Owen R. Dix measured layering and schistosity orientations for the geometric analysis. Bruce D. Wilson collected the Oakwood data for halite strain analysis, assisted greatly with data processing, and provided critical discussion. Rachel J. Burks carried out the fold-shape analysis for folds in Grand Saline and Avery Island Domes. Michael P. Roberts and Arthur G. Goldstein assisted with running program THETA and with matrix multiplication.

Christopher J. Talbot, University of Uppsala, Sweden, provided the catalyst, through his published work, for the review in part I. He also suggested many improvements to the manuscript; any errors of fact or interpretation that remain are my own. I would also like to thank the following for reading the manuscript: Robert W. Baumgardner, Jr., L. F. Brown, Jr., Jules DuBar, Thomas E. Ewing, and Noel Tyler of the Bureau of Economic Geology; and Sharon Mosher and William R. Muehlberger of the Department of Geological Sciences, The University of Texas at Austin.

I would also like to thank the following for their contributions: Joann Haddock and Dorothy C. Johnson did word processing and Fannie M. Sellingsloh typeset the report under the direction of Lucille C. Harrell. Figures were drafted by Mark T. Bentley, Barbara Hartmann, Jamie McClelland, Margaret L. Evans, John T. Ames, Robert S. Baum, Richard M. Platt, Jeff Horowitz, Margaret R. Day, Byron P. Holbert, and Kerza A. Prewitt under the direction of Richard L. Dillon. Text illustration photography was by James A. Morgan. The report was designed by Jamie S. Haynes and edited by Amanda R. Masterson and Jean Trimble.

REFERENCES

Ala, M. H., 1974, Salt diapirism in southern Iran: American Association of Petroleum Geologists Bulletin, v. 58, no. 9, p. 1758–1770.

Anthony, Mike, and Wickham, John, 1978, Finite-element simulation of asymmetric folding: Tectonophysics, v. 47, no. 1/2, p. 1–14.

Atwater, G. I., and Forman, M. J., 1959, Nature of growth of southern Louisiana salt domes and its effect on petroleum accumulation: American Association of Petroleum Geologists Bulletin, v. 43, no. 11, p. 2592–2622.

Balk, Robert, 1937, Structural behavior of igneous rocks: Geological Society of America Memoir 5, 177 p.

___ 1949, Structure of Grand Saline salt dome, Van Zandt County, Texas: American Association of Petroleum Geologists Bulletin, v. 33, no. 11, p. 1791–1829.

___ 1953, Salt structure of Jefferson Island salt dome, Iberia and Vermilion Parishes, Louisiana: American Association of Petroleum Geologists Bulletin, v. 37, no. 11, p. 2455–2474.

Biot, M. A., 1965, Theory of similar folding of the first and second kind: Geological Society of America Bulletin, v. 76, no. 2, p. 251–258.

Boulter, C. A., 1976, Sedimentary fabrics and their relation to strain-analysis methods: Geology, v. 4, no. 3, p. 141–146.

Bradshaw, R. L., and McClain, W. C., 1971, Project Salt Vault: a demonstration of disposal of high-activity solidified wastes in underground salt mines: Oak Ridge National Laboratory, ORNL-4555.

Breddin, Hans, 1956, Die tectonische Deformation der Fossilien im Rheinischen Schiefergebirge: Deutsche Geologische Gesellschaft Zeitschrift, v. 106, p. 227–305.

Bucher, W. H., 1956, Role of gravity in orogenesis: Geological Society of America Bulletin, v. 67, no. 10, p. 1295–1318.

Carey, S. W., 1962, Folding: Alberta Society of Petroleum Geologists Journal, v. 10, no. 3, p. 95–144.

Carter, N. L., 1976, Steady state flow of rocks: Reviews of Geophysics and Space Physics, v. 14, no. 3, p. 301–360.

Carter, N. L., and Hansen, F. D., 1980, Mechanical behavior of Avery Island halite: a preliminary analysis: Office of Nuclear Waste Isolation, Battelle Memorial Institute, Technical Report ONWI-100, 21 p.

___ 1983, Creep of rocksalt: Tectonophysics, v. 92, no. 4, p. 275–333.

Carter, N. L., and Heard, H. C., 1970, Temperature and rate dependent deformation of halite: American Journal of Science, v. 269, no. 10, p. 193–249.

Clabaugh, P. S., 1962a, Petrofabric analysis of salt crystals from Grand Saline salt dome: University of Texas, Austin, Master's thesis, 29 p.

___ 1962b, Petrofabric study of deformed salt: Science, v. 136, no. 3514, p. 389–391.

Cloos, Ernst, 1936, Der Sierra Nevada Pluton in Californien: Neues Jahrbuch fur Mineralogie, Beilage, v. 13, no. 76, p. 355–450.

Cobbold, P. R., 1977, Description and origin of banded deformation structures; I. Regional strain, local perturbations, and deformation bands: Canadian Journal of Earth Sciences, v. 14, no. 8, p. 1721–1731.

Cobbold, P. R., and Quinquis, H., 1980, Development of sheath folds in shear regimes: Journal of Structural Geology, v. 2, no. 1/2, p. 119–126.

Collins, E. W., 1982, Surficial evidence of tectonic stability and erosion rates, Palestine, Keechi, and Oakwood salt domes, East Texas: The University of Texas at Austin, Bureau of Economic Geology Geological Circular 82-3, 39 p.

Coward, M. P., 1976, Strain within ductile shear zones: Tectonophysics, v. 34, no. 3/4, p. 181–197.

Davis, J. C., 1973, Statistics and data analysis in geology: New York, John Wiley, 550 p.

De Paor, D. G., 1980, Some limitations of the R_f/ϕ technique of strain analysis: Tectonophysics, v. 64, no. 1/2, p. T29–T31.

Dieterich, J. H., 1970, Computer experiments on mechanics of finite amplitude folds: Canadian Journal of Earth Sciences, v. 7, no. 2, p. 467–476.

Dix, O. R., and Jackson, M. P. A., 1982, Lithology, microstructures, fluid inclusions, and geochemistry of rock salt and of the cap-rock contact in Oakwood Dome, East Texas: significance for nuclear waste storage: The University of Texas at Austin, Bureau of Economic Geology Report of Investigations No. 120, 59 p.

Dixon, J. M., 1975, Finite strain and progressive deformation in models of diapiric structures: Tectonophysics, v. 28, no. 1/2, p. 89–124.

Donath, F. A., and Parker, R. B., 1964, Folds and folding: Geological Society of America Bulletin, v. 75, no. 1, p. 45–62.

Draper, N. R., and Smith, H., 1967, Applied regression analysis: New York, John Wiley, 407 p.

Dunnet, David, 1969, A technique of finite strain analysis using elliptical particles: Tectonophysics, v. 7, no. 2, p. 117–136.

Dunnet, David, and Siddans, A. W. B., 1971, Non-random sedimentary fabrics and their modification by strain: Tectonophysics, v. 12, no. 4, p. 307–325.

Eargle, D. H., 1962, Geology of core hole WP-1 Tatum Dome, Lamar County, Mississippi: U.S. Geological Survey Technical Letter Dribble - 15, Open-File Report 474–278, 46 p.

Elliott, David, 1965, The quantitative mapping of directional minor structures: Journal of Geology, v, 73, no. 65, p. 865–880.

___ 1968, Interpretation of fold geometry from lineation isogonic maps: Journal of Geology, v. 76, no. 2, p. 171–190.

——— 1970, Determination of finite strain and initial shape from deformed elliptical objects: Geological Society of America Bulletin, v. 81, no. 8, p. 2221–2236.

Escher, B. G., and Kuenen, P. H., 1929, Experiments in connection with salt domes: Leidsche Geologische Mededeelingen, v. 3, no. 3, p. 151–182.

Etheridge, M. A., and Kirby, S. H., 1977, Experimental deformation of rock-forming pyroxenes: recrystallization mechanisms and preferred orientation development (abs.): American Geophysical Union Transactions, v. 58, p. 513.

Ewing, Maurice, and Ewing, J. I., 1962, Rate of salt-dome growth: American Association of Petroleum Geologists Bulletin, v. 46, no. 5, p. 708–709.

Fisher, R. A., and Yates, F., 1963, Statistical tables for biological, agricultural, and medical research: Edinburgh, Oliver and Boyd, 146 p.

Flinn, Derek, 1962, On folding during three-dimensional progressive deformation: Geological Society of London Journal, v. 118, pt. 4, p. 385–433.

——— 1965, On the symmetry principle and the deformation ellipsoid: Geological Magazine, v. 102, no. 1, p. 36–45.

___ 1978, Construction and computation of three-dimensional progressive deformations: Geological Society of London Journal, v. 135, pt. 3, p. 291–305.

Fry, Norman, 1979, Random point distributions and strain measurement in rocks: Tectonophysics, v. 60, no. 1/2, p. 89–105.

Gussow, W. C., 1968, Salt diapirism: importance of temperature, and energy source of emplacement, *in* Braunstein, Jules, and O'Brien, G. D., eds., Diapirism and diapirs: American Association of Petroleum Geologists Bulletin Memoir 8, p. 16–52.

Hambrey, M. J., 1979, Origin of foliation in glaciers: comments on a paper by R. L. Hooke and P. J. Hudleston: Journal of Glaciology, v. 22, no. 88, p. 556–558.

Hanna, S. S., and Fry, Norman, 1979, A comparison of methods of strain determination in rocks from southwest Dyfed (Pembrokeshire) and adjacent areas: Journal of Structural Geology, v. 1, no. 2, p. 155–162.

Hansen, F. D., and Carter, N. L., 1982, Creep of Avery Island rock salt, *in* First Conference on Mechanical Behavior of Salt: Pennsylvania State University, University Park.

Harrison, J. V., 1930, The geology of some salt plugs in Laristan (southern Persia): Geological Society of London Quarterly Journal, v. 86, p. 463–522.

Hartwig, G., 1923, Die Salz-'Seismogramme,' ihre tektonische und praktische Bedeutung: Kali, Verwandte Salze, und Erdol, v. 17, p. 192–197.

Henderson, J. R., 1981, Structural analysis of sheath folds with horizontal X-axes, northeast Canada: Journal of Structural Geology, v. 3, no. 3 p. 203–210.

Hooke, R. LeB., and Hudleston, P. J., 1978, Origin of foliation in glaciers: Journal of Glaciology, v. 20, no. 83, p. 285–299.

Hossack, J. R., 1968, Pebble deformation and thrusting in the Bygdin area (southern Norway): Tectonophysics, v. 5, no. 3-4, p. 315–339.

Howard, J. C., 1971, Computer simulation models of salt domes: American Association of Petroleum Geologists Bulletin, v. 55, no. 3, p. 495–513.

Hoy, R. B., Foose, R. M., and O'Neill, B. J., Jr., 1962, Structure of Winnfield salt dome, Winn Parish, Louisiana: American Association of Petroleum Geologists Bulletin, v. 46, no. 8, p. 1444–1459.

Hudleston, P. J., 1973a, Fold morphology and some geometrical implications of theories of fold development: Tectonophysics, v. 16, no. 1/2, p. 1–46.

___ 1973b, The analysis and interpretation of minor folds developed in the Moine rocks of Monar, Scotland: Tectonophysics, v. 17, no. 1/2, p. 89–132.

——— 1976, Recumbent folding in the base of the Barnes Ice Cap, Baffin Island, Northwest Territories, Canada: Geological Society of America Bulletin, v. 87, no. 12, p. 1684–1692.

___ 1977, Similar folds, recumbent folds, and gravity tectonics in ice and rocks: Journal of Geology, v. 85, no. 1, p. 113–122.

___ 1980, The progressive development of inhomogeneous shear crystallographic fabric in glacial ice: Journal of Structural Geology, v. 2, no. 1-2, p. 189–196.

Hudleston, P. J., and Hooke, R. LeB., 1980, Cumulative deformation in the Barnes Ice Cap and implications for the development of foliation: Tectonophysics, v. 66, no. 1/3, p. 127–146.

Hudleston, P. J., and Stephansson, Ove, 1973, Layer shortening and fold-shape development in the buckling of single layers: Tectonophysics, v. 17, no. 4, p. 299–321.

Huner, J., Jr., 1939, Geology of Caldwell and Winn Parishes: Louisiana Geological Survey Bulletin 15, 356 p.

Jackson, M. P. A., 1981a, Strain analysis of halite in the Oakwood core, *in* Kreitler, C. W., and others, Geology and geohydrology of the East Texas Basin, a report on the progress of nuclear waste isolation feasibility studies (1980): The University of Texas at Austin, Bureau of Economic Geology Geological Circular 81-7, p. 183–187.

___ 1981b, Upward flow of diapiric rock salt and the formation of anhydrite cap rock in Oakwood Dome, East Texas (abs.): Geological Society of America, Abstracts with Programs, v. 13, no. 7, p. 479.

Jackson, M. P. A., and Dix, O. R., 1981, Geometric analysis of macroscopic structures in Oakwood salt core, *in* Kreitler, C. W., and others, Geology and geohydrology of the East Texas Basin, a report on the progress of nuclear waste isolation feasibility studies (1980): The University of Texas at Austin, Bureau of Economic Geology Geological Circular 81-7, p. 177–182.

Jackson, M. P. A., and Seni, S. J., 1983, Geometry and evolution of salt structures in a marginal rift basin of

the Gulf of Mexico, East Texas: Geology, v. 11, no. 3, p. 131–135.

___ 1984a, The domes of East Texas, *in* Presley, M. W., ed., The Jurassic of East Texas: East Texas Geological Society, p. 163–239.

——— 1984b, Suitability of salt domes in the East Texas Basin for nuclear waste isolation: final summary of geologic and hydrogeologic research (1978 to 1983): The University of Texas at Austin, Bureau of Economic Geology Geological Circular 84-1, 128 p.

Kent, P. E., 1966, Temperature conditions of salt dome intrusions: Nature, v. 211, no. 5056, p. 1387.

___ 1970, The salt plugs of the Persian Gulf region: Leicester Literary and Philosophical Society Transactions, v. 64, p. 56–88.

___ 1979, The emergent Hormuz salt plugs of southern Iran: Journal of Petroleum Geology, v. 2, no. 2, p. 117–144.

Kern, H., 1977, Preferred orientation of experimentally deformed limestone, marble, quartzite, and rock salt at different temperatures and states of stress: Tectonophysics, v. 39, no. 1-3, p. 103–120.

Kier, R. S., Garner, L. E., and Brown, L. F., Jr., 1977, Land resources of Texas: The University of Texas at Austin, Bureau of Economic Geology Special Publication, scale 1:500,000.

Kreitler, C. W., Collins, E. W., Davidson, E. D., Dix, O. R., Donaldson, G. A., Dutton, S. P., Fogg, G. E., Giles, A. B., Harris, D. W., Jackson, M. P. A., Lopez, C. M., McGowen, M. K., Muehlberger, W. R., Pennington, W. D., Seni, S. J., Wood, D. H., and Wuerch, H. V., 1981, Geology and geohydrology of the East Texas Basin, a report on the progress of nuclear waste isolation feasibility studies (1980): The University of Texas at Austin, Bureau of Economic Geology Geological Circular 81-7, 207 p.

Kreitler, C. W., and Dutton, S. P., 1983, Origin and diagenesis of cap rock, Gyp Hill and Oakwood salt domes, Texas: The University of Texas at Austin, Bureau of Economic Geology Report of Investigations No. 131, 58 p.

Kreitler, C. W., and Muehlberger, W. R., 1981, Geochemical analyses of salt, Grand Saline Dome, East Texas, *in* Kreitler, C. W., and others, Geology and geohydrology of the East Texas Basin, a report on the progress of nuclear waste isolation feasibility studies (1980): The University of Texas at Austin, Bureau of Economic Geology Geological Circular 81-7, p. 188–194.

Kupfer, D. H., 1962, Structure of Morton Salt Company Mine, Weeks Island salt dome, Louisiana: American Association of Petroleum Geologists Bulletin, v. 46, no. 8, p. 1460–1467.

___ 1968, Relationship of internal to external structure of salt domes: American Association of Petroleum Geologists Memoir 8, p. 79–89.

_____ 1970, Mechanism of intrusion of Gulf Coast salt, *in* Kupfer, D. H., ed., Proceedings, Symposium on Geology and Technology of Gulf Coast Salt: Louisiana State University, School of Geoscience, p. 25–66.

——— 1974, Boundary shear zones in salt stocks, *in* Coogan, A. H., ed., Fourth Symposium on Salt: Northern Ohio Geological Society, v. 1, p. 215–225.

——— 1976, Shear zones inside Gulf Coast salt stocks help delineate spines of movement: American Association of Petroleum Geologists Bulletin, v. 60, no. 9, p. 1434–1447.

Laing, W. P., 1977, Structural interpretation of drill core from folded and cleaved rocks: Economic Geology, v. 72, no. 4, p. 671–685.

Law Engineering and Testing Company, 1983, Geothermal studies of seven interior salt domes: Report prepared for Office of Nuclear Waste Isolation, Battelle Memorial Institute, ONWI-289, 46 p.

Le Theoff, Bernard, 1979, Non-coaxial deformation of elliptical particles: Tectonophysics, v. 53, no. 1/2, p. T7–T13.

Lisle, R. J., 1977a, Clastic grain shape and orientation in relation to cleavage from the Aberystwyth Grits, Wales: Tectonophysics, v. 39, no. 1-3, p. 381–395.

___ 1977b, Estimation of the tectonic strain ratio from the mean shape of deformed elliptical markers: Geologie en Mijnbouw, v. 56, no. 2, p. 140–144.

___ 1979, Strain analysis using deformed pebbles: the influence of initial pebble shape: Tectonophysics, v. 60, no. 3/4, p. 263–277.

Lotze, Franz, 1957, Steinsalz und Kalisalze, Part I: Berlin, Gebruder Borntraeger, 466 p.

Marjoribanks, R. W., 1976, The relation between microfabric and strain in a progressively deformed quartzite sequence from central Australia: Tectonophysics, v. 32, no. 1/2, p. 269–294.

Martin, R. G., 1980, Distribution of salt structures, Gulf of Mexico, Sheet 2: U.S. Geological Survey, Miscellaneous Field Studies Map MF-1213, scale 1:2,500,000.

Martinez, J. D., Thoms, R. L., Kolb, C. R., Kumar, M. B., Wilcox, R. E., and Newchurch, E. J., 1978, An investigation of the utility of Gulf Coast salt domes for the storage or disposal of radioactive wastes, volume 1: Louisiana State University, Institute for Environmental Studies, Contract Report EW-78-C-05-5941/53, 390 p.

Matthews, P. E., Bond, R. A. B., and Van den Berg, J. J., 1974, An algebraic method of strain analysis using elliptical markers: Tectonophysics, v. 24, no. 1, p. 31–67.

Meier, M. F., and Post, Austin, 1969, What are glacier surges?: Canadian Journal of Earth Sciences, v. 6, no. 4, p. 807–817.

Mellis, O., 1942, Gefugediagramme in stereographischer Projecktien: Zeitschrift mineralogische und petrographische Mitteilungen, v. 53, p. 330–353.

Milnes, A. G., and Hambrey, M. J., 1976, A method of estimating cumulative strains in glacier ice: Tectonophysics, v. 34, no. 3/4, p. T23–T27.

Minnigh, L. D., 1979, Structural analysis of sheath-folds in a meta-chert from the Western Italian Alps: Journal of Structural Geology, v. 1, no. 4, p. 275–282.

Muehlberger, W. R., 1959, Internal structure of the Grand Saline salt dome, Van Zandt County, Texas: University of Texas, Austin, Bureau of Economic Geology Report of Investigations No. 38, 23 p.

Muehlberger, W. R., and Clabaugh, P. S., 1968, Internal structure and petrofabrics of Gulf Coast salt domes: American Association of Petroleum Geologists Memoir 8, p. 90–98.

Mukhopadhyay, Dhruba, and Sengupta, Subhashish, 1979, "Eyed folds" in Precambrian marbles from southeastern Rajasthan, India: Geological Society of America Bulletin, Part I, v. 90, no. 4, p. 397–404.

Nance, D., and Wilcox, R. E., 1979, Lithology of the Rayburn's Dome salt core: Louisiana State University, Institute for Environmental Studies, 307 p.

Nance, D., Rovik, J., and Wilcox, R. E., 1979, Lithology of the Vacherie salt dome core: Louisiana State University, Institute for Environmental Studies, 343 p.

O'Donnell, L., 1935, Jefferson Island salt dome, Iberia Parish, Louisiana: American Association of Petroleum Geologists Bulletin, v. 19, no. 11, p. 1602–1644.

Office of Nuclear Waste Isolation, 1982, Evaluation of area studies of the U.S. Gulf Coast salt dome basins: location recommendation report: Battelle Memorial Institute, ONWI-109, 95 p.

Paterson, W. S. B., 1981, The physics of glaciers (2d ed.): Oxford, Pergamon Press, 380 p.

Peach, C. J., and Lisle, R. J., 1979, A Fortran IV program for the analysis of tectonic strain using deformed elliptical markers: Computers and Geosciences, v. 5, no. 3/4, p. 325–334.

Pfiffner, O. A., and Ramsay, J. G., 1982, Constraints on geological strain rates: arguments from finite strain states of naturally deformed rocks: Journal of Geophysical Research, v. 87, no. B1, p. 311–321.

Post, Austin, 1972, Periodic surge origin of folded medial moraines on Bering piedmont glacier, Alaska: Journal of Glaciology, v. 11, no. 62, p. 219–226.

Post, Austin, and LaChapelle, E. R., 1971, Glacier ice: Seattle, University of Washington Press, 111 p.

Quinquis, H., Audren, C., Brun, J. P., and Cobbold, P. R., 1978, Intense progressive shear in Ile de Groix blueschists and compatibility with subduction or obduction: Nature, v. 273, no. 5657, p. 43–45.

Ragan, D. M., 1969, Structures at the base of an ice fall: Journal of Geology, v. 77, no. 6, p. 647–667.

Ramberg, Hans, 1964, Note on model studies of folding of moraines in piedmont glaciers: Journal of Glaciology, v. 5, no. 38, p. 207–218.

___ 1981, Gravity, deformation, and the Earth's crust in theory, experiments and geological application (2d ed.): London, Academic Press, 452 p.

Ramsay, J. G., 1967, Folding and fracturing of rocks: New York, McGraw-Hill, 568 p.

___ 1976, Displacement and strain: Royal Society of London Philosophical Transactions, Series A, v. 283, p. 3–25.

___ 1980, Shear zone geometry: a review: Journal of Structural Geology, v. 2, no. 1-2, p. 83–99.

Ramsay, J. G., and Allison, I., 1979, Structural analysis of shear zones in an alpinised Hercynian granite: Schweizerische Mineralogische Petrographische Mitteilungen, v. 59, p. 251–279.

Ramsay, J. G.,and Graham, R. H., 1970, Strain variation in shear belts: Canadian Journal of Earth Sciences, v. 7, no. 3, p. 786–813.

Reynolds, E., and Gloyna, E. F., 1960, Reactor fuel waste disposal project, permeability of rock salt and creep of underground cavities, final report: University of Texas, Austin, 40 p.

Richter-Bernburg, Gerhard, 1980, Salt tectonics, interior structures of salt bodies: Bulletin des Centres de Recherches Exploration-Production Elf-Aquitaine, v. 4, no. 1, p. 373–393.

Rickard, M. J., 1971, A classification diagram for fold orientations: Geological Magazine, v. 108, no. 1, p. 23–26.

Roberts, B., and Siddans, A. W. B., 1971, Fabric studies in the Llwyd Mawr Ignimbrite, Caernarvonshire, North Wales: Tectonophysics, v. 12, no. 4, p. 283–306.

Rogers, G. S., 1918, Intrusive origin of the Gulf Coast salt domes: Economic Geology, v. 13, p. 447–485.

Rondeel, H. E.,and Storbeck, F., 1978, Errors in geological compass determinations of the attitude of planar structures: Geologische Rundschau, v. 67, no. 3, p. 913–919.

Ross, J. V., and Nielsen, K. C., 1978, High-temperature flow of wet polycrystalline enstatite: Tectonophysics, v. 44, no. 1/4, p. 233–261.

Rousell, D. H., 1976, Preferred crystallographic orientation of quartz from deformed quartzite breccia of the Onaping Formation, Sudbury Basin: Canadian Journal of Earth Sciences, v. 13, no. 9, p. 1347–1350.

Sannemann, D., 1968, Salt-stock families in northwestern Germany: American Association of Petroleum Geologists Memoir 8, p. 261–270.

Sarkar, S., Chanda, S. K., and Bhattacharyya, A., 1982, Soft-sediment deformation fabric in the Precambrian Bhander oolite, central India: Journal of Sedimentary Petrology, v. 52, no. 1, p. 95–107.

Schwerdtner, W. M., 1966, Preferred orientation of halite in a "saltseismogram," *in* Geology, geochemistry, mining: Proceedings, Second Symposium on Salt, Northern Ohio Geological Society, p. 70–84.

___ 1967, Intragranular gliding in domal salt: Tectonophysics, v. 5, no. 5, p. 353–380.

Schwerdtner, W. M., Bennett, P. J., and Janes, T. W., 1977, Application of L-S fabric scheme to structural mapping and paleostrain analysis: Canadian Journal of Earth Sciences, v. 14, no. 5, p. 1021–1032.

Seni, S. J., and Jackson, M. P. A., 1983a, Evolution of salt structures, East Texas diapir province, part 1: sedimentary record of halokinesis: American Association of Petroleum Geologists Bulletin, v. 67, no. 8, p. 1219–1244.

___ 1983b, Evolution of salt structures, East Texas diapir province, part 2: patterns and rates of halokinesis: American Association of Petroleum Geologists Bulletin, v. 67, no. 8, p. 1245–1274.

——— 1984, Sedimentary record of Cretaceous and Tertiary salt movement, East Texas Basin: times, rates, and volumes of salt flow and their implications for nuclear waste isolation and petroleum exploration: The University of Texas at Austin, Bureau of Economic Geology Report of Investigations No. 139, 89p.

Serata, S., and Gloyna, E. F., 1959, Development of design principle for disposal of reactor fuel waste into underground salt cavities, Reactor Fuel Waste Disposal Project: University of Texas, Austin, 173 p.

Sharp, R. P., 1958, Malaspina Glacier, Alaska: Geological Society of America Bulletin, v. 69, no. 6, p. 617–646.

Shimamoto, Toshihiko, and Ikeda, Yukio, 1976, A simple algebraic method for strain estimation from deformed ellipsoidal objects. 1. Basic theory: Tectonophysics, v. 36, no. 4, p. 315–337.

Siddans, A. W. B., 1980, Analysis of three-dimensional, homogeneous, finite strain using ellipsoidal objects: Tectonophysics, v. 64, no. 1, p. 1–16.

Stocklin, Jovan, 1968, Salt deposits of the Middle East, *in* Mattox, R. B., ed., Saline deposits: Geological Society of America Special Paper 88, p. 157–181.

Talbot, C. J., 1974, Fold nappes as asymmetric mantled gneiss domes and ensialic orogeny: Tectonophysics, v. 24, no. 1/2, p. 259–276.

——— 1977, Inclined and asymmetric upward-moving gravity structures: Tectonophysics, v. 42, no. 2/4, p. 159–181.

——— 1979, Fold trains in a glacier of salt in southern Iran: Journal of Structural Geology, v. 1, no. 1, p. 5–18.

——— 1981, Sliding and other deformation mechanisms in a glacier of salt, S. Iran, *in* McClay, K. R., and Price, N. J., eds., Thrust and nappe tectonics: Oxford, Geological Society of London, p. 173–183.

Talbot, C. J., and Jarvis, R. J., 1984, Age, budget, and dynamics of an active salt extrusion in Iran: Journal of Structural Geology, v. 6, no. 5, p. 521–533.

Talbot, C. J., and Rogers, E. A., 1980, Seasonal movements in a salt glacier in Iran: Science, v. 208, no. 4442, p. 395–397.

Talbot, C. J., Tully, C. P., and Woods, P. J. E., 1982, The structural geology of Boulby (Potash) Mine, Cleveland, United Kingdom: Tectonophysics, v. 85, no. 3–4, p. 167–204.

Taylor, R. E., 1938, Origin of the cap rock of Louisiana salt domes: Louisiana Geological Survey Bulletin 11, 191 p.

Thiessen, R. L., and Means, W. D., 1980, Classification of fold interference patterns: a re–examination: Journal of Structural Geology, v. 2, no. 3, p. 311–316.

Thoms, R. L., Mogharrebi, M., and Gehle, R. M., 1982, Geomechanics of borehole closure in salt domes: Dallas, Texas, Gas Processors Association, Proceedings of 61st Annual Convention, p. 228–230.

Trusheim, Ferdinand, 1960, Mechanism of salt migration in northern Germany: American Association of Petroleum Geologists Bulletin, v. 44, no. 9, p. 1519–1540.

Tullis, Jan, 1977, Preferred orientation of quartz produced by slip during plane strain: Tectonophysics, v. 39, no. 1/3, p. 87–102.

Urai, J. L., 1983, Water assisted dynamic recrystallization and weakening in polycrystalline bischofite: Tectonophysics, v. 96, no. 1/2, p. 125–157.

U.S. Department of Energy, 1983, Proposed general guidelines for recommendation of sites for nuclear waste repositories: Federal Register, Part II, vol. 48, no. 26, p. 5670–5682.

Vernon, R. H., 1975, Deformation and recrystallization of a plagioclase grain: American Mineralogist, v. 60, no. 9/10, p. 884–888.

Vita-Finzi, C., 1979, Rates of Holocene folding in the Coastal Zagros near Bandar Abbas, Iran: Nature, v. 278, no. 5705, p. 632–633.

Washburn, Bradford, 1935, Morainic bandings of Malaspina and other Alaskan glaciers: Geological Society of America Bulletin, v. 46, no. 12, p. 1876–1890.

Wegmann, C. E., 1963, Tectonic patterns at different levels: Geological Society of South Africa Transactions, A. L. du Toit Memorial Lecture no. 8, v. 66 annexure, p. 1–78.

Wenkert, D. D., 1979, The flow of salt glaciers: Geophysical Research Letters, v. 6, no. 6, p. 523–526.

White, S. H., 1976, The effects of strain on the microstructures, fabrics, and deformation mechanisms in quartzite: Royal Society of London Philosophical Transactions, Series A, v. 283, p. 69–86.

Wynne-Edwards, H. R., 1963, Flow folding: American Journal of Science, v. 261, no. 11, p. 793–814.

Zak, Israel, and Freund, Raphael, 1980, Strain measurements in eastern marginal shear zone of Mount Sedom salt diapir, Israel: American Association of Petroleum Geologists Bulletin, v. 64, no. 4, p. 568–581.